Justus-Liebig-University Gießen
Faculty 11: Internal Medicine
Signal Transduction of Cellular Motility

Regulation of carcinoma cell motility by the GTPase isoforms Rac1 and Rac1b

---

Regulation der Motilität von Karzinomzellen durch die GTPase-Isoformen Rac1 und Rac1b

Doctoral thesis
for the degree of doctor of natural sciences
- Dr. rer. nat. -
at the faculty of Biology and Chemistry
of the University of Gießen

submitted by
Johannes Markus Klinke

Gießen, February 2020

First supervisor:	Prof. Dr. Reinhard Dammann Institute of Genetics Justus-Liebig-University Gießen Heinrich-Buff-Ring 58-62, 35392 Gießen
Second supervisor:	Prof. Dr. Klaudia Giehl Professorship for Signal Transduction of Cellular Motility Justus-Liebig-University Gießen Aulweg 128, 35392 Gießen
Committee member:	Prof. Dr. Sandra Hake Institute of Genetics Justus-Liebig-University Gießen Heinrich-Buff-Ring 58-62, 35392 Gießen
Committee member:	Prof. Dr. Albrecht Bindereif Institute of Biochemistry Justus-Liebig-University Gießen Heinrich-Buff-Ring 17, 35392 Gießen
Date of oral defense:	February 17th, 2020

Table of Contents

List of figures

List of tables

List of abbreviations

A	ampere
ARM	armadillo-repeat motif
bp	base pair
B2M	β-2-microglobulin
bHLH	basic helix-loop-helix
BSA	bovine serum albumin
c (unit prefix)	centi
CAM	chorioallantoic membrane
Ch.	chapter
dH_2O	distilled water
ddH_2O	double-distilled water
DMSO	dimethyl sulfoxide
DNA	deoxyribonucleic acid
DTT	1,4-Dithio-DL-threit(ol)
E-Cadherin	epithelial cadherin
E. coli	*Escherichia coli*
ECM	extracellular matrix
EDTA	ethylenediaminetetraacetic acid
EGF	epidermal growth factor
EGFP	enhanced green fluorescent protein
ECL	enhanced chemiluminescence
EMT	epithelial-to-mesenchymal transition
ER	endoplasmatic reticulum
ESRP1/2	epithelial splicing regulatory protein 1/2
FC	fold change
Fig.	figure
g	gram
x g	earth's gravitational acceleration (9,81 m/s^2)
GAP	GTPase activating protein
GAPDH	glyceraldehyde-3-phosphate dehydrogenase
GDI	guanosine nucleotide dissociation inhibitor
GDP	guanosine diphosphate
GEF	guanosine nucleotide exchange factors

GTP	guanosine triphosphate
h	hour
HA	human influenza hemagglutinin
hnRNP A1	heterogeneous nuclear ribonucleoprotein A1
HRP	horseradish peroxidase
kb	kilo base pairs
kDa	kilodalton
l (unit)	liter
m (unit prefix)	milli
m (unit)	meter
µ (unit prefix)	micro
M	molar (mol per liter)
m/v	mass per volume
MET	mesenchymal-to-epithelial transition
min	minutes
MMP	matrix metalloproteinase
n (unit prefix)	nano
N-Cadherin	neural cadherin
NLS	nuclear localization signal
NSCLC	non-small cell lung cancer
nt	nucleotide
OD	optical density
P100	membranous, insoluble protein fraction
$p120^{ctn}$	p120-catenin
PAK1	p21-activated kinase 1
PBS	phosphate-buffered saline
PBR	polybasic region
PCR	polymerase chain reaction
PDAC	pancreatic ductal adenocarcinoma
qRT-PCR	quantitative reverse transcriptase-PCR
Rac1	Ras-related C3 botulinum toxin substrate 1
RBP	RNA-binding protein
RNA	ribonucleic acid
ROS	reactive oxygen species

rpm	rounds per minute
RRM	RNA recognition motif
RT	room temperature
RTK	receptor tyrosine kinase
s (unit)	second
S100	cytosolic, soluble protein fraction
SD	standard deviation
SDS	sodium dodecyl sulfate
SDS-PAGE	SDS-polyacrylamide gel electrophoresis
SIP1	Smad-interacting protein 1 (also known as ZEB2)
sqRT-PCR	semi quantitative RT-PCR
SRSF1/3	serine/arginine-rich splicing factor 1/3
Tab.	table
TBS	tris-buffered saline
TGFβ1	transforming growth factor β1
TβR-I/-II	TGFβ receptor type I/type II
Tris	Tris(hydroxymethyl)-aminomethane
Tween®20	polyoxyethylene (20) sorbitan monolaurate
U	units
UV	ultraviolet
V	volts
v/v	volume per volume
WB	western blot
wt	wildtype
ZEB	zinc-finger E-box-binding homeobox

1 Introduction

1.1 Tumor metastasis and epithelial-to-mesenchymal transition

1.1.1 Metastasis in pancreatic and lung cancer

In highly developed countries, malignant neoplasms are the second leading cause of death after cardiovascular diseases. One of six deaths worldwide is caused by cancer, a disease that encompasses uncontrolled cell growth and the spreading of abnormal human cells throughout the body (American Cancer Society, 2018). In this work, different cell lines derived from human pancreatic und lung carcinoma patients were analyzed.

Pancreatic neoplasmic malignancies are the fourth leading cause of cancer-related deaths in women and men. Over 90 % of patients diagnosed with pancreatic cancer die of the disease, whereby the 5-year survival rate is only 5 % (American Cancer Society, 2018). Lung cancer accounts for the most cancer-related deaths with a 5-year survival rate of 13 % (American Cancer Society, 2018). About 95 % of pancreatic cancers are pancreatic ductal adenocarcinoma (PDAC) derived from epithelial cells lining the exocrine pancreatic ducts (Iovanna *et al.*, 2012). Most lung cancers are non-small cell lung cancers (NSCLC), which are further divided into the squamous cell carcinoma, large cell carcinoma and adenocarcinoma. With about 40 % of all lung tumors, adenocarcinomas are the most common lung cancer type and arise from the epithelial cells lining the small bronchi, bronchioles and alveoli (Kadara *et al.*, 2012). The bad prognoses of pancreatic and lung cancers are due to the fact, that both diseases are commonly diagnosed at a late stage when the tumors have already metastasized and the cancer cells spread regionally and distantly (Herbst *et al.*, 2008; Ryan *et al.*, 2014). In PDAC, this is reinforced by a very aggressive tumor biology, a rapid progression to an invasive and metastatic carcinoma as well as a strong intrinsic drug- and chemotherapeutic resistance (Ryan *et al.*, 2014).

The thorough understanding of tumor metastasis marks the major challenge in cancer research. In general, metastasis is the dissemination of tumor cells from the primary tumor site to colonize distant organs and form secondary tumor nests (Steeg, 2016). Tumor cells invade the surrounding tissue, enter the blood or lymphatic circulation and are transported throughout the body as circulating tumor cells. These cells leave the blood stream by extravasation and colonize the new tissue to form secondary tumors (Kölbl *et al.*, 2016).

1.1.2 Epithelial-to-mesenchymal transition in cancer

It is generally accepted, that most epithelial-derived carcinomas do not arise *de novo*, but undergo a multistep progression, beginning with precursor lesions and progressing to carcinomas *in situ* culminating in invasive, metastatic carcinomas. These histological and genetically distinct steps are characterized by a stepwise de-differentiation of the cells and the accumulation of genetic alterations and mutations. Among many others, the activating mutation of the *KRAS* oncogene and loss of the *P53* tumor suppressor are the most prominent examples (Iovanna *et al.*, 2012; Yatabe *et al.*, 2011). During this progression these cells lose their comparably static, epithelial properties and gain mesenchymal, metastatic traits by a process called epithelial-to-mesenchymal transition (EMT). EMT is a highly coordinated process, which plays an important role during embryogenesis, development, wound healing as well as tissue regeneration. EMT is re-activated during tumorigenesis in a less orderly fashion (Kalluri and Weinberg, 2009). The changes in cellular morphology and protein expression during EMT were summarized in Fig. 1.1. Due to the complex nature of EMT the following section will highlight only some hallmark events of the process.

The early events of EMT consist of the deconstruction of epithelial cell-cell junctions, which establish the permeability barrier function of epithelial tissues and are essential for epithelial integrity (Hartsock and Nelson, 2008). Tight junctions, which seal epithelial tissues, are dissolved by downregulation of Claudin, Occludin and Zonula occludens 1 (ZO1). Adherens junctions, which connect the Actin cytoskeleton of neighboring cells, are dissolved by cleaving and subsequently degrading epithelial Cadherins (E-Cadherin). Additionally, gap junctions and desmosomes, which connect the Cytokeratin intermediate filaments of neighboring cells, are disrupted by Connexin downregulation (Huang *et al.*, 2012). As a consequence, epithelial cells lose their apico-basal polarity, which is functionally and physically integrated into the junction architecture (St Johnston and Ahringer, 2010).

Tumor cells undergoing EMT also drastically rearrange their cytoskeleton. The peripheral and cortical Actin cytoskeleton is preplaced by Actin stress fibers to allow cell migration and directed motility. Actin dynamics and rearrangements during cell migration are regulated by RhoGTPases (Lawson and Ridley, 2018), which will be assessed in more detail in Ch. 1.3.1. Additionally, the Cytokeratin intermediate filaments are replaced by Vimentin. Both regulate trafficking of organelles and membrane-associated proteins, but differ in the proteins that are transported to the membrane (Lamouille *et al.*, 2014).

Another characteristic of EMT is the switch in the protein expression of cell adhesion transmembrane proteins, like Cadherins and Integrins. Downregulation of E-Cadherin during

EMT is accompanied by an increased expression of mesenchymal neural Cadherin (N-Cadherin). Homotypic N-Cadherin interactions are much weaker than E-Cadherin interactions, which allows tumor cell migration and invasion. Neo-expression and upregulation of N-Cadherin in epithelial-derived tumors are associated with a more aggressive behavior and poor patient prognosis (Gloushankova *et al.*, 2017; Luo *et al.*, 2018). Integrins anchor the epithelial cells to extracellular matrix (ECM) components of the basement membrane and also facilitate apico-basal polarity. During EMT, epithelial-specific Integrins, which mediate long lasting cell-matrix connections at the basal cell side, are replaced by mesenchymal Integrins, which exhibit more transient adhesive properties (Micalizzi *et al.*, 2010). Another protein, which is affected during EMT is $p120^{ctn}$. The armadillo-repeat motif-containing (ARM) protein is a master regulator of Cadherin stability and modulator of RhoGTPase activity, thereby playing a role in cytoskeleton reorganization. $p120^{ctn}$ interacts with and stabilizes Cadherins on the intracellular transmembrane domain where it inhibits endocytoses and promotes adhesion (Kourtidis *et al.*, 2013). Upon downregulation of E-Cadherin during EMT, $p120^{ctn}$ accumulates in the cytoplasm and nucleus. Aberrant subcellular localization of $p120^{ctn}$ plays a functionally diverse role in cancer progression and can promote invasion and motility (Menke and Giehl, 2012). The $p120^{ctn}$ gene (*CTNND1*) contains four alternative exons and four alternative transcription start sites, which encodes 64 potential different isoforms. The isoforms are named after their start sites (1-4) and alternatively spliced exons (A-D). The functional differences of the different isoforms of $p120^{ctn}$ are largely unexplored (Pieters *et al.*, 2012). But a change in the isoform ratio is observed during EMT (Zhang *et al.*, 2014).

For cancer cells to leave the primary tumor and invade the surrounding tissues, extensive ECM remodeling and degradation is necessary, which is another hallmark characteristic of EMT. EMT-related changes of the Integrin repertoire of a cell are correlated with the increased expression and exocytosis of proteases, like matrix metalloproteinases (MMP) and ADAM family proteases (Peixoto *et al.*, 2019). MMPs degrade the structural components of the ECM and thereby enable invasion. Furthermore, MMPs are involved in the degradation of transmembrane proteins, like E-Cadherin, and activation of precursor zymogens in the ECM (Chen *et al.*, 2013).

Altogether, EMT is an important process during tumorigenesis and metastasis. But it is important to note, that EMT is not a binary process with two distinct epithelial and mesenchymal cell populations. EMT rather occurs in a gradual manner with different expression levels of epithelial and mesenchymal markers as well as partial or hybrid EMT states (Pastushenko and Blanpain, 2019).

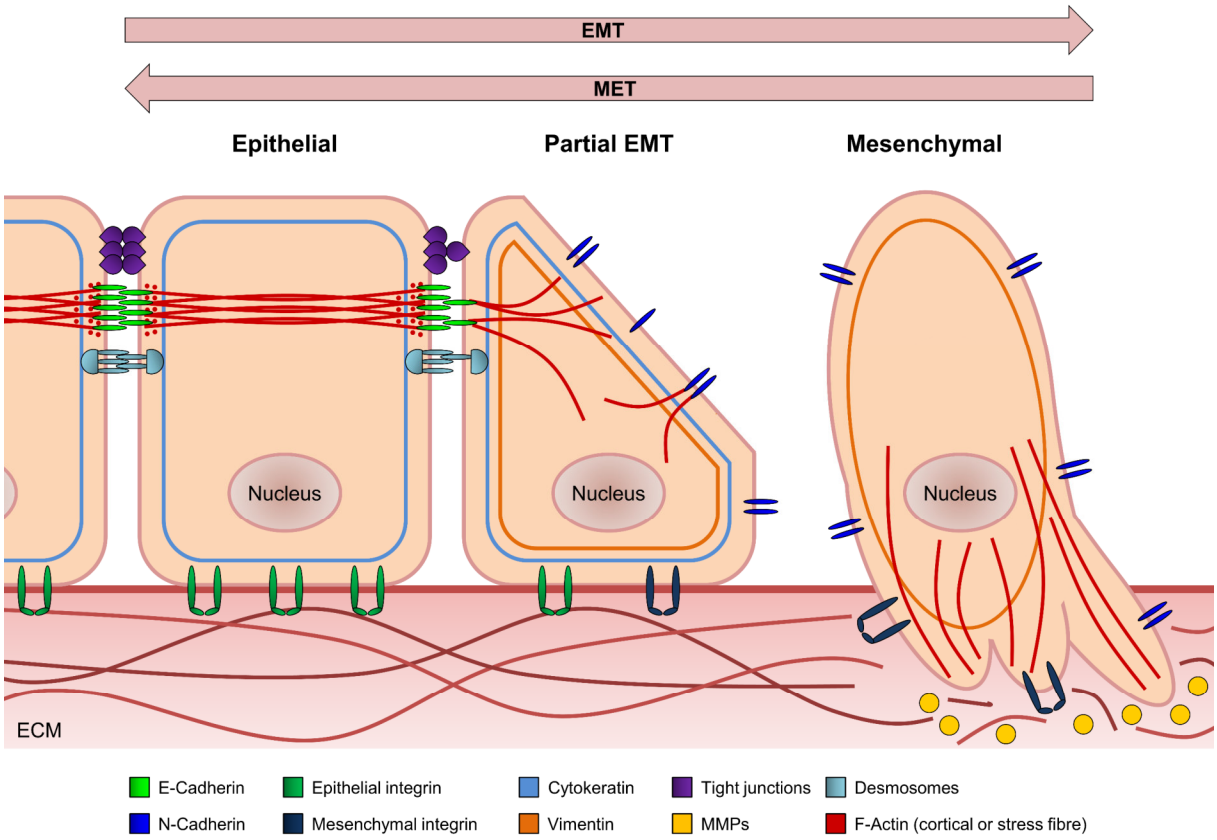

Fig. 1.1: Schematic changes of protein expression patterns and cellular morphology during epithelial-to-mesenchymal transition. During tumor progression epithelial cells de-differentiate and gain mesenchymal invasive traits by a process called epithelial-to-mesenchymal transition (EMT). This figure depicts epithelial cells losing their apico-basal polarity, dissolving the epithelial cell-cell junctions, which include adherens and tight junctions as well as desmosomes, and drastically rearranging their cytoskeleton. Furthermore, the Cytokeratin intermediate filaments are downregulated and replaced by Vimentin. The cells undergo a Cadherin and Integrin switch, replacing E-Cadherin with N-Cadherin and epithelial-specific Integrins with mesenchymal ones. The extracellular matrix (ECM) is remodeled in part through exocytosis of matrix metalloproteinases (MMP). EMT is a reversible process with partial hybrid states. Mesenchymal cells can revert to form epithelia through the reverse process called mesenchymal-to-epithelial transition (MET). This figure was altered according to Lamouille *et al.* (2014) with the permission of the *Springer Nature* journal (license number: 4557540030740).

1.1.3 EMT-specific transcription factors

Numerous transcription factors play an important role in EMT and MET. During tumorigenesis, multiple transcription repressors and activators were shown to be re-expressed and capable of inducing EMT (Pastushenko and Blanpain, 2019). Some of these transcription factors influence their own expression in positive feedback loops and alter the expression ratios of other transcription factors by spatial-temporal cooperation, thereby acting in a concerted manner to induce EMT (Tran *et al.*, 2011). Next to promoter hypermethylation, chromatin modifications play an important role in the transcriptional repression and downregulation of epithelial genes during EMT (Wawruszak *et al.*, 2019). In the following, the focus will be laid on a subset of highly characterized master regulators of EMT, which were analyzed in the course of this work.

Snail (syn. Snail1) and Slug (syn. Snail2) represent the best analyzed members of the *SNAIL* family of zinc-finger transcription factors (Phillips and Kuperwasser, 2014). Despite a strong homology of the Snail and Slug proteins, they possess important functional differences. While *SNAIL*-knockout mice die at gastrulation, *SLUG*-null mice survive, but show tissue and stem cell defects (Dhasarathy *et al.*, 2011). The Snail and Slug proteins differ mainly in their middle regions, which are important for posttranslational regulation and differential protein-protein-interactions (Phillips and Kuperwasser, 2014). Both proteins contain an N-terminal SNAG domain, which is important for the nuclear localization and transcriptional repression. The sequence-specific DNA-binding is mediated by a C-terminal zinc-finger domain (Phillips and Kuperwasser, 2014). Both transcription factors repress epithelial genes by binding to E-box promoter sequences. They alter the gene expression by recruiting proteins for histone modifications and chromatin remodeling (Chen *et al.*, 2014; Dong *et al.*, 2012). Besides downregulating E-Cadherin and the tight junction protein Occludin, Snail and Slug are involved in the upregulation of N-Cadherin, Fibronectin, MMPs, Twist1 and ZEB1 as well as ZEB2 (Casas *et al.*, 2011; Dhasarathy *et al.*, 2011; Phillips and Kuperwasser, 2014).

The zinc-finger E-box-binding homeobox transcription factors 1 (ZEB1) and 2 (ZEB2) also bind to regulatory E-box DNA sequences in promoter regions through their zinc-finger domains. ZEB1 and ZEB2 activate or repress gene expression through association with chromatin remodeling factors (Fardi *et al.*, 2019). The two proteins show only a 43 % homology, which explains their functional differences, but contain highly conserved N- and C-terminal zinc-finger clusters, which show an 88 % and 93 % sequence homology, respectively. Major structural differences between ZEB1 and ZEB2 are found in the middle regions. These regions are responsible for several functions including protein-protein interactions (Fardi *et al.*, 2019). Several ZEB-responsive genes were identified. In NSCLC cells, ZEB1 upregulates N-Cadherin, Vimentin, the fibroblast growth factor receptor 1 (FGFR1) and ZEB2, but represses the expression of E-Cadherin and the epithelial cell adhesion molecule (EpCAM) (Gemmill *et al.*, 2011). ZEB2, which is also named Smad-interacting protein 1 (SIP1) and was identified through its role in TGFβ signaling, also participates in E-Cadherin repression and upregulates MMPs and Twist1 (Yalim-Camci *et al.*, 2019).

Twist1 is a member of the basic helix-loop-helix (bHLH) family of transcriptional regulators, which play important roles in lineage specification, prenatal development and differentiation. Twist1 was identified as a master regulator of mesoderm development (Yang *et al.*, 2010). Like Snail, Slug, ZEB1 and ZEB2, Twist1 regulates transcription by binding to E-box elements in promoter regions and influencing chromatin remodeling as well as histone modifications (Yang

et al., 2010; Yang *et al.*, 2012). Twist1-dependent transcriptional regulation is mediated through homo-dimerization or hetero-dimerization with other bHLH family members. The diversity of dimerization possibilities explains the dual mode of the transcriptional output (Tang *et al.*, 2016). Twist1 plays a crucial role in EMT and is responsible for the induction or repression of gene expression of several EMT-related genes. For example, Twist1 downregulates the expression of E-Cadherin as well as β-Catenin and induces N-Cadherin, Fibronectin and smooth-muscle Actin gene expression (Yang *et al.*, 2012).

1.1.4 The role of TGFβ1 as an EMT inducer

Several signaling pathways were implemented in the reprogramming of gene expression patterns of epithelial cells. Among the numerous signaling cascades involved, transforming growth factor β (TGFβ) signaling inherits a predominant role in EMT induction (Lamouille *et al.*, 2014).

In humans, three highly homologous TGFβ ligands (TGFβ1-3) function as the primary mediators of TGFβ signaling and are secreted as inactive homodimeric protein complexes and sequestered in the ECM. Upon Integrin-mediated release and subsequent activation, TGFβ can bind to the respective receptors and mediate signal transduction cascades (Morrison *et al.*, 2013; Shi *et al.*, 2011). TGFβ1, the best characterized member, which mediates its signaling effects through transmembrane serine/threonine kinase receptors. These tetrameric receptor complexes consist of two type I (TβR-I) and two type II (TβR-II) receptors. Upon binding of the dimeric ligand, the transmembrane proteins oligomerize allowing the TβR-II to trans-phosphorylate the TβR-I (Hata and Chen, 2016). The downstream signal transduction cascades are separated into two groups, the Smad-dependent or canonical and the Smad-independent or non-canonical TGFβ1 signaling pathways. During canonical TGFβ1 signaling the activated TβR-I phosphorylates C-terminal serine residues of the regulatory Smads (or R-Smads), Smad2 and Smad3. The two phosphorylated R-Smads form a heteromeric complex with the common-Smad Smad4 (or Co-Smad), which is essential for nuclear trans-localization (Kamato *et al.*, 2013). In the nucleus, the Smad complex interacts with a variety of transcription cofactors and initiates transcriptional activation or repression of several target genes (Hata and Chen, 2016). TGFβ complements Smad-mediated signaling effects by non-canonical, Smad-independent signaling pathways. These include the PI3K/Akt, MAPK (e.g. ERK1/2, p38 and JNK) and RhoGTPase (e.g. RhoA, Rac1 and Cdc42) signaling cascades (Zhang *et al.*, 2013; Zhang, 2017).

The pleiotropic growth factor TGFβ1 has two distinct and paradoxical functions during tumorigenesis. In normal human epithelia and early-stage carcinomas, TGFβ1 exerts cytostatic

effects and acts as a tumor suppressor by inducing cell cycle arrest and apoptotic reactions. Prolonged TGFβ1 stimulation during cancer progression reverses the inhibitory effects and promotes carcinoma growth, invasion and metastasis (Morrison *et al.*, 2013). Increased TGFβ1 expression, secretion and activation were shown to induce EMT in a wide variety of cancers. The prolonged treatment of NSCLC cells with TGFβ1 led to increased cancer cell stemness and induced changes in the protein expression patterns consistent with EMT (Gemmill *et al.*, 2011; Pirozzi *et al.*, 2011). Amongst others, Rac1 was shown to play a pivotal role in antagonizing the TGFβ1 growth inhibitory response and driving migratory and EMT responses (Ungefroren *et al.*, 2011). Additionally, it was observed, that pharmacological inhibition of TGFβ1 signaling reversed the EMT-related Cadherin switch and upregulation of Snail as well as Twist1 in A459 cells (Kim and Kim, 2013). Furthermore, mutational abrogation of TGFβ1 signaling during cancer progression plays an important role in malignancy-related EMT. In about 80 % of PDAC patients, the *DPC4* gene (Smad4) is deleted or contains a loss-of-function mutation. Smad4 is thought to counteract tumorigenesis through its role in TGFβ-mediated growth inhibition (Shin *et al.*, 2017). Altogether, TGFβ1 signaling inherits a predominant function in cancer progression and induction of EMT, which can be explained by the diverse physiological functions of TGFβ1 and the multitude of signaling nodes and cross talks involved.

1.2 Alternative splicing and EMT

1.2.1 The role of alternative splicing during cancer progression and EMT

The drastic changes in protein expression and cell morphology, which occur during EMT require multiple levels of regulation. In the last two decades, the post-transcriptional regulation through alternative splicing has emerged as an additional major contributor to EMT fine-tuning (Pradella *et al.*, 2017).

The human genome contains only 22.000 genes, whereas over 250.000 different proteins are known to be expressed. This increased protein diversity is enabled by alternative splicing of about 90 % of human gene products, thereby regulating the expression of several, sometimes functionally opposing protein isoforms from a single gene (Lee and Rio, 2015; Pennisi, 2005). Alternative splicing is regulated by *cis*- and *trans*-acting factors. *Cis*-acting factors include the consensus splice site sequences and the grade of conservation of these sequences. Additionally, intronic and exonic splicing enhancer as well as silencer sequences affect the splicing outcome of alternative exons (Graveley, 2009). These enhancer or silencer sequences are recognized by *trans*-acting splicing factors, which are RNA-binding proteins (RBP), that inhibit or facilitate splicing of a nearby splice site (Pradella *et al.*, 2017). The balance of alternative exon out-

splicing or retention is influenced by the ratio and relative abundance of several splicing enhancers and inhibitors. The outcome can be shifted through splicing factor expression changes, shuttling of these proteins between the nucleus and cytoplasm as well as changes in the activity state of different splicing factors (Warzecha and Carstens, 2012).

Two major classes of ubiquitously expressed splicing factors were identified to regulate alternative splicing processes, the heterogeneous nuclear ribonucleoproteins (hnRNP) and serine/arginine-rich splicing factors (SRSF). In general, hnRNPs bind to silencer sequences and promote exon out-splicing, whereas SRSF proteins generally promote alternative exon inclusion by interacting with enhancer elements (Piekielko-Witkowska *et al.*, 2010). The hnRNP protein family consists of twenty members, which fulfill a wide variety of functions including alternative splicing, mRNA stabilization, transcriptional regulation and nuclear export. The hnRNP A1 protein is the best characterized member of this family and contains two N-Terminal RNA recognition motifs (RRM), which mediate specific target RNA binding (Roy *et al.*, 2017). The overexpression of hnRNP A1 was identified in several tumor types including liver, gastric and pancreatic cancer and correlated with increased invasion and EMT (Chen *et al.*, 2018b; Cogoi *et al.*, 2017; Zhou *et al.*, 2013b). The SRSF proteins are the second major family of ubiquitously expressed RBPs. Twelve human SRSF proteins were described, which consist of one or two N-Terminal RRMs and a serine/arginine-rich C-terminal domain containing multiple Arg-Ser dipeptide repeats (Corbo *et al.*, 2013). SRSF proteins are essential for constitutive splicing of pre-mRNA, but also play an important role in alternative splicing, nuclear export of mature mRNA, non-sense mediated decay and translation (Das and Krainer, 2014). SRSF1 (also known as ASF/SF2) and SRSF3 (also known as SRp20) are the best characterized SRSF family members. SRSF1 contains two RRMs, whereas SRSF3 is the smallest family member with only one RRM (Richardson *et al.*, 2011). SRSF1 protein amounts are generally maintained in constant levels in normal tissues through different regulatory mechanisms. Increased protein expression of SRSF1 was described in several tumor types including mammary and NSCLC lung cancers, where it possessed oncogenic functions including enhanced EMT progression as well as increased proliferation and survival (Anczuków *et al.*, 2012; Ezponda *et al.*, 2010; Gout *et al.*, 2012). SRSF3 was also shown to be highly expressed in several cancer types including lung, breast and colon cancer cells, where it promoted cell cycle progression, proliferation and cancer cell stemness (Corbo *et al.*, 2012; Jia *et al.*, 2010). Interestingly, antagonistic functions of SRSF1 and SRSF3 were also observed during alternative splicing of *RAC1* pre-mRNA in colorectal cancer cells (see Fig 1.5) (Gonçalves *et al.*, 2009).

In addition to SRSFs and hnRNPs, several tissue type-specific splicing factors were identified. Changes in the expression ratios of these splicing factors were observed during EMT in several different cancer types, including breast and lung cancer cells (Fici *et al.*, 2017; Yang *et al.*, 2016). The epithelial splicing regulatory proteins 1 (ESRP1) and 2 (ESRP2) promote the expression of epithelial protein isoforms and will be addressed in more detail in Ch. 1.2.2.
The RNA-binding motif protein 47 (RBM47) was also shown to promote epithelial-specific splicing patterns and is frequently downregulated during EMT, which correlated with metastatic traits in breast cancer cells (Vanharanta *et al.*, 2014). The RNA-binding FOX protein 2 (RBFOX2) however, is an essential regulator of mesenchymal tissue-specific splicing and was shown to drive EMT in normal and cancerous ovarian and mammary cells by promoting the expression of mesenchymal protein isoforms (Braeutigam *et al.*, 2014; Venables *et al.*, 2013). The protein expression changes of ubiquitously expressed and tissue type-specific splicing factors during EMT is schematically illustrated in Fig. 1.2.

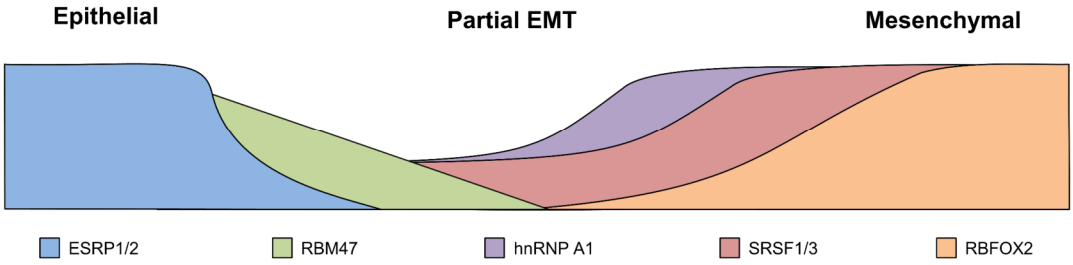

Fig. 1.2: Changes in the protein expression levels of ubiquitously expressed and tissue type-specific splicing factors during EMT in cancer. The figure schematically depicts the changes in the protein expression levels of several ubiquitously expressed and tissue type-specific splicing factors during Cancer-associated EMT. Early in the process the epithelial tissue-specific splicing factors ESRP1 and ESRP2 as well as RBM47 are downregulated, whereas the mesenchymal tissue-specific alternative splicing factor RBFOX2 is upregulated in advanced EMT. The ubiquitously expressed splicing factors hnRNP A1 and SRSF1 as well as SRSF3 are overexpressed in several cancer entities during EMT progression. This figure was altered according to Pradella *et al.* (2017) under the terms of the creative commons attribution 4.0 international license.

1.2.2 Epithelial splicing regulatory proteins and their role in carcinogenesis and metastasis

ESRP1 and ESRP2 are the best characterized tissue type-specific splicing factors, which promote the generation of epithelial-specific isoforms and were shown to be expressed exclusively in epithelial cells under normal conditions (Warzecha *et al.*, 2009b). Both, ESRP1 and ESRP2, were observed to be essential for mammalian development and proper skin barrier functions in the epidermis as knockout mice developed cleft lips and palates (Bebee *et al.*, 2015).

The paralogous proteins ESRP1 and ESRP2 show a 60 % homology in their amino acid sequences and contain three highly conserved tandem RRMs, that are 80-90 % identical between the two proteins (Dominguez *et al.*, 2010; Hayakawa *et al.*, 2017). ESRP1 and ESRP2 recognize and bind GGU/UGG-rich motifs on pre-mRNAs. The splicing outcome depends on the localization of the ESRP-binding motif within the pre-mRNA sequence. If the binding site is positioned within a downstream intron of a cassette or alternative exon, ESRPs promote exon inclusion. Binding of ESRPs to motifs within or upstream of a regulated exon leads to the out-splicing of the respective exon (Warzecha *et al.*, 2010; Yang *et al.*, 2016).

ESRP1 and ESRP2 were identified as master regulators of an extensive epithelial-specific splicing network and were shown to regulate some gene products with EMT-related functions, such as the maintenance of cell-cell and cell-matrix adhesion as well as epithelial cell polarity. Additionally, components of the MAPK pathway and proteins involved in cell motility as well as regulators and effectors of RhoGTPases are affected by ESRPs (Dittmar *et al.*, 2012; Warzecha *et al.*, 2009b; Warzecha *et al.*, 2010; Yang *et al.*, 2016). In a few select cases gene products targeted by ESRPs were shown to produce isoforms with differential and even opposing functions. Confirmed targets are the fibroblast growth receptor 2 (*FGFR2*), cluster of differentiation 44 (*CD44*) and $p120^{ctn}$ (*CTNND1*). The alternative isoforms were shown to exhibit preferred expression in epithelial or mesenchymal cells and influence EMT in many different ways (Warzecha *et al.*, 2009a; Warzecha *et al.*, 2009b).

Downregulation of ESRP1 and ESRP2 was highlighted as an obligate and general event at the onset of EMT during cancer progression (see Fig. 1.2). Low expression ratios of ESRP1 and ESRP2 were also correlated to tumor aggressiveness and a higher risk of metastasis in early breast and oral squamous cancer progression (Fici *et al.*, 2017; Ishii *et al.*, 2014). Conversely, high ESRP1 and ESRP2 protein expression levels were correlated to a favorable outcome and better overall survival in colorectal cancer patients (Deloria *et al.*, 2016). However, contradicting studies exist, which linked increased ESRP1 and ESRP2 protein expression levels to cancer progression in colorectal and breast cancers (Fagoonee *et al.*, 2017; Gökmen-Polar *et al.*, 2019). Therefore, the precise role of ESRP1 and ESRP2 in carcinogenesis remains the topic of many controversial debates and further research is necessary to fully understand the specific roles of these splicing factors in cancer progression and metastasis.

1.3 The Rho family GTPases Rac1 and Rac1b

1.3.1 RhoGTPases and cell migration

Carcinoma cells undergoing EMT gain mesenchymal traits, which include increased motility and invasion. Cell migration is a multistep process, which requires spatial regulation of Actin cytoskeleton rearrangements and cell adhesion to allow dynamic cell elongation and directed motility (Yilmaz and Christofori, 2009). Members of the Rho family of small guanosine triphosphatases (RhoGTPases) are essential players in the coordination of cell migration and invasion by regulating Actin cytoskeleton dynamics and focal adhesion complex turnover (Lawson and Ridley, 2018; Nagano *et al.*, 2012). There are twenty family members of RhoGTPases with RhoA, Rac1 and Cdc42 being the most extensively studied and best characterized representatives regarding their roles in cell migration (Lawson and Ridley, 2018). RhoA regulates the formation of Actin stress fibers and the assembly of contractile Actin-myosin filaments, which are involved in the retraction of the rear of the cell during migration. Cdc42 and Rac1 are located in the leading edge of the migrating cells. While Cdc42 regulates Actin polymerization during filopodia formation, Rac1 influences the polymerization of Actin to form lamellipodia and membrane ruffles (Raftopoulou and Hall, 2004).

1.3.2 The small RhoGTPase Rac1

The Ras-related C3 botulinum toxin substrate 1 (Rac1) is a ubiquitously expressed small G-protein and plays an important role in cytoskeleton rearrangements. Rac1 acts molecular switch regulating cell scattering, migration, invasion and metastasis. Especially at the leading edge of motile cells, Rac1 influences Actin polymerization and promotes the formation of lamellipodia and membrane ruffles (Raftopoulou and Hall, 2004). But Rac1 was also shown to be involved in signal transduction pathways, that control proliferation, the production of reactive oxygen species (ROS), cell adhesion, survival, differentiation and malignant transformation (Wertheimer *et al.*, 2012).

Rac1 proteins, like other RhoGTPases, are molecular switches that cycle between inactive, GDP-bound and active, GTP-bound states. Once activated they interact with effector proteins and thereby control signal transduction pathways important for migratory responses (Arnst *et al.*, 2017). The GDP-GTP cycle of the Rac1 and the different factors involved in regulating Rac1 activity are schematically depicted in Fig. 1.3. Guanosine nucleotide exchange factors (GEFs) interact with GDP-loaded Rac1 proteins, thereby catalyzing the release of GDP allowing the much more abundant GTP to be bound (Vetter and Wittinghofer, 2001). GTPase activating proteins (GAPs) are negative regulators of Rac1 proteins enhancing the intrinsic

GTPase activity and thereby driving the hydrolysis of GTP to GDP (Vetter and Wittinghofer, 2001). The nucleotide exchange from GDP to GTP within the Rac1 nucleotide binding pocket induces a conformational change of the two flexible switch domains, thereby stabilizing the GTP for hydrolysis within the binding pocket. This conformational change is essential for the vast majority of interactions of activated Rac1 proteins with their downstream effectors (see Fig. 1.3 and Fig. 1.4 C) (Arnst *et al.*, 2017; Vetter and Wittinghofer, 2001). Another group of factors involved in the regulation of RhoGTPase activity are Rho guanosine nucleotide dissociation inhibitors (RhoGDIs) (Garcia-Mata *et al.*, 2011). Rac1 is post-translationally modified at the C-terminal CAAX-box by incorporation of a geranyl-geranyl or less frequently a farnesyl group at cysteine residue 189. Additionally, a 16-carbon fatty acid palmitate is added at cysteine residue 178 through S-palmitoylation to increase hydrophobicity and ensure membrane localization (Bustelo *et al.*, 2012). RhoGDI exerts dual inhibitory effects as it interacts with the prenyl-group of Rac1, thereby extracting it from the plasma membrane and sequestering it in the cytoplasm (Grizot *et al.*, 2001). Additionally, the N-terminal domain of RhoGDI interacts with the switch I and II regions of the nucleotide binding pocket of the Rac1 when GDP is bound. Thereby, it inhibits GDP dissociation by stabilizing the conformation of the two switch domains (Grizot *et al.*, 2001). Dissolution of the Rac1-RhoGDI complex is essential for subsequent membrane association and GEF-mediated activation of Rac1 (Garcia-Mata *et al.*, 2011). Another important functional region of Rac1 is the C-terminal polybasic region (PBR) (see Fig. 1.4). Next to an important role in ensuring membrane localization, the positively charged PBR (PVKKRKRK) contains a nuclear localization signal (NLS), indicating possible functions of Rac1 proteins in the nucleus (Lam and Hordijk, 2013; Lanning *et al.*, 2004).

Rac1 can be activated by a wide variety of extracellular signals and stimuli, e.g. growth factors, cell-cell- and cell-matrix-mediated signaling or external stress factors. The signals are forwarded through transmembrane receptor proteins, which include tyrosine-kinase receptors (RTKs), G-protein-coupled receptors (GPCRs) and Integrin-mediated focal adhesion as well as Cadherin-mediated cell-cell adhesion (Ehrlich *et al.*, 2002; Wertheimer *et al.*, 2012). The activated receptors stimulate GEFs, which subsequently promote guanosine nucleotide exchange. GTP-bound Rac1 then influences myriads of different downstream effectors and signal transduction pathways (Marei and Malliri, 2017). Activated Rac1 regulates the spatio-temporal polymerization and branching of the Actin cytoskeleton in part through the activation of the WAVE regulatory complex and the subsequent activation of the Actin-related protein 2 and 3 complex (Arp2/3) (Chen *et al.*, 2017a). Furthermore, Rac1-GTP interacts with and

activates the p21-activated kinase 1 (PAK1), which is a key downstream effector protein of Rac1. A vast array of over 50 downstream targets of active PAK1 were described, which include the before mentioned Arp2/3 complex, the LIM kinase (LIMK) as well as several transcription factors (Baker *et al.*, 2014; Barros *et al.*, 2009). Additionally, extensive cross talks with Ras-mediated MAPK as well as PI3K signal transduction pathways were described (Imamichi *et al.*, 2005; Makrodouli *et al.*, 2011). Active Rac1 is also involved in the p38-MAPK signaling cascades during stress response (Chen *et al.*, 2018a) and regulates transcription via the Jun N-terminal kinase (JNK) and the transcription factor c-Jun (Imamichi *et al.*, 2005). Rac1 is involved in Smad-independent TGFβ signaling through the type I TGFβ receptor ALK5 (Santibáñez *et al.*, 2010). Additionally, a role of Rac1 in direct regulation of Smad proteins was described (Ungefroren *et al.*, 2011).

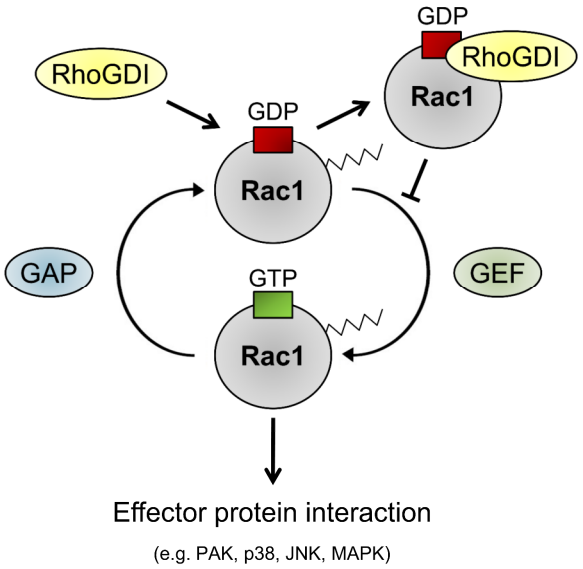

Fig. 1.3: Regulation of Rac1 activity by GEFs, GAPs and RhoGDIs. The figure schematically depicts the cycling of Rac1 between an inactive, GDP-bound and active, GTP-bound state. The guanosine nucleotide exchange factor (GEF), GTPase activating protein (GAP) and Rho guanosine nucleotide dissociation inhibitor (RhoGDI) are involved in regulating Rac1 activity and are also shown. Geranyl-geranyl group (denticulated line). This figure was altered according to Wertheimer *et al.* (2012) (license number: 4583720468400) and Lawson and Ridley (2018) (license number: 4583721453551) with permission of the respective journals.

1.3.3 The alternatively spliced Rac1 isoform Rac1b

At the end of the last century, an alternatively spliced Rac1 isoforms, termed Rac1b, was identified in colorectal cancer cells (Jordan *et al.*, 1999). Since then, it has been shown to be overexpressed in several other tumor types, including breast, pancreatic, lung and thyroid carcinomas (Faria *et al.*, 2016; Jordan *et al.*, 1999; Mehner *et al.*, 2014; Schnelzer *et al.*, 2000; Zhou *et al.*, 2013a). Rac1b differs from Rac1 only by insertion of 57 nts, which encodes the 19

amino acid alternative exon 3b. It is inserted in-frame downstream of exon 3 and lies within the 3` end of the switch II region (Jordan *et al.*, 1999) (see Fig. 1.4 A).

Rac1b was characterized as a self-activating, constitutively GTP-bound GTPase. This is due to the structural and conformational changes the insertion exon 3b confers to this isoform (Fiegen *et al.*, 2004). Specifically, the exon 3b peptide was shown to be natively unstructured in solution, thereby leading to a highly motile and more flexible switch II region in comparison to the Rac1 counterpart. Additionally, exon 3b leads to an open conformation of the switch I region independent of the nature of the bound nucleotide (see Fig. 1.4 C). As a consequence, Rac1b exhibits an accelerated nucleotide exchange rate (Fiegen *et al.*, 2004; Orlichenko *et al.*, 2010). Since GTP is much more abundant than GDP within the cytoplasm, Rac1b is rendered in a predominantly GTP-bound state (Fiegen *et al.*, 2004; Vetter and Wittinghofer, 2001). Rac1b also exhibits an impaired GTP-hydrolysis, since the switch regions cannot stabilize the GTP nucleotide for hydrolysis within the nucleotide binding pocket. This is reinforced by the weaker interaction of Rac1b with Rac-specific GAPs like IQGAP1 and β-PIX in comparison to Rac1 (Orlichenko *et al.*, 2010).

The inability of the Rac1b switch regions to adapt a closed conformation upon GTP binding explains the altered effector protein binding pattern of Rac1b (see Fig. 1.4 B). Rac1b was shown to be unable to interact PAK1, JNK or RhoGDI (Matos *et al.*, 2003; Singh *et al.*, 2004). In contrast, Rac1b was observed to interact more efficiently with $p120^{ctn}$, the receptor for activated C kinase 1 (RACK1), β-Catenin and the small GTPase GDP dissociation stimulator (SmgGDS) in comparison to Rac1 (Orlichenko *et al.*, 2010). Thereby, Rac1b regulates distinct cellular responses. Rac1b was shown to be unable to promote lamellipodia formation, but retains the ability to stimulate the NF-κB signaling pathway to the same extent as Rac1 (Matos *et al.*, 2003). Moreover, Rac1b drastically increases cell survival in the presence of only minimal growth stimuli by initiating anti-apoptotic signaling and drives cell cycle progression by stimulating the NF-κB-mediated expression and accumulation of cyclin-D1 (Faria *et al.*, 2017; Matos and Jordan, 2005). Due to the NLS within the C-terminal PBR, nuclear Rac1b was shown to influence Wnt3A independent Wnt target gene transcription as transcriptional co-activator (Esufali *et al.*, 2007; Pethe *et al.*, 2011).

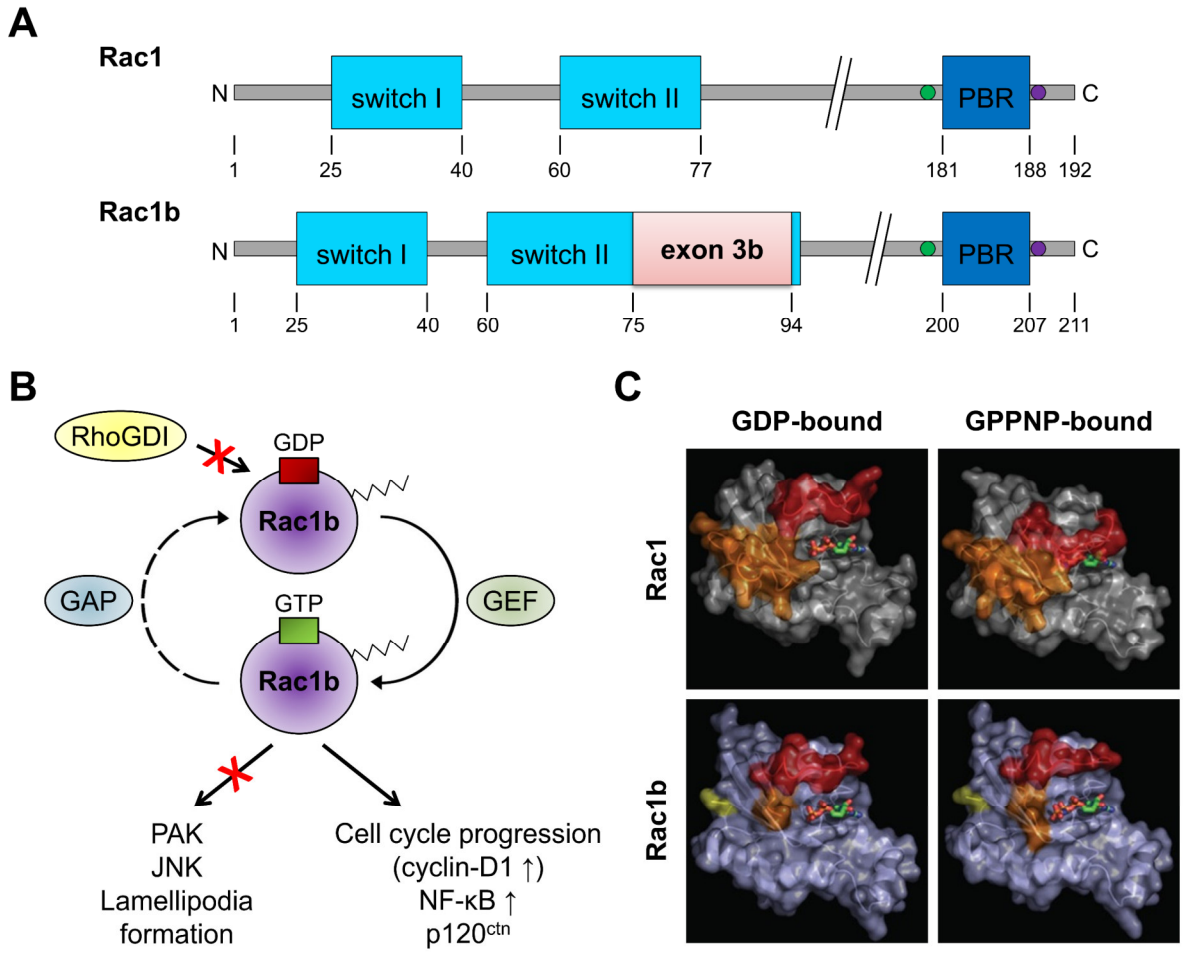

Fig. 1.4: Structural and functional differences between Rac1 and Rac1b. (**A**) Linear presentation of the domain structure of Rac1 (top) and Rac1b (bottom) including the functional switch I and II regions (light blue), the C-terminal polybasic region (PBR, dark blue) as well as the cysteine residues important for post-translational S-palmitoylation (green dot) and geranyl-geranylation (purple dot). Exon 3b (light red). (**B**) Schematic depiction of Rac1b GDP-GTP cycling. This figure exemplifies altered regulator and effector protein binding patterns as well as distinct cellular responses in comparison to Rac1 (compare with Fig. 1.3). This figure section was altered according to Fiegen *et al.* (2004) with permission of the *Journal of Biological Chemistry* (license number: 4583740485396). (**C**) Depicted are the nucleotide-dependent conformational changes of the switch I (red) and switch II regions (orange) of Rac1 (top panel) and Rac1b (bottom panel). GPPNP is an uncleavable GTP analog. This figure section was taken from Orlichenko *et al.* (2010) with permission of the *Journal of Biological Chemistry* (license number: 4576460598836).

The generation of Rac1 or Rac1b isoforms depends on different splicing factors, which regulate exon 3b out-splicing or retention during *RAC1* pre-mRNA maturation (see Fig. 1.5). ESRP1, SRSF3 and hnRNP A1 have been shown to promote exon 3b out-splicing, whereas SRSF1 promotes retention of the alternative exon (Gonçalves *et al.*, 2009; Ishii *et al.*, 2014; Pelisch *et al.*, 2012).

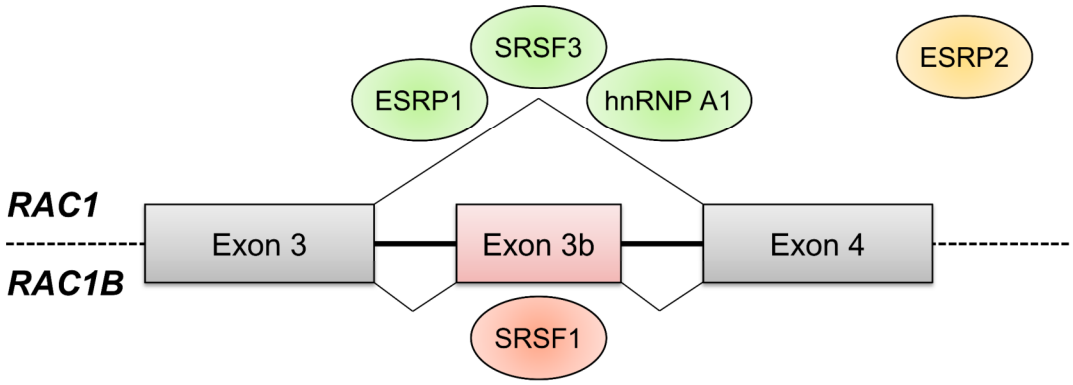

Fig. 1.5: Splicing factors involved in alternative *RAC1* pre-mRNA splicing. Different splicing enhancers (red) and inhibitors (green) regulate exon 3b retention or out-splicing during *RAC1* pre-mRNA maturation. The splicing factors ESRP1, SRSF3 and hnRNP A1 promote exon 3b out-splicing, whereas SRSF1 regulates exon 3b retention. A role of ESRP2 in *RAC1* pre-mRNA splicing was not described.

1.3.4 Differential roles of Rac1 and Rac1b in cancer progression and EMT

Aberrant Rac1 signaling plays a pivotal role in cancer progression and metastasis, although functionally relevant Rac1 mutations are very rarely found in human tumors (Schnelzer *et al.*, 2000). Instead, the overexpression and hyperactivation of Rac1 proteins are more commonly observed and were shown to drive tumorigenic processes and promote carcinoma cell motility as well as EMT in several tumor types, including colorectal, lung and pancreatic cancer cells (Espina *et al.*, 2008; Hage *et al.*, 2009; Shen *et al.*, 2014). In pancreatic cancer, Rac1 overexpression is involved in early Actin rearrangements during development of neoplastic lesions, whereas a knockdown of Rac1 reduced tumor formation and prolonged survival (Heid *et al.*, 2011). Rac1 hyperactivation in cancer is most commonly caused by deregulation of upstream factors, for example Rac-GEFs. Enhanced activity of phosphatidylinositol (3,4,5)-triphosphate-dependent Rac exchanger 1 (P-Rex1) was linked to increased cell migration and aggressive behavior in human breast cancer cells (Montero *et al.*, 2011). The T lymphoma invasion and metastasis-inducing factor 1 (Tiam1) was shown to be overexpressed in lung adenocarcinomas and colorectal cancer cells and promoted EMT progression and tumor cell invasion via elevated Rac1 activity (Izumi *et al.*, 2019; Zhu *et al.*, 2019).

Rac1b is overexpressed in several tumor types. In metastatic colorectal cancer patients, Rac1b overexpression correlated with a poor prognosis as it promoted anti-apoptotic responses (Alonso-Espinaco *et al.*, 2014; Henriques *et al.*, 2015; Matos *et al.*, 2008). Additionally, enhanced Rac1b expression was identified as a driving-force during K-Ras-induced lung tumorigenesis and linked to MMP-induced EMT in breast, lung and pancreatic cancer (Cichon *et al.*, 2015; Mehner *et al.*, 2014; Stallings-Mann *et al.*, 2012). Interestingly, Rac1b was also

shown to antagonize Rac1 activity. Rac1b interfered with platelet-derived growth factor (PDGF)-dependent Rac1 activity as it decreased the amount of membrane-bound Rac1 in a competitive manner (Nimnual *et al.*, 2010). Together with our collaboration partner, the group of Prof. Dr. Hendrik Ungefroren of the university hospital in Lübeck, our group identified antagonistic activities of Rac1 and Rac1b in TGFβ-induced EMT and migration in pancreatic carcinoma cells (Ungefroren *et al.*, 2013). More recently, the group of Ungefroren could also confirm this observation in breast carcinoma cells (Melzer *et al.*, 2017). Nevertheless, the precise role Rac1b in carcinogenesis and, moreover, the functional differences between Rac1 and Rac1b are controversially debated and remain to be fully elucidated.

1.4 Aim of this work

The aim of this work was to specify functional differences between the two GTPase isoforms Rac1 and Rac1b and to analyze potential differential roles in tumor cell migration as well as EMT in pancreatic and lung carcinoma cells. Rac1b was characterized as a constitutively active GTPase isoform of Rac1 and shown to be overexpressed in various tumor types (Fiegen *et al.*, 2004). Initial experiments of this work aimed to elucidate mRNA and protein expression levels of Rac1 and Rac1b in different pancreatic and lung cell lines. Thereby, cells with high Rac1b amounts were identified and further characterized by analyzing the EMT status and invasive capacity. Since the presence of RhoGTPases within the plasma membrane or cytoplasm depend on their activity (Garcia-Mata *et al.*, 2011), another aim of this work was to characterize differences in subcellular localization of Rac1 and Rac1b. To further elucidate the dependency of Rac1 and Rac1b activity on the subcellular localization, not only endogenous and ectopically expressed wildtype proteins, but also constitutively active and dominant negative mutants were examined. Since both proteins contain a NLS within their C-terminal PBR (Lam and Hordijk, 2013), possible differences in the nuclear localization of Rac1 and Rac1b were addressed. The chorioallantoic membrane (CAM) invasion assay was re-established in the group as a part of this work to analyze carcinoma cell invasion *in vivo*. This assay was applied aiming to identify putative effects of different Rac1 and Rac1b protein expression levels on the invasive potential of various carcinoma cells.

Another aim of this work was to analyze the splicing factors involved in *RAC1* pre-mRNA splicing (see Fig. 1.5). Thereby, putative cross talks between these splicing factors and Rac1 isoforms as well as possible roles in EMT were supposed to be examined. Moreover, the analysis of these proteins after treating lung and pancreatic carcinoma cells with TGFβ1 aimed to uncover further putative functions during EMT.

2 Material and methods

2.1 Material

2.1.1 Chemicals

All standard chemicals, which were used in this work, but are not listed below, were purchased from the following companies in analytical quality: AppliChem (Darmstadt), Biozym (Hessisch-Oldendorf), Capricorn (Ebsdorfergrund), Carl Roth (Karlsruhe), Merck Millipore (Darmstadt), Serva Electrophoresis (Heidelberg), Sigma-Aldrich (Taufkirchen), Thermo Fisher Scientific (Langenselbold) and VWR (Darmstadt).

Tab. 2.1: Chemicals

Chemical	Supplier
30% Acrylamide (Rotiphorese® Gel A)	Carl Roth, Karlsruhe
2% Bisacrylamide (Rotiphorese® Gel B)	Carl Roth, Karlsruhe
Bovine serum albumin, Fraction V (pH 7,0)	Serva Electrophoresis, Heidelberg
Diethyl pyrocarbonate (DEPC) BioChemica	AppliChem, Darmstadt
Dulbecco's Modified Eagle medium (DMEM, high glucose)	Thermo Fisher Scientific, Langenselbold
Fetal bovine serum (FCS)	Capricorn, Ebsdorfergrund
Keratinocyte serum-free medium (1 x)	Thermo Fisher Scientific, Langenselbold
Mayer's hemalum solution (for microscopy)	Merck Millipore, Darmstadt
Opti-MEM™ I reduced serum media	Thermo Fisher Scientific, Langenselbold
Paraplast Plus® (for tissue embedding)	Sigma-Aldrich, Taufkirchen
Powdered milk (blotting grade)	Carl Roth, Karlsruhe
Roswell Park Memorial Institute-1640 medium (RPMI-1640)	Thermo Fisher Scientific, Langenselbold
Roti®-Histokitt II (synthetic mounting solution)	Carl Roth, Karlsruhe
Roti®-Histol (for histology)	Carl Roth, Karlsruhe
Shandon Eosin Y (alcoholic)	Thermo Fisher Scientific, Langenselbold
SuperSignal™ West Pico PLUS chemiluminescent substrate	Thermo Fisher Scientific, Langenselbold
0,05% Trypsin-EDTA (1x), phenol red	Thermo Fisher Scientific, Langenselbold

2.1.2 Consumables

All consumables, which were used in this work, but are not listed below, were purchased from the current supplier in standard quality.

Tab. 2.2: Consumables.

Consumable	Supplier
Adhesive clear PCR seal sheets	Biozym, Hessisch-Oldendorf
Durapore™ artificial silk plaster tape (9,2 m x 2,5 cm)	3M Science, Neuss
Cell culture dishes (6 cm, 10 cm)	Sarstedt, Nümbrecht
Histosette® II tissue processing cassettes and lids	VWR, Darmstadt
Millex-GS sterile filter (0,22 µm)	Merck Millipore, Darmstadt
Microtome blade R35 pfm (stainless steel)	Feather Safety Razor, Osaka, JPN
PCR Plate Multiply®, 96 wells	Sarstedt, Nümbrecht
Protran BA 85 nitrocellulose transfer membrane	GE Healthcare, Freiburg
Silicone mat (thickness 0,5 mm, transparent)	Karl Späh, Scheer
SuperFrost Ultra Plus® adhesive microscopic slides	Carl-Roth, Karlsruhe
TC plate (6-well, 12-well)	Sarstedt, Nümbrecht
Whatman® chromatography paper	GE Healthcare, Freiburg

2.1.3 Devices and laboratory instruments

Tab. 2.3: Devices and laboratory instruments.

Device	Supplier
BlueMarine™ 100 horizontal electrophoresis chamber	Serva Electrophoresis, Heidelberg
Cold Plate EG1150 C (for tissue embedding)	Leica Mikrosysteme, Wetzlar
Cooling centrifuge Heraeus Megafuge 16R	Thermo Fisher Scientific, Langenselbold
DFC310 FX (microscopic light source)	Leica Mikrosysteme, Wetzlar
ELx800 absorbance microplate reader	Biotek, Bad Friedrichshall
Fully enclosed tissue processor ASP300S	Leica Biosystems, Wetzlar
Fusion SL4-3500.WL chemiluminescence imaging system	Vilber Lourmat, Eberhardzell
Heated paraffin embedding module EG1140H	Leica Biosystems, Wetzlar

HeatSealer S100 and plate adapter	Eppendorf, Hamburg
Inverse fluorescence microscope Olympus IX81	Olympus, Hamburg
Inverse light microscope Axiovert 25	Carl Zeiss, Wetzlar
King Craft® power drill KBM 40F	Aldi Süd, Mühlheim a. d. Ruhr
Mastercycler® personal	Eppendorf, Hamburg
Microm HM 355S microtome	Thermo Fisher Scientific, Langenselbold
Mini blotting chamber B2157	Sigma-Aldrich, Taufkirchen
Nanodrop 1000 spectrophotometer	Thermo Fisher Scientific, Langenselbold
Optima MAX-E ultracentrifuge (100.000 rpm)	Beckman-Coulter, Krefeld
LI-COR Odyssey CLx	LI-COR Bioscience, Bad Homburg
LI-COR Odyssey Sa	LI-COR Bioscience, Bad Homburg
Reflected light microscope DM750	Leica Mikrosysteme, Wetzlar
Reflected light microscope DMLA	Leica Mikrosysteme, Wetzlar
SensoQuest Labcycler Basic	SensoQuest, Göttingen
Slide staining set	Medite, Burgdorf
Sterile laminar flow cabinet	Integra Biosciences, Fernwald
Stratagene Mx3005P Real time PCR Cycler	Agilent Technologies, Frankfurt am Main
Thermomixer® compact	Eppendorf, Hamburg
UV-Transilluminator GeneFlash	Syngene Bio Imaging, Cambridge, UK
Vertical electrophoresis chamber (10 x 8 cm)	Sigma-Aldrich, Taufkirchen
X-Cite 120PC Q (fluorescent light source)	Olympus, Hamburg

2.1.4 Software

Tab. 2.4: Software.

Software (Version)	Developer
CellSens Dimension (1.6)	Olympus, Hamburg
Citavi (6.3.0)	Swiss Academic Software, Wädenswil, CH
Fiji (1.52i)	Schindelin *et al.* (2012)
Fusion (15.18)	Vilber Lormat, Eberhardzell
Gen5 (2.00)	Biotek, Bad Friedrichshall
GraphPad Prism5 (5.03)	GraphPad Software, La Jolla, CA, USA
Image Studio Lite (5.2)	LI-COR Bioscience, Bad Homburg
Inkscape (0.48)	Inkscape, Boston, MA, USA

Leica QWin (3)	Leica Mikrosysteme, Wetzlar
Microsoft Excel (2016)	Microsoft, Unterschleißheim
Microsoft Word (2016)	Microsoft, Unterschleißheim
Microsoft PowerPoint (2016)	Microsoft, Unterschleißheim
MxPro qPCR Software (4.10)	Agilent Technologies, Frankfurt am Main
NanoDrop 1000 (3.8.1)	PeqLab, Erlangen
Vector NTI (10)	Thermo Fisher Scientific, Langenselbold

2.1.5 Enzymes, markers, kits and reagents for molecular biology

Tab. 2.5: Enzymes, markers, kits and reagents for molecular biology.

Enzymes, markers, kits and reagents	Origin (Cat. No.)
1 kb DNA ladder	New England Biolabs, Frankfurt am Main (#N3232)
100 bp DNA ladder	New England Biolabs, Frankfurt am Main (#N3231)
Alkaline phosphatase, calf intestinal (CIP)	New England Biolabs, Frankfurt am Main (#M0290)
CloneJET PCR Cloning Kit	Thermo Fisher Scientific, Langenselbold (#K1231)
DNA-spin™ Plasmid DNA Purification Kit	iNtRON Biotechnology, Seongnam, KOR (#17096)
DNA-midi™ GT Plasmid DNA Extraction Kit (Gravity)	iNtRON Biotechnology, Seongnam, KOR (#17254)
Deoxyribonucleotides (dNTPs) (10 mM each)	Sigma-Aldrich, Taufkirchen (#D7295)
Hot Start *Taq* 2 x Master Mix	New England Biolabs, Frankfurt am Main (#M0496)
High range molecular weight marker	Sigma-Aldrich, Taufkirchen (#S8320)
my-Budget 5 x Hot-Start *Taq* PCR-Mix (ready to load)	Bio-Budget, Krefeld (#80-64020000-75)
NucleoBond® Finalizer	Macherey-Nagel, Düren (#740519.20)
NucleoSpin® Gel and PCR Clean-Up Kit	Macherey-Nagel, Düren (#740609)
Oligo $d(T)_{23}$ VN random primers (50 µM)	New England Biolabs, Frankfurt am Main (#S1327)
PageRuler Prestained protein ladder	Thermo Fisher Scientific, Langenselbold (#26617)
ProtoScript® II Reverse Transcriptase	New England Biolabs, Frankfurt am Main (#M0368)

QuikChange II Site-Directed Mutagenesis Kit	Agilent Technologies, Frankfurt am Main (#200524)
Q5™ Hot Start High-Fidelity Polymerase	New England Biolabs, Frankfurt am Main (#M0493)
Restriction enzymes and buffers	New England Biolabs, Frankfurt am Main (#diverse)
RNase-free DNase Set	Qiagen, Hilden (#79254)
RNeasy Plus Mini Kit	Qiagen, Hilden (#74106)
SensiMix™ SYBR No-ROX Kit	Bioline, Luckenwalde (#QT650)
T4 DNA ligase and buffer	New England Biolabs, Frankfurt am Main (#M0202)

2.1.6 Transfection reagents

Tab. 2.6: Transfection reagents.

Transfection reagent	Origin (Cat. No.)
Lipofectamine™ RNAiMAX	Thermo Fisher Scientific, Langenselbold (#13778075)
Lipofectamine™ LTX w. PLUS™ Reagent	Thermo Fisher Scientific, Langenselbold (#15338100)
Polyetherimide (PEI)	Sigma-Aldrich, Taufkirchen (#700193)

2.1.7 Plasmids

The plasmids listed below were generated in the course of this work, if not indicated otherwise**.**

Tab. 2.7: Plasmids. Abbreviation: HA (human influenza hemagglutinin), wt (wildtype).

Plasmid	Reference
pcDNA3.1(+)	Thermo Fisher Scientific, Langenselbold
pcDNA3.1(+)/HA-ESRP1 #6	this work
pcDNA3.1(+)/HA-ESRP2 #4	this work
pCGN/HA	Tanaka and Herr (1990)
pCGN/HA-Rac1 wt	provided by Prof. Dr. Klaudia Giehl
pCGN/HA-Rac1 V12 #4	this work
pCGN/HA-Rac1 N17 #5	this work
pCGN/HA-Rac1b wt	Ungefroren *et al.* (2013)

pCGN/HA-Rac1b V12 #15	this work
pCGN/HA-Rac1b N17 #3	this work
pEGFP-C1 and -C3	Clonetech, Saint-Germain-en-Laye, FRA
pEGFP-C1/Rac1 wt	Dreissigacker *et al.* (2006)
pEGFP-C1/Rac1b wt	provided by Prof. Dr. Klaudia Giehl
pGEM/ESRP1	Sino Biological, Wayne, PA, USA
pJET1.2/Blunt	Thermo Fisher Scientific, Langenselbold
pJET1.2/ESRP1 (*BamH*I/*Not*I) #3	this work
pJET1.2/ESRP2 (*BamH*I^2) #3	this work
pJET1.2/ESRP2 (*BamH*I/*Xba*I) #6	this work
pORF/ESRP2	Applied Biological Materials, Richmond, BC, CAN

2.1.8 Oligonucleotides

All primers were designed in the course of this work and purchased from Biomers.net GmbH (Ulm), if not indicated otherwise. Standard RT-PCR oligonucleotides, which were not published, but are frequently used in our group, were kindly provided by Prof. Dr. Andre Menke. The appropriate primers were marked.

2.1.8.1 PCR primers for cloning, sequencing and site-directed *in vitro* mutagenesis

Tab. 2.8: PCR primers for cloning. Underlined: start or stop codon; italic: restriction sites.

Oligonucleotide	Sequence (5'-3')
ESRP1_*BamH*I-FWD	GAA *GGA TCC* ATG ACG GCC TCT C
ESRP1_*Not*I-REV	GAA *GCG GCC GC*T TAA ATA CAA ACC
ESRP2_*BamH*I-FWD	GAA *GGA TCC* ATG ACT CCG CCG
ESRP2_*BamH*I-REV	GAA *GGA TCC* CTA CAA ACA CAC CCA TTC
ESRP2_*Xba*I-REV	GAA *TCT AGA* CTA CAA ACA CAC CCA TTC CTT G

Tab. 2.9: Sequencing primers.

Oligonucleotide	Sequence (5'-3')
ESRP1_Middle	TGG CAG TCT TCA GAT CAA GAT ATT
ESRP2_Middle	TCA AAG GGC TCA ACG TGG

Tab. 2.10: PCR primers for site-directed *in vitro* mutagenesis. Underlined: mutated codon 12 or 17.

Oligonucleotide	Sequence (5'-3')
Rac1(V12)-FWD	GTG GTG GGA GAC GTA GCT GTA GGT AAA AC
Rac1(V12)-REV	GTT TTA CCT ACA GCT ACG TCT CCC ACC AC
Rac1(N17)-FWD	GGA GCT GTA GGT AAA AAT TGC CTA CTG ATC AG
Rac1(N17)-REV	CTG ATC AGT AGG CAA TTT TTA CCT ACA GCT CC

2.1.8.2 Primers for RT-PCR

Tab. 2.11: PCR primers for semiquantitative RT-PCR.

Oligonucleotide	Sequence (5'-3')	Reference
Actin-For Actin-Back	GAC TAC CTC ATG AAG ATC CT GCG GAT GTC CAC GTC ACA CT	Nuessle *et al.* (2011)
E-Cad-for2 E-Cad Kl-Ba	ACC ACC TTA GAG GTC AGC GT CCG CCT CTC TCG AGT CCC CT	Prof. Dr. Andre Menke, Gießen
ESRP1_sq-FWD ESRP1_sq-REV	GTT CGC CAC AGA TAT TCG TA ATGGTAACTTACATGGCGG	This work
ESRP2_sq-FWD ESRP2_sq-REV	GAT GTG GTG GAC AGT GAG TGT CGC TTT ATA CAC CTC AA	This work
hnRNPA1-sq-FWD hnRNPA1-sq-REV	TGC CTT TGT AAC CTT TGA CGT GT ACT GTG CTT GGC TGA GTT CAC	Guo *et al.* (2013)
N-Cad-sense N-Cad-antisense	TAA AAT ATG ATG AAG AAG GTG GAG G TGA GGA ATT AAG GGA GCT CA	Prof. Dr. Andre Menke, Gießen
Rac1b qFor1 Rac1b FL-Back	TGA ATC TGG GCT TAT GGG ATA CA TTA CAA CAG CAG GCA TTT TCT CTT C	Prof. Dr. Andre Menke, Gießen
SRSF1_sq-FWD SRSF1_sq-REV	GAG ATG GCA CTG GTG TCG TG TGC GAC TCC TGC TGT TGC TTC	Guo *et al.* (2013)
SRSF3_q2-FWD SRSF3_q2-REV	AAC AAG ACG GAA TTG GAA CG TGG GCC ACG ATT TCT ACT TC	Gonçalves *et al.* (2009)
Vim-For Vim-Back	TGG CAG GTC TTG ACC TTG AA GGT CAT CGT GAT GCT GAG AA	Prof. Dr. Andre Menke, Gießen

Tab. 2.12: PCR primers for quantitative RT-PCR.

Oligonucleotide	Sequence (5'-3')	Reference (Cat. No.)
Hs_ACTB_1_SG (QuantiTect®)	Sequences not available	Qiagen, Hilden (#QT00095431)
Hs_B2M_1_SG (QuantiTect®)	Sequences not available	Qiagen, Hilden (#QT00088935)
Hs_CDH1_1_SG (QuantiTect®)	Sequences not available	Qiagen, Hilden (#QT00080143)
Hs_ESRP1_1_SG (QuantiTect®)	Sequences not available	Qiagen, Hilden (#QT00085694)
Hs_ESRP2_1_SG (QuantiTect®)	Sequences not available	Qiagen, Hilden (#QT00066066)
Hs_GAPDH_1_SG (QuantiTect®)	Sequences not available	Qiagen, Hilden (#QT00079247)
Rac1b qFor1 Rac1b qBack1	TGA ATC TGG GCT TAT GGG ATA CA GGT TAT ATC CTT ACC GTA CGT TTC TCC	Prof. Dr. Andre Menke, Gießen
RPLP0-qPCR-fp RPLP0-qPCR-rp	GTC GGA GGA GTC GGA CGA G GCC TTT ATT TCC TTG TTT GTC AAA	Prof. Dr. Andre Menke, Gießen
Hs_SNAI1_1_SG (QuantiTect®)	Sequences not available	Qiagen, Hilden (#QT00010010)
Hs_SNAI2_1_SG (QuantiTect®)	Sequences not available	Qiagen, Hilden (#QT00044128)
Hs_TWIST1_1_SG (QuantiTect®)	Sequences not available	Qiagen, Hilden (#QT00011956)
Hs_VIM_1_SG (QuantiTect®)	Sequences not available	Qiagen, Hilden (#QT00095795)
Hs_ZEB1_1_SG (QuantiTect®)	Sequences not available	Qiagen, Hilden (#QT00020972)
Hs_ZEB2_1_SG (QuantiTect®)	Sequences not available	Qiagen, Hilden (#QT00008554)

2.1.8.3 siRNAs for gene silencing

Tab. 2.13: siRNAs for gene silencing.

Oligonucleotide	Target sequence (5'-3')	Reference (Cat. No.)
siESRP1_SMARTpool (ON-TARGETplus) (4 siRNAs)	CCC GGU AUA UUG AGG UUU A CAA UGA UUU CAG AGC CUU A GGA CAG CAU UGC CCU AUU A AGU CAG GGC ACG AGG UUU A	Dharmacon, München (#L-020672-01-0005)
siESRP2_SMARTpool (ON-TARGETplus) (4 siRNAs)	CCA CAU GGG CGU CCG CUA U ACA AGG GCA UGC UGG GUA A GAC UUA AUC CUC CUA GUU U AGG AAU GGG UGU GUU UGU A	Dharmacon, München (#L-014523-00-0005)
Non-targeting Pool (ON-TARGETplus) (4 siRNAs)	UGG UUU ACA UGU CGA CUA A UGG UUU ACA UGU UGU GUG A UGG UUU ACA UGU UUU CUG A UGG UUU ACA UGU UUU CCU A	Dharmacon, München (#D-001810-10-05)
siRAC1_SMARTpool (ON-TARGETplus) (4 siRNAs)	GUG AUU UCA UAG CGA GUU U GUA GUU CUC AGA UGC GUA A AUG AAA GUG UCA CGG GUA A GAA CUG CUA UUU CCU CUA A	Dharmacon, München (#L-003560-00-0005)
Hs_RAC1_6_HP	AUG CAU UUC CUG GAG AAU AUA	Qiagen, Hilden (#SI02655051)
Rac1-specific siRNA	GCA AAC AGA UGU GUU CUU ATT	Melzer *et al.* (2017)
Rac1b-si1A	CAG UUG GAG AAA CGU ACG GTT	Qiagen, Hilden (#1027423)
Rac1b-si2B	CGU ACG GUA AGG AUA UAA CTT	Ungefroren *et al.* (2013)

2.1.9 Prokaryotic and eukaryotic cells

2.1.9.1 *Escherichia coli* strains

OneShot TOP10 *E. coli* Thermo Fisher Scientific, Langenselbold

2.1.9.2 Eukaryotic cell lines

Tab. 2.14: Eukaryotic cell lines. (1) American tissue culture collection (ATCC), (2) German collection of microorganisms and cell cultures (DSMZ). Abbreviations: NSCLC (Non-small cell lung cancer).

Organ of origin	Cell line	Tumor type and properties	Reference
Pancreas	BxPC-3	Adenocarcinoma	CRL-1687™ (1)
	Capan-1	Adenocarcinoma, metastasis (liver)	HTB-79™ (1)
	Capan-2	Adenocarcinoma	HTB-80™ (1)
	Colo357	Adenocarcinoma, metastasis (lymph node)	Morgan *et al.* (1980)
	H6c7	Non tumorigenic, immortalized pancreatic duct epithelial cells	Radulovich *et al.* (2008)
	MIA PaCa-2	Carcinoma	CRL-1420™ (1)
	PANC-1	Epithelioid carcinoma	CRL-1469™ (1)
Lung	A549	Carcinoma	CCL-185™ (1)
	Colo699	Adenocarcinoma, metastasis (pleural effusion)	ACC 196 (2)
	HCC44	Carcinoma (NSCLC)	ACC 534 (2)
	HTB-55	Adenocarcinoma, metastasis (pleural effusion)	HTB-55™ (1)
	H1299	Carcinoma (NSCLC), metastasis (lymph node)	CRL-5803™ (1)
	H2122	Adenocarcinoma (NSCLC), metastasis (pleural effusion)	CRL-5985™ (1)
	H23	Adenocarcinoma (NSCLC)	CRL-5800™ (1)
	H358	Bronchioalveolar carcinoma (NSCLC), metastasis (alveolus)	CRL-5807™ (1)
Kidney	HEK293	Embryonic kidney cells	CRL-1573™ (1)
Mouse	NIH/3T3	Embryonic mouse fibroblast cells	CRL-1658™ (1)

Tab. 2.15: Stably expressing cell clones. All stably expressing H23 cell lines were generated by Prof. Dr. Andre Menke and kindly provided for this work.

Stably expressing cell clone	Plasmid
H23/EGFP A3	pEGFP-C1
H23/EGFP-Rac1 D1	pEGFP-C1/Rac1
H23/EGFP-Rac1 D2	pEGFP-C1/Rac1
H23/EGFP-Rac1b B1	pEGFP-C1/Rac1b
H23/EGFP-Rac1b B3	pEGFP-C1/Rac1b

2.1.10 Antibodies

2.1.10.1 Primary antibodies

Tab. 2.16: Primary antibodies. Buffers: (1) = 1 x TBS, (2) = 3 % BSA in 1 x TBS/T, (3) 5 % powdered milk in 1 x TBS. Abbreviations: Bl. (blocking), kDa (kilodalton), mAb (monoclonal), ms (mouse), MW (molecular weight), pAb (polyconal), rb (rabbit).

Antibody (Clone)	Dilution (buffer)	Bl.	MW [kDa]	Species	Origin (Cat. No.)
α-Tubulin (B-5-1-2)	1:5.000 in (1)	(3)	50,1	ms, mAb	Sigma-Aldrich, Taufkirchen (#T5198)
β-Actin (AC-15)	1:4.000 in (1)	(3)	42,0	ms, mAb	Sigma-Aldrich, Taufkirchen (#A5441)
Caveolin	1:3.000 in (1)	(3)	20,5	rb, pAb	Becton Dickinson, Heidelberg (#610059)
E-Cadherin (36)	1:4.000 in (2)	(3)	97,5	ms, pAb	Becton Dickinson, Heidelberg (#610182)
E-Cadherin (24E10)	1:5.000 in (2)	(3)	97,5	rb, mAb	Cell Signaling Technology, Frankfurt am Main (#3195S)
ESRP1	1:1.000 in (2)	(3)	75,6	rb, pAb	Thermo Fisher Scientific, Langenselbold (#PA5-25833)
ESRP2	1:1.000 in (2)	(3)	77,4	rb, pAb	Thermo Fisher Scientific, Langenselbold (#PA5-21110)
GAPDH	1:5.000 in (1)	(3)	35,9	rb, pAb	Rockland, Limerick, PA, USA (#600-401-A33)
GFP (7.1 and 13.1)	1:1.000 in (1)	(3)	26,9	ms, mAb	Roche, Mannheim (#11 814 460 001)
GFP-HRP (GG4-2C2.12.10)	1:3.000 in (1)	(3)	26,9	ms, mAb	Miltenyi, Bergisch Gladbach (#130-091-833)
HA-tag (12CA5)	1:1.000 in (2)	(3)	-	ms, mAb	Roche, Mannheim (#11 583 816 001)
HA-tag-HRP (GG8-1F3.3.1)	1:2.000 in (1)	(3)	-	ms, mAb	Miltenyi, Bergisch Gladbach (#130-091-972)
hnRNP A1 (9H10)	1:2.000 in (2)	(3)	38,7 / 34,2	ms, mAb	Sigma-Aldrich, Taufkirchen (#R4528)
Lamin A/C	1:2.000 in (2)	(3)	74,1 / 65,1	rb, pAb	Cell Signaling Technology, Frankfurt am Main (#2032)
N-Cadherin (32)	1:2.000 in (2)	(3)	99,8	ms, mAb	Becton Dickinson, Heidelberg (#610920)
N-Cadherin	1:500 in (2)	(3)	99,8	rb, pAb	Takara Bio Inc., Kusatsu, JPN (#M 142)
$p120^{ctn}$ (S-19)	1:1.000 in (2)	(3)	65,6 - 108,2	rb, pAb	Santa Cruz Biotechnology, Heidelberg (#sc-1101)
Rac1 (102)	1:1.000 in (2)	(3)	21,6	ms, mAb	Becton Dickinson, Heidelberg (#610650)

Rac1b	1:2.000 in (2)	(3)	23,6	rb, pAb	Merck Millipore, Darmstadt (#09-271)
RhoGDIα (K21)	1:1.000 in (1)	(3)	23,2	rb, pAb	Santa Cruz Biotechnology, Heidelberg (#sc-359)
RhoGDIα (G-2)	1:1.000 in (1)	(3)	23,2	ms, mAb	Santa Cruz Biotechnology, Heidelberg (#sc-373724)
Snail	1:1.000 in (2)	(3)	29,1	rb, pAb	Abcam, Cambridge, UK (#ab17732)
Snail (C15D3)	1:1.000 in (2)	(3)	29,1	rb, mAb	Cell Signaling Technology, Frankfurt am Main (#3879)
Vimentin XP® (D21H3)	1:1.000 in (2)	(3)	53,7	rb, mAb	Cell Signaling Technology, Frankfurt am Main (#5741)
Vimentin (V9)	1:500 in (2)	(3)	53,7	ms, mAb	Sigma-Aldrich, Taufkirchen (#V6630)

2.1.10.2 Secondary antibodies

Tab. 2.17: Secondary antibodies for western blotting. All secondary antibodies were diluted in 1 x TBS buffer. Abbreviations: CF (cyanine-based fluorescent dye), gt (goat), hr (horse), HRP (horseradish peroxidase), H+L (heavy and light chain), pAb (polyclonal).

Antibody	Dilution	Species	Origin (Cat. No.)
Anti-mouse IgG (H+L), CF™ 680	1:150.000	gt, pAb	Biotrend, Köln (#20065)
Anti-mouse IgG (H+L), CF™ 770	1:150.000	gt, pAb	Biotrend, Köln (#20077)
Anti-rabbit IgG (H+L), CF™ 680	1:150.000	gt, pAb	Biotrend, Köln (#20067)
Anti-rabbit IgG (H+L), CF™ 770	1:150.000	gt, pAb	Biotrend, Köln (#20078)
Anti-mouse IgG, HRP-linked	1:5.000	hr, pAb	New England Biolabs, Frankfurt am Main (#7076)
Anti-rabbit IgG, HRP-linked	1:5.000	gt, pAb	New England Biolabs, Frankfurt am Main (#7074)

Tab. 2.18: Secondary antibodies for immunofluorescent staining. All secondary antibodies were diluted in 0,3 % BSA in 1 x CMF-PBS buffer. Abbreviations: gt (goat), HRP (horseradish peroxidase), H+L (heavy and light chain), pAb (polyclonal).

Antibody	Dilution	Species	Origin (Cat. No.)
Anti-mouse IgG (H+L), Cy3-linked	1:1.000	gt, pAb	Dianova, Hamburg (#115-165-003)
Anti-mouse IgG (H+L), AlexaFluor® 488-linked	1:1.000	gt, pAb	Thermo Fisher Scientific, Langenselbold (#A-11001)
Anti-rabbit IgG (H+L), Cy3-linked	1:1.000	gt, pAb	Dianova, Hamburg (#111-166-045)
Anti-rabbit IgG (H+L), AlexaFluor® 488-linked	1:1.000	gt, pAb	Thermo Fisher Scientific, Langenselbold (#A-11008)

2.1.11 Growth factors

Tab. 2.19: Growth factors.

Growth factor	Working concentration and buffer	Origin (Cat. No.)
Human epidermal growth factor (EGF)	5 ng/ml in ddH_2O	PeproTech, Hamburg (#AF-100-15)
Human transforming growth factor β1 (TGFβ1)	10 ng/ml in ddH_2O	PeproTech, Hamburg (#100-21)

2.2 Methods

2.2.1 Microbiological methods

2.2.1.1 Cultivation of *Escherichia coli* bacteria

E. coli bacteria were cultivated in sterile Lysogeny-Broth (LB) medium. Bacterial cultures on LB agar plates were incubated at 37 °C, whereas liquid cultures were incubated at 37 °C and 200 rpm to ensure oxygen distribution. Transformed *E. coli* bacteria were cultivated in LB medium, which contained the appropriate antibiotic for selection. The antibiotics were added to the LB medium at a final concentration of 100 µl/ml ampicillin, 50 µg/ml kanamycin and 50 µl/ml spectinomycin.

LB liquid medium

1,0 % (m/v) Tryptone
0,5 % (m/v) Yeast extract
1,0 % (m/v) NaCl
pH 7,5 in ddH_2O

LB agar medium

1,5 % (m/v) agar in LB medium

2.2.1.2 Transformation of chemically competent *E. coli* TOP10

200 µl of chemically competent *E. coli* bacteria TOP10 (see Ch. 2.2.1.3) were thawed on ice. After adding 0,1 to 0,2 µg of plasmid DNA and 100 µl of TCM buffer (4 °C), the transformation mixture was incubated for 30 min on ice. Following a heat shock for 3 min at 42 °C, the mixture was shortly cooled on ice for 1 min before adding 700 µl of LB medium (room temperature) and incubating the mixture for 1 h at 37 °C and 300 rpm. Afterwards, a 100 or 200 µl aliquot of the mixture was plated onto LB agar plates containing the appropriate antibiotic. Commercially available competent *E. coli* One Shot® TOP10 (Thermo Fisher Scientific) were transformed according to the manufacturer's protocol „*Transforming competent cells*".

TCM buffer

10 mM Tris/HCl
10 mM $CaCl_2$
10 mM $MgCl_2$
pH 7,5 in ddH_2O

2.2.1.3 Production of chemically competent *E. coli*

Chemically competent *E. coli* TOP10 used for plasmid transformation were generated by incubating the cells with calcium chloride to puncture the bacterial cell walls and membranes. A bacterial liquid broth culture (100 ml) was incubated until an optical density of 0,4-0,6 at a wavelength of 600 nm (OD_{600}) was detected. After centrifugation for 10 min at 2000 x g and 4 °C, the bacterial pellet was resuspended with 25 ml of a cold, sterile 100 mM $CaCl_2$ solution (4 °C). After incubating the suspension for 1 h on ice, a second centrifugation was carried out for 10 min at 2000 x g and 4 °C. The bacterial pellet was resuspended in 5 ml of a sterile 100 mM $CaCl_2$ solution (4 °C) containing 30 % (v/v) glycerol. The chemically competent *E. coli* TOP10 were portioned into 600 µl aliquots and frozen in an ethanol-dry ice solution immediately. The aliquots were stored at -80 °C.

2.2.2 Molecular biological methods

2.2.2.1 Isolation of plasmid DNA

The small-scale isolation of plasmid DNA for restriction analysis and cloning was carried out using the DNA-spin™ Plasmid DNA Purification kit (iNtRON Biotechnology). The plasmid DNA was isolated from a 1,5 ml overnight bacterial liquid broth culture according to the manufacturer's protocol. Large-scale isolation of plasmid DNA for cloning and transfections of eukaryotic cells was performed using the DNA-midi™ GT Plasmid DNA Extraction kit (iNtRON Biotechnology). In this case, the plasmid DNA was extracted from a 100-200 ml overnight liquid broth culture. After eluting the plasmid DNA from the binding columns it was concentrated using the NucleoBond® Finalizer kit (Macherey-Nagel) according to the protocol „Plasmid DNA concentration and desalting". The plasmid DNA was eluted in 250-500 µl 1 x TE buffer. Afterwards, the DNA concentration was determined using the NanoDrop 1000 spectrophotometer (see Ch. 2.2.2.3).

1 x TE buffer

10 mM Tris/HCl
5 mM EDTA
pH 8,8 in ddH_2O

2.2.2.2 Isolation of whole cell RNA

The isolation of whole cell RNA was performed by using the RNeasy Mini kit (Qiagen) according to the protocol "Purification of Total RNA from Animal Cells using Spin

Technology" with the following modifications. Depending on the size of the culture dish, the cells were lysed in 350 µl (30 mm and 6 well) and 600 µl (60 mm) RLT buffer containing 1 % (v/v) 2-Mercaptoethanol. The lysates were passed 6-8 times through a 25 G needle fitted onto a RNase-free syringe. The digestion of genomic DNA was carried out using the RNase-free DNase Set (Qiagen) according to the protocol "On-Column DNase Digestion". The whole cell RNA was eluted from the RNeasy spin columns using 50 µl sterile DEPC-H_2O. The RNA concentration was determined with the NanoDrop 1000 spectrophotometer (see Ch. 2.2.2.3). The RNA was reversely transcribed into cDNA for RT-PCR experiments (see Ch. 2.2.2.11).

2.2.2.3 Determining concentration of nucleic acids with the NanoDrop 1000 spectrophotometer

The concentration of nucleic acids of DNA and RNA samples was determined with the NanoDrop 1000 spectrophotometer (Thermo Fisher Scientific). 2 µl of the nucleic acid solution was applied to the lower measurement pedestal of the NanoDrop spectrophotometer. The sample extinction was measured at a wavelength of 260 nm as well as 280 nm. A ratio of absorbance at 260 nm and 280 nm of 1,8 indicated pure DNA, whereas a ratio of 2,0 represented a pure RNA solution.

2.2.2.4 Hydrolysis of DNA with restriction endonucleases

Two different types of restriction reactions were carried out with various restriction enzymes and buffers of New England Biolabs. Analytical restriction reactions were performed to identify the presence and correct orientation of an insert cloned into a vector backbone. Preparative restriction reactions were performed to prepare large amounts of insert and vector DNA for cloning experiments. The reaction mixtures were composed of the following components:

Analytical restriction reaction

x µl plasmid DNA (~ 0,5 µg)
1 µl restriction buffer (10 x)
0,25 U restriction enzyme (10 U/µl) per µg DNA
add ddH_2O (sterile) to 10 µl

Preparative restriction reaction

30 µl plasmid DNA (or 5 µg)
5 µl restriction buffer (10 x)
1-2 µl restriction enzyme (10-20 U/µl)
add ddH_2O (sterile) to 50 µl

The restriction reaction was carried out for 1-2 h at 37 °C.

2.2.2.5 Dephosphorylation of 5' DNA phosphate groups

Plasmid DNA fragments, which were hydrolyzed with blunt-end cutting restriction enzymes, were dephosphorylated to prevent re-ligation by using the lkaline phosphatase enzyme and buffer system of New England Biolabs. The dephosphorylation reaction mixture was composed of the following components:

Dephosphorylation reaction

30 µl plasmid DNA (hydrolyzed)
5 µl NEBuffer (10 x)
2 µl alkaline phosphatase, calf intestinal (CIP) (10 U/µl)

The dephosphorylation reaction was carried out for 30 min at 37 °C. Afterwards the alkaline phosphatase was heat inactivated for 20 min at 75 °C.

2.2.2.6 Ligation of DNA fragments

The ligation of the ESRP1 and ESRP2 inserts into the pcDNA3.1(+) vector was performed using the T4 DNA ligase system of New England Biolabs. The insert DNA was cloned into 50 ng vector DNA at an insert-to-vector ratio of 3:1. The size-dependent amount of insert DNA was calculated using the following equation:

$$\text{Amount}_{\text{Insert}}\,[\text{ng}] = \frac{\text{Amount}_{\text{Vektor}}\,[\text{ng}]\ \text{x}\ \text{Size}_{\text{Insert}}\,[\text{bp}]}{\text{Size}_{\text{Vektor}}\,[\text{bp}]}\ \text{x}\ \text{V}$$

(V: molar surplus of insert-to-vector DNA [dimensionless])

The ligation reaction mixture was composed of the following components:

Ligation reaction

x µl vector DNA (50 ng)
y µl insert DNA (calculated amount)
2 µl T4 buffer (10 x)
1 µl T4 DNA ligase (5 U/µl)
add ddH_2O (sterile) to 20 µl

The ligation reaction was carried out either for 1 h at room temperature or overnight at 16 °C. Afterwards, the T4 DNA ligase was heat inactivated for 20 min at 65 °C. The ligation of blunt ended PCR products into the pJET1.2-blunt plasmid was performed according to the manufacturer's manual "Blunt-End Cloning Protocol" of the CloneJET PCR cloning kit (Thermo Fisher Scientific).

2.2.2.7 Agarose gel electrophoresis of DNA and RNA fragments

Agarose gel electrophoresis was applied to separate DNA and RNA molecules based on their size and charge. TAE agarose gels were produced at an agarose concentration of 1-2 % (w/v) and contained either ethidium bromide (Sigma-Aldrich) or Midori Green Advance (Biozym). The DNA or RNA samples were mixed with at least 20 % (v/v) 5 x DNA sample buffer and transferred into the sample loading pockets of the gels. By applying 5 µl of the 100 bp DNA ladder or 1 kb DNA ladder (New England Biolabs), the size of the DNA and RNA fragments were analyzed after electrophoretic separation. Depending on the size of the gel, the electrophoretic separation was carried out for 1 h at 70 V (60 ml) or 1,5 h at 100 V (120 ml). Afterwards, the nucleic acid-intercalating dyes were visualized using the GeneFlash UV transilluminator (Syngene Bio Imaging).

TAE buffer

40 mM Tris/HCl, pH 8,0
20 mM acetic acid
1 mM EDTA

10 x DNA sample buffer

0,25 % (m/v) Orange G
50 % (v/v) glycerol
1 mM EDTA

2.2.2.8 Isolation of DNA fragments from agarose gels

DNA fragments were separated by agarose gel electrophoresis (see Ch. 2.2.2.7) and the respective bands excised from the agarose gel. The DNA fragments were extracted using the NucleoSpin® Gel and PCR Clean-Up kit (Macharey-Nagel) according to the manufacturer's protocol „DNA extraction from agarose gels".

2.2.2.9 Amplification of DNA fragments for cloning using polymerase chain reaction

Polymerase chain reactions (PCR) were performed to amplify ESRP1 and ESRP2 cDNA fragments, which were subsequently cloned into pJET1.2/blunt plasmids. The PCR experiments were performed using the Q5 Hot Start High-Fidelity DNA polymerase (New England Biolabs). A single PCR reaction mixture was composed of the following components:

PCR reaction (1 x)

x µl template DNA (100 ng)
2,5 µl forward primer (10 µM)
2,5 µl reverse primer (10 µM)
1 µl dNTPs (10 mM each)
10 µl GC enhancer (5 x)
10 µl Q5 reaction buffer (5 x)
0,5 µl Q5 Hot Start High-Fidelity polymerase (2 U/µl)
add ddH_2O (sterile) to 50 µl

The elongation time depended on the size of the DNA fragment used as template, whereas the annealing temperatures depended on the specific primer pairs, which were used to insert specific restriction sites upstream of the start codon and downstream of the stop codon (see Tab. 2.20).

Tab. 2.20: Reaction conditions for cloning primers. Abbreviations: Atm (annealing temperature), Et (elongation time).

Primer pair	Reaction conditions	Amplicon size
ESRP1_*BamH*I-FWD ESRP1_*Not*I-REV	Atm: 70 °C, Et: 2 min	2066 bp
ESRP2_*BamH*I-FWD ESRP2_*BamH*I-REV	Atm: 70 °C, Et: 2 min	2172 bp
ESRP2_*BamH*I-FWD ESRP2_*Xba*I-REV	Atm: 70 °C, Et: 2 min	2172 bp

The PCR experiments were carried out in the SensoQuest Labcycler Basic (SensoQuest) using the amplification protocol shown in Tab. 2.21 below. A successful amplification was verified by performing agarose gel electrophoresis with 5 µl of the respective PCR product (see Ch. 2.2.2.7). If the amplified DNA fragments were used for cloning experiments, the amplicons were purified using the NucleoSpin® Gel and PCR Clean-Up kit (Macharey-Nagel, Düren) according to the manufacturer's protocol „PCR Clean-Up".

Tab. 2.21: Amplification protocol for PCRs using the Q5 Hot Start High-Fidelity polymerase.

Phase	Temperature	Duration	Cycles
Initial denaturation	98 °C	2:00 min	1x
Denaturation	98 °C	45 s	35 x
Annealing	70 °C	1:00 min	
Elongation	72 °C	2:00 min	
Final elongation	72 °C	4:00 min	1 x
Hold	8 °C	infinite	-

2.2.2.10 Site-directed *in vitro* mutagenesis to generate Rac1 and Rac1b mutants

The QuikChange II Site-directed Mutagenesis kit (Agilent Technologies) was used to generate constitutive active G12V and dominant negative T17N mutants of wildtype Rac1 and Rac1b for transient expression in mammalian cells. The PCR-based *in vitro* mutagenesis experiments were performed using specific mutagenic primers (see Tab. 2.10) and pCGN expression plasmids encoding either HA-tagged wildtype Rac1 or Rac1b (see Tab. 2.7). The coding sequence at codon 12 of Rac1 and Rac1b was altered from 5'-GGA-3' (glycine) to 5'-GCA-3' (valine) and codon 17 was altered from 5'-ACT-3' (threonine) to 5'-AAT-3' (asparagine). The primers were designed according to the manufacturer's manual "Mutagenic Primer Design". The *in vitro* mutagenesis reaction was performed according to the protocols "Mutant Strand Synthesis Reaction (Thermal Cycling)" and "*DpnI* Digestion of the Amplification Products". The reaction conditions depended on the primers used and the size of the template DNA (see Tab. 2.22). Afterwards, the plasmids were transformed into chemically competent *E. coli* TOP10 (see Ch. 2.2.1.2) and isolated (see Ch. 2.2.2.1). The point mutations were verified by Sanger sequencing at the GATC Biotech company.

Tab. 2.22: Reaction conditions for mutagenic primers. Abbreviations: Atm (annealing temperature), Et (elongation time).

Primer pair	Reaction conditions	Amplicon size
Rac1(V12)-FWD Rac1(V12)-REV	Atm: 60 °C, Et: 8:30 min	8079 bp (*RAC1*) or 8136 bp (*RAC1B*)
Rac1(V12)-REV Rac1(N17)-REV	Atm: 60 °C, Et: 8:30 min	8079 bp (*RAC1*) or 8136 bp (*RAC1B*)

2.2.2.11 Synthesis of cDNA for gene expression analysis

The cDNA used for RT-PCR experiments was generated from whole cell RNA isolates using the ProtoScript® II reverse transcriptase system (New England Biolabs). Therefore, 1 µg of whole cell RNA was mixed with 1 µl of Oligo $d(T)_{23}$ VN random primers (50 µM) as well as 1 µl of a dNTP solution (10 mM each). The solution was diluted by adding 8 µl of RNase-free ddH_2O. The secondary and tertiary structures of the RNA molecules were dissolved for 5 min at 65 °C. The mixture was incubated on ice for 5 min before 4 µl of ProtoScript II buffer (5 x), 2 µl of 0,1 M DTT, 3 µl of RNase-free ddH_2O and 1 µl of ProtoScript II reverse transcriptase enzyme (200 U/µl) were added. The mixture was incubated for 5 min at 25 °C, before the reverse transcription reaction took place for 60 min at 42 °C. Afterwards, the reverse transcriptase enzyme was heat inactivated for 20 min at 65 °C. After cooling the samples on ice, 5 µl of cDNA solution were diluted in 45 µl nuclease-free ddH_2O (1/10) as a working solution for semi quantitative and quantitative RT-PCR experiments. The quality of the cDNA was assessed by performing semi quantitative RT-PCR experiments to detect the mRNA amounts of *ACTB* (β-Actin) (see Ch. 2.2.2.12).

2.2.2.12 Semi quantitative reverse transcriptase-polymerase chain reaction (sqRT-PCR)

Semi quantitative reverse transcriptase-polymerase chain reactions (sqRT-PCR) were performed to analyze the mRNA quantities of *RAC1* isoforms, different splicing factors and EMT-related factors. The PCR experiments were performed using the ready to load my-Budget 5 x Hot-Start *Taq* PCR mix (Bio-Budget). As template DNA, 1 µl of the diluted cDNA samples (1/10) was added to the reaction mixture. PCR reactions without template DNA were performed to identify possible unspecific amplifications and contaminations. A single sqRT-PCR reaction mixture was composed of the following components:

sqRT-PCR reaction (1 x)

1 µl template cDNA (1/10)
1 µl forward and reverse primers (10 µM each)
4 µl my-Budget 5 x Hot-Start *Taq* PCR mix (ready to load)
add 14 µl of nuclease-free ddH_2O (sterile) to 20 µl

The annealing temperature, the elongation time and the number of amplification cycles depended on the primer pair used in the sqRT-PCR experiments and are listed in Tab. 2.23 below.

Tab. 2.23: Reaction conditions for sqRT-PCR primers. Abbreviations: At (annealing time), Atm (annealing temperature), Et (elongation time), Cy (amplification cycles).

Primer Pair	Reaction conditions	Amplicon size
Actin-For Actin-Back	58 °C (Atm), 45 s (At), 45 s (Et), 25 x (Cy)	312 bp
E-Cad-for2 E-Cad Kl-Ba	47 °C (Atm), 60 s (At), 60 s (Et), 30 x (Cy)	633 bp
ESRP1_sq-FWD ESRP1_sq-REV	58 °C (Atm), 45 s (At), 45 s (Et), 35 x (Cy)	251 bp
ESRP2_sq-FWD ESRP2_sq-REV	60 °C (Atm), 45 s (At), 45 s (Et), 35 x (Cy)	249 bp
hnRNPA1-sq-FWD hnRNPA1-sq-REV	56 °C (Atm), 45 s (At), 60 s (Et), 40 x (Cy)	612 bp (isoform *A1A*) 768 bp (isoform *A1B*)
N-Cad-sense N-Cad-antisense	53 °C (Atm), 45 s (At), 45 s (Et), 35 x (Cy)	317 bp
Rac1b qFor1 Rac1b FL-Back	53 °C (Atm), 45 s (At), 60 s (Et), 35 x (Cy)	428 bp (*RAC1*) 485 bp (*RAC1B*)
SRSF1_sq-FWD SRSF1_sq-REV	58 °C (Atm), 45 s (At), 45 s (Et), 30 x (Cy)	213 bp
SRSF3_q2-FWD SRSF3_q2-REV	58 °C (Atm), 45 s (At), 45 s (Et), 30 x (Cy)	213 bp
Vim-For Vim-Back	57 °C (Atm), 45 s (At), 60 s (Et), 35 x (Cy)	750 bp

The sqRT-PCR experiments were carried out in the SensoQuest Labcycler Basic (SensoQuest) under consideration of the primer-specific reaction conditions. The standard amplification protocol is shown in Tab. 2.24 below.

Tab. 2.24: Amplification protocol for sqRT-PCRs using the ready to load my-Budget 5 x Hot-Start *Taq* PCR mix.

Phase	Temperature	Duration	Cycles
Initial denaturation	94 °C	4:00 min	1x
Denaturation	94 °C	45 s	28 - 35 x
Annealing	47 - 60 °C	45 s	
Elongation	72 °C	45 s - 1:00 min	
Final elongation	72 °C	10:00 min	1 x
Hold	8 °C	infinite	-

The mRNA amounts were analyzed by performing agarose gel electrophoresis with 10 µl of the respective PCR product (see Ch. 2.2.2.7).

2.2.2.13 Quantitative reverse transcriptase-polymerase chain reaction (qRT-PCR)

SYBR green-based, quantitative reverse transcriptase-polymerase chain reactions (qRT-PCR) were performed to analyze the relative mRNA quantities of *RAC1B*, different splicing factors and EMT-related factors. Specific primer pairs for the detection of the *RAC1B* and *RPLP0* mRNAs were used, whereas predesigned, commercially available QuantiTect® primers (Qiagen) were applied to detect the mRNA levels of *ESRP1*, *ESRP2*, *ACTB*, *CDH1*, *VIM* and different EMT-specific transcription factors (see Tab. 2.12). Each sample was analyzed in a duplicate. A single qRT-PCR reaction mixture was composed of the following components:

qRT-PCR reaction (1 x)

1 µl template cDNA (1/10)
1 µl forward and reverse primers (10 µM each)
or 2 µl QuantiTect® primer solution (10 x)
10 µl SensiMix™ SYBR No-ROX PCR mix (2 x) (Bioline)
add 8 µl of nuclease-free ddH_2O (sterile) to 20 µl

The 96-well PCR plate was sealed by pressing adhesive clear PCR seal sheets (Biozym) onto the PCR plate for 5 s using the HeatSealer S100 (Eppendorf). The qRT-PCR experiments were carried out in the Stratagene Mx3005P real time PCR cycler (Agilent Technologies) using the protocol “SYBR Green (with Dissociation Curve)” of the MxPro qPCR software. The product accumulation was measured at the end of each elongation step. Additionally, a dissociation curve was generated to verify the absence of primer-dimers and contaminations. The fold

change in relative mRNA quantities was calculated by the $2^{-\Delta\Delta Ct}$ method (see Ch. 2.2.6.2). The amplification and dissociation curve protocols were listed in Tab. 2.25 below.

Tab. 2.25: Amplification protocol for qRT-PCRs using the 2 x SensiMix™ SYBR No-ROX kit and the Stratagene Mx3005P real time PCR cycler.

Phase	Temperature	Duration	Cycles
Initial denaturation	95 °C	5:00 min	1x
Denaturation	95 °C	45 s	40 x
Annealing	55 °C	45 s	
Elongation	72 °C	1:00 min	
Dissociation curve	95 °C	1:00 min	1 x
	55 °C	30 s	
	95 °C	30 s	

2.2.3 Cell biological methods

2.2.3.1 Cultivation of eukaryotic cells

Different adherent eukaryotic cells were grown and maintained in tissue culture dishes (10 cm), which contained 10 ml of DMEM growth medium. The H23 cell clones were cultured in DMEM growth medium, which was supplemented with 1,0 mg/ml G418 for selection of stably transfected cells. The immortalized human pancreatic duct epithelial cells H6c7 were grown and maintained in specialized growth medium. The cells were incubated at 37 °C, 8 % CO_2 and 90 % relative humidity in a HERAcell 150i CO_2 incubator (Thermo Fisher Scientific). The growth medium was replaced every 2-3 days.

As soon as the eukaryotic cell layer reached 90-100 % in confluency a small amount of the cells was sub cultured into a new culture dish. Cell detachment was achieved by washing the cells with 1 x CMF-PBS and incubating them in a 0,05 % Trypsin-EDTA mixture (Thermo Fisher Scientific) for 1-5 min at 37 °C, 8 % CO_2 and 90 % relative humidity in a CO_2 incubator. Afterwards, the cells were resuspended in 5 ml of DMEM growth medium and sedimented by light centrifugation for 3 min at 200 x g. The cells were resuspended in DMEM growth medium and a suitable dilution was transferred into a new culture dish.

DMEM growth medium

10 % (v/v) fetal calf serum (FCS)
1 % (v/v) Minimum essential medium non-essential amino acids (100 x)
1 % (v/v) GlutaMAX™ (200 mM L-alanyl-L-glutamine)
in Dulbecco's Modified Eagle Medium, high glucose (DMEM)

Specialized growth medium for H6c7 cells

50 % (v/v) Roswell Park Memorial Institute (RPMI)-1640 medium
50 % (v/v) Keratinocyte serum-free medium
5 % (v/v) fetal calf serum (FCS)
1 % (v/v) GlutaMAX™ (200 mM L-alanyl-L-glutamine)
50 µg/ml bovine pituitary extract
5 ng/ml epidermal growth factor (EGF)

1 x CMF-PBS (calcium- and magnesium-free phosphate-buffered saline)

140 mM NaCl
2,7 mM KCl
8 mM Na_2HPO_4 x 2 H_2O
15 mM KH_2PO_4
pH 7,4 in ddH_2O

2.2.3.2 Cryopreservation of eukaryotic cells

For cryopreservation, the cells were detached from the cell culture dishes as described in Ch. 2.2.3.1. After centrifugation, 1 ml of the resuspended cell suspension was given into a Nunc™ CryoTube™ vial (Thermo Fisher Scientific), which contained 1 ml of DMEM cryo medium. The homogenized mixture was transferred into a freezing container filled with 100 % (v/v) isopropanol, which was stored at -80 °C for 2-3 days, thereby freezing the cells slowly over a period of time. For long term cryopreservation the cryo vials were transferred into liquid nitrogen.

For re-culturing, the frozen cells were thawed by transferring the cryo vials into a 37 °C water bath for less than 1 min. The cells were sedimented for 3 min at 200 x g and seeded into an appropriate tissue culture dish containing fresh DMEM growth medium. The medium was exchanged on the next day.

DMEM cryo medium

Dulbecco's Modified Eagle medium (DMEM, high glucose)
20 % (v/v) fetal calf serum (FCS)
1 % (v/v) MEM Non-essential amino acids (100 x)
1 % (v/v) GlutaMAX™ (200 mM L-alanyl-L-glutamine)
10 % (v/v) dimethyl sulfoxide (DMSO)

2.2.3.3 Determining cell number with a Neubauer chamber

A Neubauer improved counting chamber was used to determine the cell number. Therefore, the cells were detached from the cell culture dishes and the cell suspension transferred onto a Neubauer chamber. The total number of cells were counted in four large corner squares. The mean cell number was multiplied with the factor x 10^4 to determine the number of cells per ml. The suitable amount of the cell suspension containing the desired number of cells was transferred into a tissue culture dish or plate containing DMEM growth medium.

2.2.3.4 Transient plasmid DNA transfection of PANC-1 and H358 cells with Lipofectamine LTX

The transient plasmid transfections of PANC-1 and H358 cells were carried out using the transfection reagent Lipofectamine LTX® as well as the Plus™ reagent (Thermo Fisher Scientific). One day prior to the transfection, 4 x 10^5 PANC-1 cells were seeded into each well of a 6-well tissue culture plate. This resulted in a 50-60 % confluency on the day of transfection. Approximately 3 x 10^5 H358 cells were seeded into each well of a 6-well tissue culture plate two days prior to plasmid transfection. On the day of plasmid transfection, the growth medium was removed and replaced by 1,5 ml of fresh growth medium per well. The plasmid DNA and transfection reagent complexes were generated as follows. Reaction A: 9 µl of Lipofectamine® LTX were given to 100 µl of sterile Opti-MEM I (Thermo Fisher Scientific). Reaction B: 2,5 µg plasmid DNA and 2,5 µl of Plus™ reagent were diluted in the 100 µl Opti-MEM I. Both reaction mixtures were vortexed and incubated for 10 min at room temperature, before combining the two mixtures and incubating them for another 10 min at room temperature. The DNA-lipid complexes were carefully given onto the cells. The cells were incubated for 6 h before changing the medium. Afterwards, the cells were incubated for 24 to 96 h before RIPA lysates were prepared. In case of an incubation time longer than 24 h, the DMEM growth medium was changed one day after the transfection.

2.2.3.5 Transient plasmid DNA transfection of H1299 cells with PEI

H1299 cells were transiently transfected using polyetherimide (PEI). One day prior to the transfection, 1 x 10^6 H1299 cells were seeded into 10 cm culture dishes. This resulted in a 60-70 % confluency on the next day. On the day of plasmid transfection, the growth medium was removed and replaced by 4 ml growth medium. The plasmid DNA and transfection reagent complexes were generated by diluting 31,5 µl of PEI (1 µg/µl) and 15 µg of plasmid DNA in 500 µl DMEM medium without supplements. The reaction mixture was incubated for 10 min at room temperature before giving the DNA-lipid complexes onto the cells. After incubating the cells for 3 h, 6 ml of DMEM growth medium was added to each tissue culture dish. The transfected cells were incubated for 48 h.

2.2.3.6 siRNA transfection of H358, HTB-55 and Colo357 cells with Lipofectamine RNAiMAX

On the day prior to the siRNA transfection, Colo357, H358 and HTB-55 cells were seeded into a 6-well or 12-well tissue culture plate, which resulted in a confluency of 60-80 % on the day of the transfection. The cell number, the amount of siRNA, Lipofectamine RNAiMAX and Opti-MEM I depended on the cell line and size of the culture plate used (see Tab. 2.26). The siRNA and transfection reagent complexes were generated as follows. Reaction A: The respective amount of Lipofectamine® RNAiMAX was diluted in Opti-MEM I. Reaction B: The appropriate amount of siRNA was added to Opti-MEM I. Both reaction mixtures were combined, mixed by vortexing and incubated for 5 min at room temperature, before the siRNA-lipid complexes were given onto the cells. The growth medium was replaced on the next day before repeating the siRNA transfection. Another 24 h later the growth medium was exchanged again. RIPA lysates or RNA isolates were generated after an additional incubation time of 48 h. Total incubation times: 96 h (after first. transfection), 72 h (after second transfection).

Tab. 2.26: Transfection conditions for siRNA transfections of Colo357, H358 and HTB-55 cells in 6- and 12-well tissue plates.

Cell line	Tissue plate	Cell count [cells/well]	siRNA-concentration	Lipofectamine RNAiMAX	Opti-MEM I
Colo357	6-well	4,0 x 10^5	50 nM	9 µl	100 µl
	12-well	2,0 x 10^5	50 nM	4 µl	50 µl
H358	6-well	8,0 x 10^5	37,5 nM	7,5 µl	100 µl
	12-well	4,0 x 10^5	30 nM	3 µl	50 µl
HTB-55	6-well	1,0 x 10^6	37,5 nM	7,5 µl	100 µl
	12-well	3,5 x 10^5	30 nM	3 µl	50 µl

2.2.3.7 Immunofluorescent staining of fixed Colo357 and H358 cells

The subcellular localization of endogenous Rac1 and Rac1b was analyzed in Colo357 and H358 cells by immunofluorescent staining. The Colo357 (3-4 x 10^5 cells/well) and H358 cells (1-2 x 10^5 cells/well) were seeded onto small glass coverslips (diameter: 15 mm) within a 12-well tissue culture plate. After 48 h the cells were fixed for 10 min with 2,5 % (m/v) paraformaldehyde in 1 x CMF-PBS at room temperature. After fixation with paraformaldehyde, the cell membranes were permeabilized for 10 min at room temperature using 0,1 % (v/v) Triton® X-100 in 1 x CMF-PBS. Alternatively, the cells were fixed with an ice-cold methanol-acetone (1:1) solution (-20 °C) for 10 min at room temperature without a subsequent permeabilization step. Non-specific antibody binding was blocked by incubating the cells with 3 % BSA in 1 x CMF-PBS for 1 h at room temperature.

After washing the cells with 1 x CMF-PBS, they were covered with 20 µl of a primary antibody solution containing the mouse monoclonal anti-Rac1 and the rabbit polyclonal anti-Rac1b antibodies (each diluted at 1:300 in 0,2 % BSA in 1 x CMF-PBS each). The cells were incubated for 30 min at room temperature in a light-protected container, before again adding 20 µl of the primary antibody solution and repeating the incubation. Afterwards, the cells were washed, covered with 50 µl of the secondary antibody solution containing the AlexaFluor® 488-coupled and Cy3-coupled secondary antibodies (see Tab. 2.18) as well as DAPI (1 µg/µl). The cells were incubated for 30 min at room temperature in the dark, before repeating this step. The cells were mounted onto a drop of Mowiol solution on microscopic slides after carefully washing the glass coverslips containing the cells with 1 x CMF-PBS and ddH_2O. The immunofluorescently stained Rac1 and Rac1b proteins as well as the DAPI-stained cell nuclei were visualized using the GFP, Cy3, and DAPI filters of the Olympus XI 81 fluorescent microscope.

Mowiol mounting solution

10 % (m/v) Mowiol 4-88
25 % (v/v) glycerol
50 % (v/v) 0,2 M Tris/HCl, pH 8,5
in ddH_2O

2.2.3.8 Long-term TGFβ1 stimulation of H358 and HTB-55 cells

H358 and HTB-55 cells were treated with TGFβ1 to induced EMT. Therefore, 1-2 x 10^5 cells were seeded into each well of a 6-well tissue plates. The cells were treated with 10 ng/ml $TGFβ_1$ every second day for up to twelve days. Cells treated with 0,2 mM citrate served as controls. As soon as the cell layer reached 90-100 % in confluency, the cells were sub cultured into a new 6-well tissue culture plate. On the twelfth day, RIPA cell lysates were prepared. In rescue experiments, the H358 cells were transfected with pcDNA3.1(+)/HA-ESRP1 and HA-ESRP2 plasmids at the sixth and eighth day of TGFβ1 stimulation, respectively (see Ch. 2.2.3.4).

2.2.4 Protein biochemical methods

2.2.4.1 Preparation of RIPA cell lysates

RIPA cell lysates were prepared to isolate proteins from eukaryotic cells. For that, the cells were washed with cold 1 x TBS (4 °C) and lysed in RIPA buffer, which contained a protease inhibitor mix. The amount of RIPA buffer used for cell lysis depended on the size of the culture dish. After adding 500 µl (10 cm), 100 µl (6-well) or 50 µl (12-well) RIPA buffer per dish or well, the cells were detached by using a cell scraper. The lysates were passed eight times through a 25 G needle fitted onto a 1 ml syringe before the insoluble cell components were sedimented by centrifugation for 15 min at 16.100 x g and 4 °C. The protein concentration in the supernatant was measured by performing a bicinchoninic acid (BCA) protein assay. The lysates were either directly used for SDS-polyacrylamide gel electrophoresis or frozen in liquid nitrogen and stored at -80 °C.

1 x RIPA buffer

50 mM Tris/HCl, pH 7,0
150 mM NaCl
0,1 % (v/v) SDS
1 % (v/v) Triton® X-100
0,5 % (m/v) Na-deoxycholate

1 x protease inhibitor mix

1,39 mM pefabloc
15 µM aprotinin
21 µM leupeptin
50 µM Trypsin inhibitor (soybean)

2.2.4.2 Separation of cytosolic and membranous proteins by subcellular fractionation

Subcellular fractionation assays were performed to separate the insoluble, membranous protein fraction (P100) from the soluble, cytosolic proteins (S100) by ultra-centrifugation at 100.000 x g. The cells were seeded into at least two 10 cm tissue culture dishes and grown to confluency, before washing the cells twice with cold 1 x CMF-PBS (4 °C) and lysing them in 250 µl hypotonic HEPES lysis buffer. After detaching the cells by using a cell scraper, the lysates were passed ten times through a 25 G needle fitted onto a 1 ml syringe. The nuclei and larger organelles were separated from the cell lysates via centrifugation for 10 min at 500 x g and 4 °C. A 100 µl aliquot of the supernatant was used as a lysate control, whereas the rest of the supernatant was separated into S100 and P100 fractions by centrifugation for 1 h at 100.000 x g and 4 °C. Afterwards, the supernatant (= S100) containing the soluble proteins was separated from the pellet, which was washed with 250 µl HEPES buffer by centrifugation for 15 min at 100.000 x g and 4 °C. The cell pellet containing the insoluble proteins (= P100) was resuspended in 50-100 µl RIPA buffer by using a micro pistil. The protein concentration of the lysate, S100 and P100 fractions was measured by performing a BCA protein assay. The fractions were either directly used for SDS-polyacrylamide gel electrophoresis or frozen in liquid nitrogen and stored at -80 °C.

1 x HEPES buffer

50 mM HEPES, pH 7.6 bei 4°C
8,6 % (m/v) saccharose
10 mM EDTA
10 mM EGTA
1 x protease inhibitor mix (see Ch. 2.2.4.1)

2.2.4.3 Extraction of nuclear proteins by ultra-centrifugation

Nuclear proteins were extracted from pancreatic and lung cells by using high speed centrifugation. Therefore, the protocol described in Nicholson *et al.* (1990) was altered as

follows. The confluently grown cells of at least two 10 cm cell culture dishes were washed twice with 1 x CMF-PBS and subsequently lysed in 300 µl buffer C. The cells were detached from the culture dish by using a cell scraper and the cell membranes were ruptured by passing the lysates ten times through a glass Dounce homogenizer. The nuclei were separated from the cell lysates via centrifugation for 5 min at 720 x g and 4 °C. The pellet containing the nuclei was resuspended in 150 µl buffer N and passed ten times through a glass Dounce homogenizer. The insoluble and soluble nuclear proteins were separated by centrifugation for 1 h at 100.000 x g and 4 °C. The protein concentration of the supernatant was measured by performing a BCA protein assay. The nuclear extracts were either directly used for SDS-polyacrylamide gel electrophoresis or frozen in liquid nitrogen and stored at -80 °C.

Buffer C:

10 mM Tris HCl pH 7.5
1 mM $MgCl_2$
1.5 mM EDTA
20 mM KCl
10 % glycerol
1 x protease inhibitor mix (see Ch. 2.2.4.1)

Buffer N

10 mM Tris HCl, pH 7.5
1 mM EDTA
1 mM DTT
600 mM KCl
1 x protease inhibitor mix (see Ch. 2.2.4.1)

2.2.4.4 Determination of the protein concentration by bicinchinonic acid protein assays

The protein concentration was measured by performing bicinchoninic acid (BCA) protein assays. The BCA assay is based on the quantitative reduction of divalent copper (Cu^2) in the presence of peptide bonds. The protein concentration was calculated by comparing the measured $OD_{562\ nm}$ values of the cell lysates with a protein solution of a known concentration. Therefore, a calibration line was created using a 2 mg/ml solution of bovine serum albumin (BSA). An ascending series of 0 µl, 2 µl, 4 µl, 6 µl, 8 µl, 10 µl and 12,5 µl of BSA solution was given into a 96-well microtiter plate. ddH_2O was added to a total volume of 20 µl. The

protein lysates were diluted at a ratio of 1/10. For that, 5 µl of protein lysate was diluted in 45 µl ddH_2O and two aliquots of 20 µl were given into 96-well microtiter plate. Afterwards, 180 µl of BCA staining reagent was given into each well containing either the diluted lysates, the calibration samples or the water control. The plate was incubated for 30 min at 37 °C. The absorption of the samples and the water control was measured in the ELx800 Absorbance Microplate Reader and the protein concentration calculated afterwards.

BCA staining reagent

50 x Vol. Pierce BCA Protein Assay Reagent A

1 x Vol. 4 % (m/v) $CuSO_4$ in ddH_2O

2.2.4.5 Sodium dodecyl sulfate-polyacrylamide gel electrophoresis (SDS-PAGE)

The protein amounts of Rac1 isoforms, splicing factors and EMT-related proteins were analyzed by western blotting. Therefore, proteins were separated by mass by performing sodium dodecyl sulfate-polyacrylamide gel electrophoresis (SDS-PAGE). In the course of this work, separating gels with an acrylamide concentration of 10 % and 13,5 % (v/v) were used, the composition of which is listed in Tab. 2.27 below.

Tab. 2.27: Composition of separating and stacking gels for SDS-PAGE.

SDS-polyacrylamide gels (Vol. for four small gels, 8 x 5 x 0,2 cm)	**Separating gels**		**Stacking gel**
	10 %	**13,5 %**	**4 %**
30 % (m/v) Acrylamide solution	13 ml	17 ml	0,76 ml
2 % (m/v) Bisacrylamide solution	5 ml	6,5 ml	0,3 ml
3 M Tris/HCl, pH 8,8	5 ml	-	-
1 M Tris/HCl, pH 6,8	-	5 ml	0,76 ml
10 % (m/v) SDS	0,4 ml	0,4 ml	0,06 ml
60 % (m/v) Saccharose	-	-	1,5 ml
ddH_2O	16,5 ml	11 ml	2,6 ml
TEMED	40 µl	40 µl	8 µl
10 % (m/v) Ammonium persulfate (APS)	250 µl	250 µl	80 µl
Separation range	30-130 kDa	20-100 kDa	-

Four gels (8 x 6 x 0,2 cm each) were produced simultaneously in a gel casting chamber (Sigma-Aldrich). Gel polymerization took place for at least 3 h at 37 °C or overnight at 4 °C. The

stacking gels were poured onto the solid separating gels and a 10-pocket sample comb inserted. After stacking gel polymerization for at least 15 min at room temperature, the polyacrylamide gel was inserted into a vertical electrophoresis chamber and covered with 1 x SDS electrophoresis buffer.

The protein samples were prepared by adding at least 20 % (v/v) 5 x SDS sample buffer and denaturing the proteins for 5 min at 95 °C. In the course of this work, 50 µg of RIPA lysates and S100 fractions as well as 25 µg of P100 and nuclear extracts were prepared and loaded into the sample pockets, respectively. The proteins were concentrated within the stacking gel for 15 min at 80 V, before the electrophoretic separation of the proteins within the separating gel took place for an additional 60-90 min at 110 V.

1 x SDS electrophoresis buffer

50 mM Tris
0,5 M glycine
0,1 % (m/v) SDS

5 x SDS sample buffer

200 mM Tris/HCl, pH 8,8
5 mM EDTA
1 M saccharose
1 mM DTT
2 % (m/v) SDS
0,1 % (m/v) bromophenol blue

2.2.4.6 Transferring proteins onto nitrocellulose membranes (western blotting)

Proteins were transferred from the SDS-polyacrylamide gel onto a nitrocellulose membrane (Protran BA85 nitrocellulose transfer membrane) through western blotting. Therefore, the separating gel was laid onto a nitrocellulose membrane air bubbles-free and covered by two Whatman® chromatography filters and fleece sponges on each side. The components were fixed within a blotting grid and inserted into a mini blotting chamber (Sigma-Aldrich) filled with transfer buffer. The transfer of the proteins was either carried out for 1 h at 70 V and room temperature or for 10 h at 20 V and 4 °C.

After western blotting, the nitrocellulose membrane was washed with ddH_2O and the protein bands stained reversibly for 5 min in Ponceau-S solution. After partly destaining in dH_2O, the membrane was documented by scanning and subsequently completely destained in 1 x TBS.

Transfer buffer

25 mM Tris/HCl
0,1 % (m/v) SDS
1,5 % glycine
20 % (v/v) methanol

Ponceau S staining solution

0,2 % (m/v) Ponceau S
3 % (m/v) trichloro acetic acid

2.2.4.7 Detection of proteins with specific antibodies

Unspecific binding of antibodies to the nitrocellulose membrane was blocked with 5 % (m/v) powdered milk in 1 x TBS for 1 h at room temperature. Afterwards, the nitrocellulose membrane was covered with the desired primary antibody solution (see Tab. 2.16). Binding of the primary antibodies was performed overnight at 4 °C. After washing the nitrocellulose membrane once with 1 x TBS/T and twice with 1 x TBS for 10 min at room temperature, it was covered with the secondary antibody solution (see Tab. 2.17) and incubated for 1 h at room temperature. Afterwards, the nitrocellulose membrane was washed as described above. The secondary antibodies were either detected using the Fusion SL4-3500.WL chemiluminescence imaging system (Vilber Lormat) or the LI-COR Odyssey SA and Clx system (LI-COR Bioscience) depending on the conjugate (see Ch. 2.2.4.8 and Ch. 2.2.4.9).

1 x TBS/T

1 x TBS + 0,1 % (v/v) Tween® 20

2.2.4.8 Detection of HRP-coupled secondary antibodies using the Fusion SL4-3500.WL

The HRP-coupled secondary antibodies were detected using the SuperSignal™ West Pico Plus chemiluminescent substrate (Thermo Fisher Scientific). The Luminol/Enhancer solution and Stable Peroxide solution were mixed at a ratio of 1:1 according to the manufacturer's protocol. The washed nitrocellulose membrane was covered with the ECL solution and incubated for 3-

5 min in a light-protected container. Afterwards, the membrane was developed using the Fusion SL4-3500.WL chemiluminescence imaging system (Vilber Lormat). Usually, the nitrocellulose membrane was exposed for 30 s to 2 min at full resolution or high sensitivity.

2.2.4.9 Detection of fluorophore-coupled secondary antibodies using the LI-COR Odyssey Sa and CLx

The cyanine-based fluorescence dye-coupled secondary antibodies were detected using the LI-COR Odyssey Sa Infrared or CLx Infrared system (LI-COR Bioscience). This system allowed the excitation of fluorescent signals at wavelengths of 685 nm (red channel) and 785 nm (green channel). Both, the red and green fluorescence signals, were detected at different intensities using the LI-COR Image Studio software. Thereby, two different primary antibodies from different species could be used for detection of two different proteins simultaneously.

2.2.5 Chorioallantoic membrane invasion assay

The chick embryonic chorioallantoic membrane (CAM) invasion model was re-established in the group as a part of this work (Hofer *et al.*, 2004; Veit *et al.*, 2004). Fertilized white chicken eggs were purchased from the poultry reproduction company LSL Rhein-Main. Due to the high number of unfertilized eggs and embryos dying during the incubation procedure, 8-10 eggs were used per cell line in each CAM invasion experiment. Upon arrival, the breeding process was initiated by immediately incubating the eggs at 37 °C and 60-70 % relative humidity.

On the fifth day of incubation, the egg shell was opened at the pointed pole. A small strip (2,5 x 2,5 cm) of artificial silk plaster tape was attached to the egg shell to cover the hole, which was then widened to a diameter of 1-2 cm by using fine preparation cutlery. The hole was covered with another strip of plaster tape to prevent dehydration. The eggs were incubated for another three days at 37 °C and 60-70 % relative humidity. The viability of the chick embryos was checked on a daily basis.

On the eighth day, the tumor cells were xenografted within a small, autoclaved silicone ring (inner diameter: 5 mm, outer diameter: 6 mm) on the surface of the CAM. The carcinoma cells were cultured in three to four 10 cm tissue culture dishes and grown to confluency. For each analyzed cell line, 1 x 10^6 carcinoma cells in 20 µl DMEM medium without supplements per egg were xenografted within the silicone ring on the surface of the CAM. The eggs were covered with plaster tape and incubated for another four days. The viability of the chick embryos was again checked on a daily basis.

On day twelve of the egg incubation, CAM sections with the silicone ring containing the cells were cut out in a rectangular shape (length: 15 mm, width: 6 mm). The retrieved sections were transferred into a 3,5 cm petri dish, which contained 4 % (v/v) formaldehyde in 1 x CMF-PBS (pH 7,6). After taking pictures of the CAM sections to document the tumor formation, the sections were fixed for 3 h to several days at 4 °C. The formaldehyde penetrated tissue at 1-2 mm/h. Afterwards , the CAM sections were transferred into Histosette® II tissue processing cassettes (VWR) with paper sheets on each side of the section to prevent tissue loss. The sections were dehydrated overnight in the fully enclosed tissue processor ASP300S (Leica Biosystems). On the following day, the CAM sections were embedded into paraffin wax in an upright standing position by using the heated paraffin embedding module EG1140H (Leica Biosystems). For that, the sections were removed from the Histosette® II tissue processing cassettes. A small drop of heated paraffin wax was given into an embedment dish, which was then transferred from the heating onto a cooling module. The CAM sections were immediately transferred into the drop of paraffin wax and kept in an upright position by using pre-heated tweezers until the paraffin wax hardened marginally. As soon as the CAM section stood by itself, it was covered with the Histosette® tissue processing cassette and heated paraffin wax completely. The tissue embedment dish was transferred onto the EG1150 C cold plate (Leica Microsystems) until the paraffin wax hardened completely.

The paraffin blocks, which were stored at -20 °C, were fixed into the Microm HM 355S microtome (Thermo Fisher Scientific) and excess paraffin was removed by cutting 30 µm slices (trim cutting). As soon as the CAM and tumor cell nests were reached, fine cuts were made at a thickness of 5 µm for hemalum eosin staining. The slices were collected on SuperFrost Ultra Plus® adhesive microscopic slides (Carl-Roth). The presence of the tumor nests within the CAM sections was checked microscopically (DM750, Leica Mikrosysteme). A series of ten to fifteen microscopic slides were generated for each paraffin block. The slides were dried and stored at room temperature.

The CAM sections were stained with hemalum eosin (HE) staining. Therefore, two or three slides of a ten or fifteen slide series were stained according to the protocol listed in Tab 2.28. To preserve the HE-stained sections, rectangular coverslips (24 x 60 mm) were mounted onto microscopic slides by using the xylene-based Roti-Histokitt II mounting solution (Carl-Roth). The mounting solution was dried overnight at room temperature. The HE-stained CAM sections were analyzed and documented with the reflected light microscope DMLA (Leica Mikrosysteme) (see also Fig. 3.7).

Tab. 2.28: Protocol for the hemalum eosin staining of CAM sections.

Duration [min]	Reagent	Repetition	Phase
60	60 °C	1 x	Deparaffinization and rehydration
5	Roti-Histol	2 x	
5	Ethanol absolute (99,6 %)	2 x	
5	Ethanol (96 %)	2 x	
5	Ethanol (70 %)	2 x	
2	dH_2O	1 x	
5	**Mayer's hemalum solution**	1 x	Hemalum staining
5	H_2O (tap)	1 x	Washing
1	Ethanol (96 %)	1 x	
4	**Shandon eosin Y (alcoholic)**	1 x	Eosin staining
short	dH_2O	1 x	Washing and dehydration
2	Ethanol (96 %)	2 x	
5	Ethanol absolute (99,6 %)	2 x	
5	Isopropanol (99,8 %)	1 x	
5	Roti-Histol	2 x	
-	Mounting with Roti-Histokitt II	-	Mounting

2.2.6 Data analysis and statistical evaluations

2.2.6.1 Densitometric analysis of western blot and sqRT-PCR experiments

Densitometric analyses for quantification of cDNA and protein bands were performed after sqRT-PCR and western blot experiments, respectively. The intensities of the bands were measured using the LI-COR Image Studio software (LI-COR Bioscience). The measured values were normalized by dividing through the value of the corresponding standard, namely the *ACTB* (sqRT-PCR) or β-Actin (western blot) band. In a second normalization step the fold change (FC) was calculated by dividing through the value of the control, which was set to 1,0. The arithmetic mean and the standard deviation were calculated by using the GraphPad Prism software. Additionally, it was applied for statistical analyses and generating graphical depictions. The statistical significance was analyzed by a one sample t-test (unpaired, two-tailed). It was distinguished between the following significance levels: $p < 0,05 = *$, $p < 0,01 = **$, $p < 0,001 = ***$.

2.2.6.2 Evaluation of qRT-PCR experiments

The product accumulation was measured at the end of each elongation step during the qRT-PCR run, whereby the amplification cycles were recorded to detect the cycle number at which the fluorescence signal exceeded a threshold (C_t).

The fold change (FC) in relative mRNA quantities was calculated by the $2^{-\Delta\Delta Ct}$ method according to Livak and Schmittgen (2001). The mean C_t values of the duplicates of the gene of interest and the reference gene were calculated. The relative mRNA amount (ΔC_t) was quantified by subtracting the mean C_t value of the reference gene from the mean C_t value of a gene of interest. The FC was calculated by subtracting the ΔC_t values of siControl, in which non-targeting siRNA was transfected, from the ΔC_t values of samples treated with specific siRNAs. The GraphPad Prism software was applied to calculate the arithmetic mean and the standard deviation of three independent experiments. Additionally, it was used for statistical analyses and generating the bar graphs. The statistical significance of mRNA quantity differences in relation to the control, which was set to 1,0, was analyzed by a one sample t-test (unpaired, two-tailed). It was distinguished between the following significance levels: $p < 0,05$ = *, $p < 0,01$ = **, $p < 0,001$ = ***.

3 Results

3.1 Differences in Rac1 and Rac1b mRNA and protein expression in pancreatic and lung carcinoma cell lines

The mRNA and protein levels of Rac1 and Rac1b were analyzed in different pancreatic and lung carcinoma cell lines. Therefore, the pancreatic carcinoma cell lines Colo357, PANC-1, MIA PaCa-2, Capan-1, Capan-2, BxPC-3 and the immortalized human pancreatic duct epithelial cells H6c7 as well as the lung carcinoma cell lines HCC44, H2122, H358, HTB-55, H23, Colo699, H1299, and A549 were used. The cDNA probes were supplied by Prof. Dr. Andre Menke, whereas the majority of the RIPA lysates were provided by Prof. Dr. Klaudia Giehl.

The differences in mRNA expression were examined through semi quantitative reverse transcriptase polymerase chain reaction (sqRT-PCR) analyses. The forward primer was complementary to the *RAC1* sequence within exon 3 directly upstream of exon 3b, whereas the reverse primer was complementary to the 3' end of the *RAC1* and *RAC1B* cDNA, respectively (see Tab. 2.11). Thereby, *RAC1* (428 bp) and *RAC1B* (485 bp) fragments were amplified simultaneously. The sqRT-PCR analysis revealed substantial differences in the *RAC1B* mRNA levels between the cell lines, but no striking variations in the amounts of *RAC1* mRNA. The pancreatic carcinoma cell lines Colo357 and Capan-2 exhibited the highest amounts *RAC1B* mRNA, whereas Capan-1, BxPC-3 and H6c7 expressed slightly lower levels. Only weak or no *RAC1B* mRNA was detected for PANC-1 and MIA PaCa-2 cells (see Fig. 3.1 A). For the lung carcinoma cell lines, the highest levels of *RAC1B* mRNA were observed in the H358 as well as HTB-55 cells, when considering the reduced amount of cDNA for H358, indicated by the *ACTB* amplicon. In comparison to that, lower *RAC1B* mRNA levels were present HCC44, H2122 and Colo699 cell lines, while only very weak amounts were identified in H23 cells. *RAC1B* mRNA expression was not detected for H1299 and A549 cells (see Fig. 3.1 B).

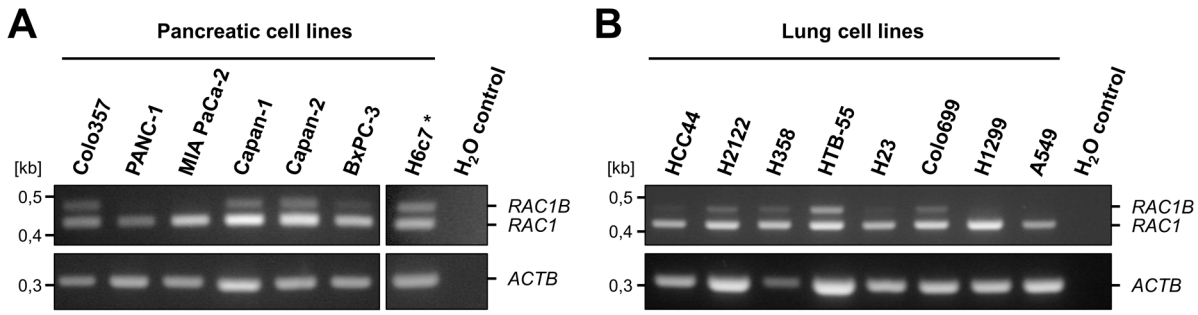

Fig. 3.1: Semi quantitative analysis of Rac1 and Rac1b mRNA levels in pancreatic and lung cell lines. Semi quantitative reverse transcriptase polymerase chain reactions (sqRT-PCR) were carried out using cDNAs from established (**A**) pancreatic and (**B**) lung cell lines. The used primer pair amplified a cDNA fragment, which included the alternative exon 3b and therefore allowed the simultaneous detection of *RAC1* and *RAC1B* cDNA (top panel). The detection of *ACTB* (β-Actin) used for normalization is displayed in the bottom panel. The figure shows representative agarose gels of three independent experiments. (*) One experiment was carried out for H6c7 cells.

The protein levels of Rac1 and Rac1b were analyzed in RIPA cell lysates by performing western blot analyses using specific anti-Rac1 and anti-Rac1b antibodies. These analyses revealed that the protein expression of Rac1b, but not Rac1, varied in different pancreatic and lung carcinoma cell lines (see Fig. 3.2 A and B). The pancreatic carcinoma cell lines Colo357 and Capan-2 displayed the highest amounts of Rac1b protein amounts in comparison to the other pancreatic cell lines. Much lower Rac1b protein levels were expressed in Capan-1, BxPC-3, H6c7 and PANC-1 cells, whereas no Rac1b expression was detected in MIA PaCa-2 (see A). For the lung carcinoma cell lines, the highest amounts of Rac1b proteins were present in H358 as well as HTB-55 cells. In comparison to that, lower levels were observed in HCC44 cells. Only very weak amounts of Rac1b were identified in H23 and Colo699 cells, whereas no Rac1b protein expression was detected for H1299 and A549 cells (see B). The anti-Rac1 antibody recognizes the C-terminal region of the Rac1 protein, which is identical in both isoforms (see Fig. 3.2 C). This dual specificity of the antibody allowed a direct comparison of Rac1 and Rac1b protein expression levels, when using only the anti-Rac1 antibody. These analyses revealed a low Rac1b-to-Rac1 protein expression ratio, even in cell lines with relatively high Rac1b protein levels (see A and B: middle panel).

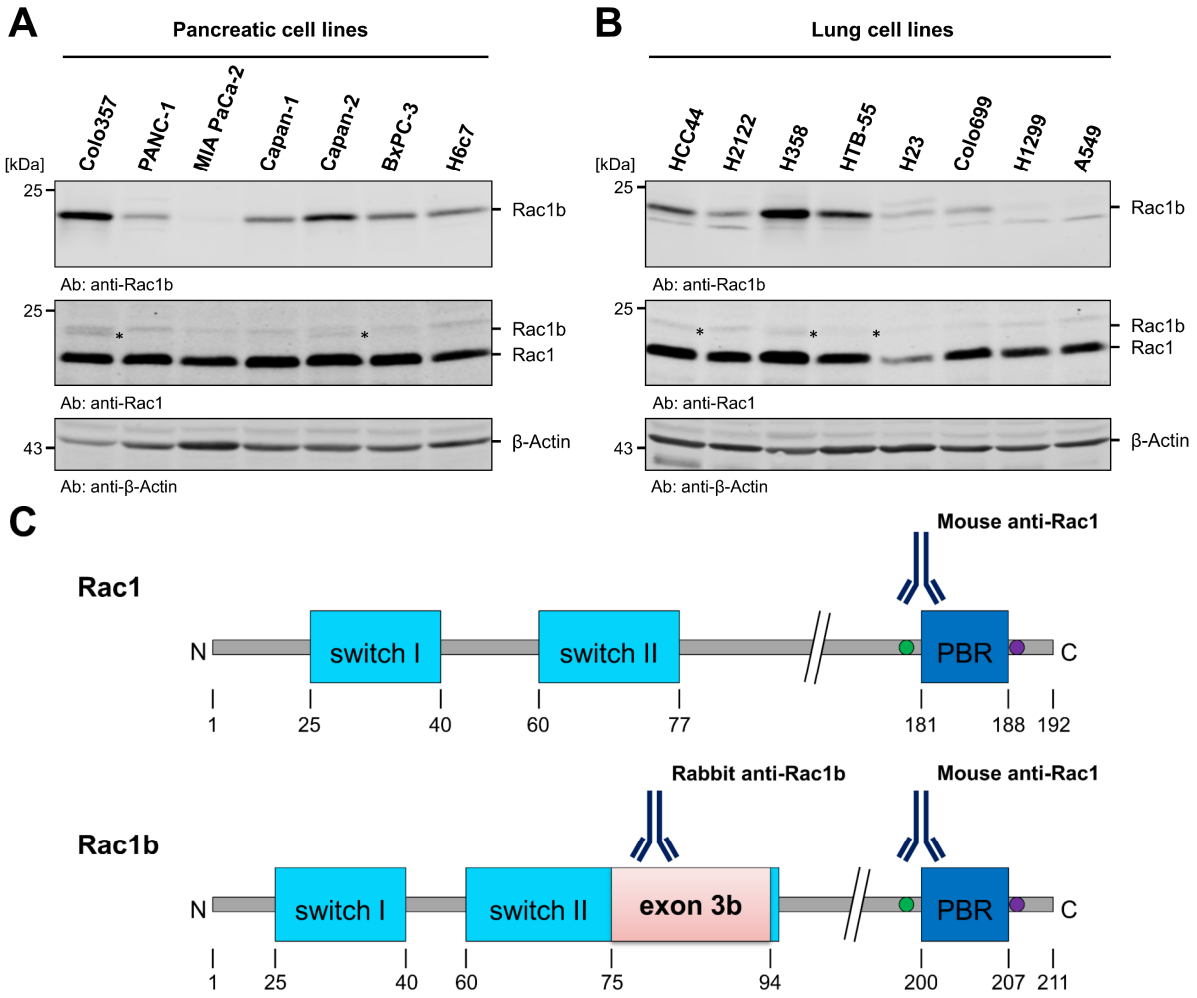

Fig. 3.2: Analysis of Rac1 and Rac1b protein amounts in pancreatic and lung cell lines using an anti-Rac1 and specific anti-Rac1b antibody. RIPA lysates of established (**A**) pancreatic and (**B**) lung cell lines were separated in 13,5 % SDS polyacrylamide gels and analyzed via western blot procedure. The protein levels of Rac1b and Rac1 were detected using a specific rabbit anti-Rac1b (top panel) and a mouse anti-Rac1 antibody (middle panel), respectively. Additionally, β-Actin was detected (bottom panel). The figure shows representative western blots of two independent experiments. (*) The detection of Rac1b with the anti-Rac1 antibody is highlighted. (**C**) Schematic presentation of the binding region of the monoclonal mouse anti-Rac1 and polyclonal rabbit anti-Rac1b antibodies within the respective amino acid sequence of Rac1 (top) and Rac1b (bottom).

The differences in Rac1b mRNA and protein levels of the various cell lines were summarized in Tab. 3.1, in which a semi quantitative appraisal of the amount of the Rac1b mRNA and protein was conducted. The Rac1 expression was comparable in all analyzed cell lines. Additionally, no differences between the mRNA and protein content of the respective Rac1 isoforms were observed. In the following experiments the pancreatic carcinoma cell line Colo357 and the lung carcinoma cells H358 and HTB-55 were analyzed more extensively, due to the high mRNA and protein amounts of the Rac1b isoform. PANC-1 pancreatic and H23 lung carcinoma cells, which are well characterized in our group, were examined as representative cell lines with low Rac1b-to-Rac1 ratios.

Tab. 3.1: Overview of the differences in Rac1b mRNA and protein contents between the analyzed pancreatic and lung cell lines. The Rac1b protein and mRNA levels were evaluated as being strong (++), weak (+) or not detectable (-). The overview is a summary of two (protein) and three independent analyses (mRNA), respectively. (*) n = 1 for mRNA expression in H6c7.

Organ of origin	Cell line	Rac1b	
		mRNA	protein
Pancreas	Colo357	++	++
	PANC-1	+	+
	MIA PaCa-2	-	-
	Capan-1	++	+
	Capan-2	++	++
	BxPC-3	+	+
	H6c7	+ *	+
Lung	HCC44	+	+
	H2122	+	+
	H358	++	++
	HTB-55	++	++
	H23	+	+
	Colo699	+	+
	H1299	-	-
	A549	-	-

3.2 Subcellular localization of Rac1 and Rac1b

The subcellular localization of Rac1 and Rac1b was analyzed for the endogenous proteins in several pancreatic and lung cell lines. Additionally, the subcellular localization of wildtype EGFP-Rac1 and EGFP-Rac1b fusion proteins was assessed, which were transiently expressed in PANC-1 cells and stably expressed in H23 cell clones. Furthermore, HA-tagged constitutive active (G12V) as well as dominant negative (T17N) Rac1 and Rac1b mutants were transiently expressed in H1299 cells to identify the influence of the activity state of the respective isoforms on their subcellular localization. Fluorescence microscopy analyses and subcellular fractionation assays were performed to identify isoform-specific differences in subcellular localization.

The localization of endogenous Rac1 and Rac1b by fluorescence microscopy was supposed to be achieved by immunofluorescent staining. However, a specific detection and thus distinction of endogenous Rac1 and Rac1b proteins with the anti-Rac1 or anti-Rac1b antibody was not

possible, because the anti-Rac1 antibody also detects the Rac1b isoform (see also Ch. 3.1). Furthermore, the anti-Rac1b antibody recognizes an additional unidentified protein with an approximate size of 55 kDa in western blot experiments (data not shown).

3.2.1 Detection of ectopically expressed wildtype EGFP-Rac1 and EGFP-Rac1b by using fluorescence microscopy

To identify differences in the subcellular localization between the Rac1 isoforms, PANC-1 cells were transiently transfected with EGFP-Rac1 and EGFP-Rac1b expression plasmids and incubated for 24 h before performing live cell imaging analysis. Differences in the subcellular localization of EGFP-Rac1 and EGFP-Rac1b were not obvious after 24 h of ectopic protein expression (data not shown). Therefore, additional live cell imaging analyses were performed with cell clones stably expressing EGFP-Rac1 and EGFP-Rac1b, namely H23/EGFP A3, H23/EGFP-Rac1 D1 and D2 as well as H23/EGFP-Rac1b B1 and B3. The fluorescence microscopic images shown in Fig. 3.3 were provided by Julia Seiz of the group of Prof. Dr. Andre Menke. The EGFP-Rac1 and EGFP-Rac1b fusion proteins were visualized at an emission wavelength of 509 nm, which is the emission maximum for enhanced green fluorescent proteins.

These analyses indicated an exclusive cytoplasmic localization of the EGFP proteins in the H23/EGFP A3 cell clone (see A-C). The EGFP-Rac1 fusion protein was localized in the cytoplasm, but also the plasma membrane of the H23/EGFP-Rac1 D1 cells, where the fluorescence signal was more intense in areas of cell-cell contacts (see E and H: arrows). EGFP-Rac1 was not present the nucleus (see D-F). A similar localization of EGFP-Rac1 was observed in the H23/EGFP-Rac1 D2 cell clone (see G-I). Stably expressed EGFP-Rac1b was predominantly localized in the plasma membrane in H23/EGFP-Rac1b B1 and B3. Also, an enhanced fluorescence signal was visible in cell-cell-contacts (see K and N: arrows). A nuclear localization of EGFP-Rac1b was also not detected (see J-O).

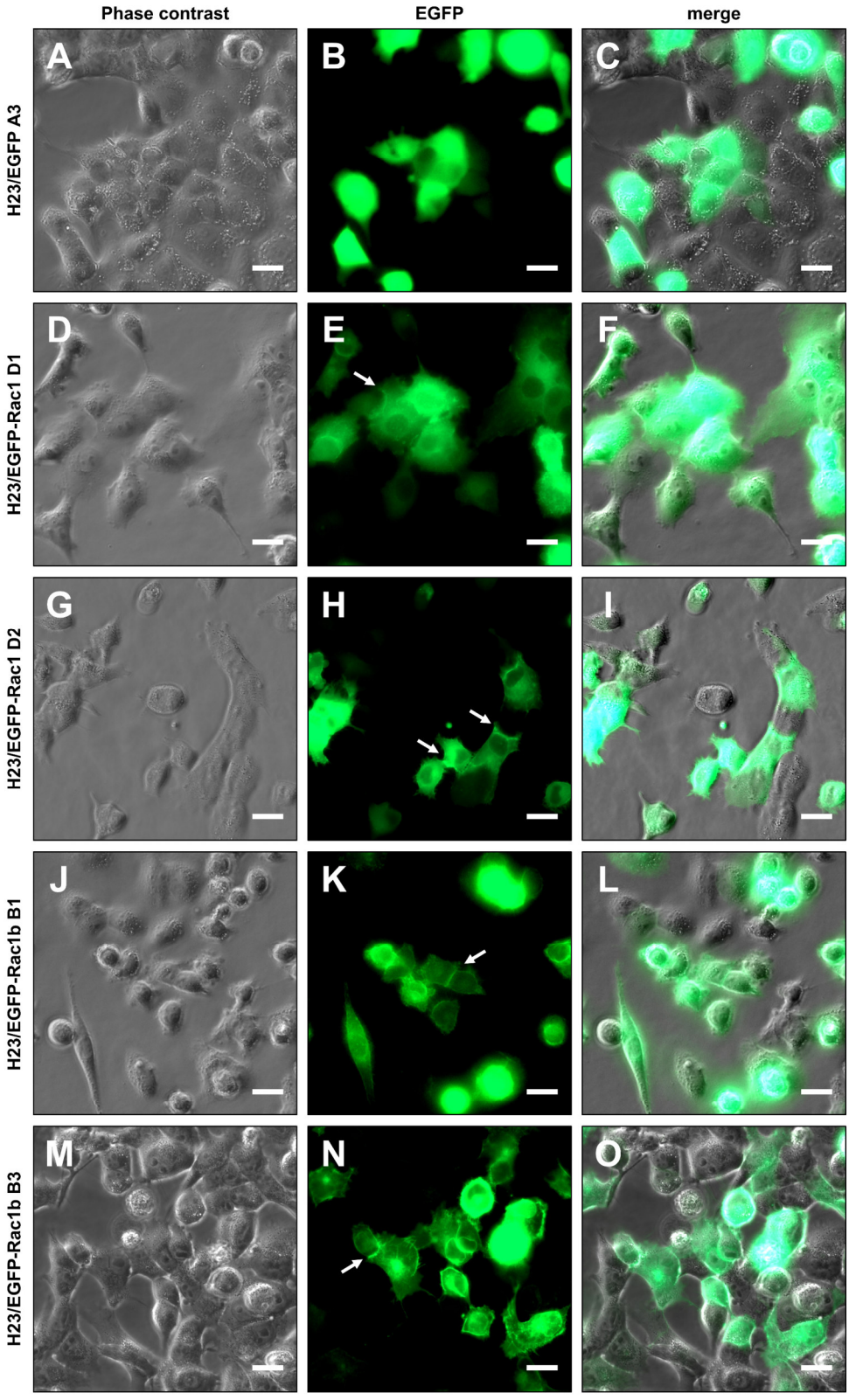

Fig. 3.3: Localization of EGFP, EGFP-Rac1 and EGFP-Rac1b in stably expressing H23 cell clones by fluorescence microscopy. The subcellular localization of ectopically expressed EGFP, EGFP-Rac1 and EGFP-Rac1b fusion proteins was analyzed by using fluorescence microscopy (B, E, H, K, N). Phase contrast images are displayed to show the cell morphology (A, D, G, J, and M). Merged images are also shown (C, F, I, L, and O). (**A-C**) H23/EGFP A3. (**D-F** and **G-I**) H23/EGFP-Rac1 clone D1 and D2. (**J-L** and **M-O**) H23/EGFP-Rac1b clone B1 and B3. The arrows in E, H, K and N indicate areas of cell-cell contacts. Scale bar: 20 µm.

3.2.2 Localization of ectopically expressed EGFP-Rac1 and EGFP-Rac1b using subcellular fractionation

In the next set of experiments, the subcellular localization of EGFP-Rac1 and EGFP-Rac1b was analyzed by subcellular fractionation assays using high speed ultra-centrifugation and western blot procedure. For that, the insoluble, membrane-containing protein fraction (P100) was separated from the fraction containing soluble proteins (S100) for 1 h via centrifugation at 100.000 x g. The subcellular fractionation assays were performed with parental H23 cells, H23/EGFP A3, H23/EGFP-Rac1 D1 and D2 as well as H23/EGFP-Rac1b B1 and B3 cell clones. The presence of EGFP-Rac1 and EGFP-Rac1b as well as endogenous Rac1 and Rac1b in the P100 and S100 fractions was analyzed by an anti-Rac1 and anti-Rac1b antibody. An anti-GFP antibody was used to detect only the EGFP-Rac1 and EGFP-Rac1b fusion proteins. RhoGDIα was detected as a marker for cytosolic proteins, whereas Caveolin served as a marker for membranous proteins. These proteins were detected in a separate western blot experiment and verified the purity of the respective fractions.

As shown in Fig. 3.4, these analyses revealed differences in the subcellular localization of both, the endogenous Rac1 and Rac1b proteins as well as the stably expressed EGFP-Rac1 and EGFP-Rac1b. Endogenous Rac1b was predominantly localized in the P100 fraction, whereas endogenous Rac1 was also present in S100. This was the case for the parental H23 cells as well as all cell clones. EGFP-Rac1 proteins were also detected within the S100 and P100 fractions (see C-D). In contrast, EGFP-Rac1b proteins exhibited an almost exclusive membranous localization within the P100 fraction (see E-F).

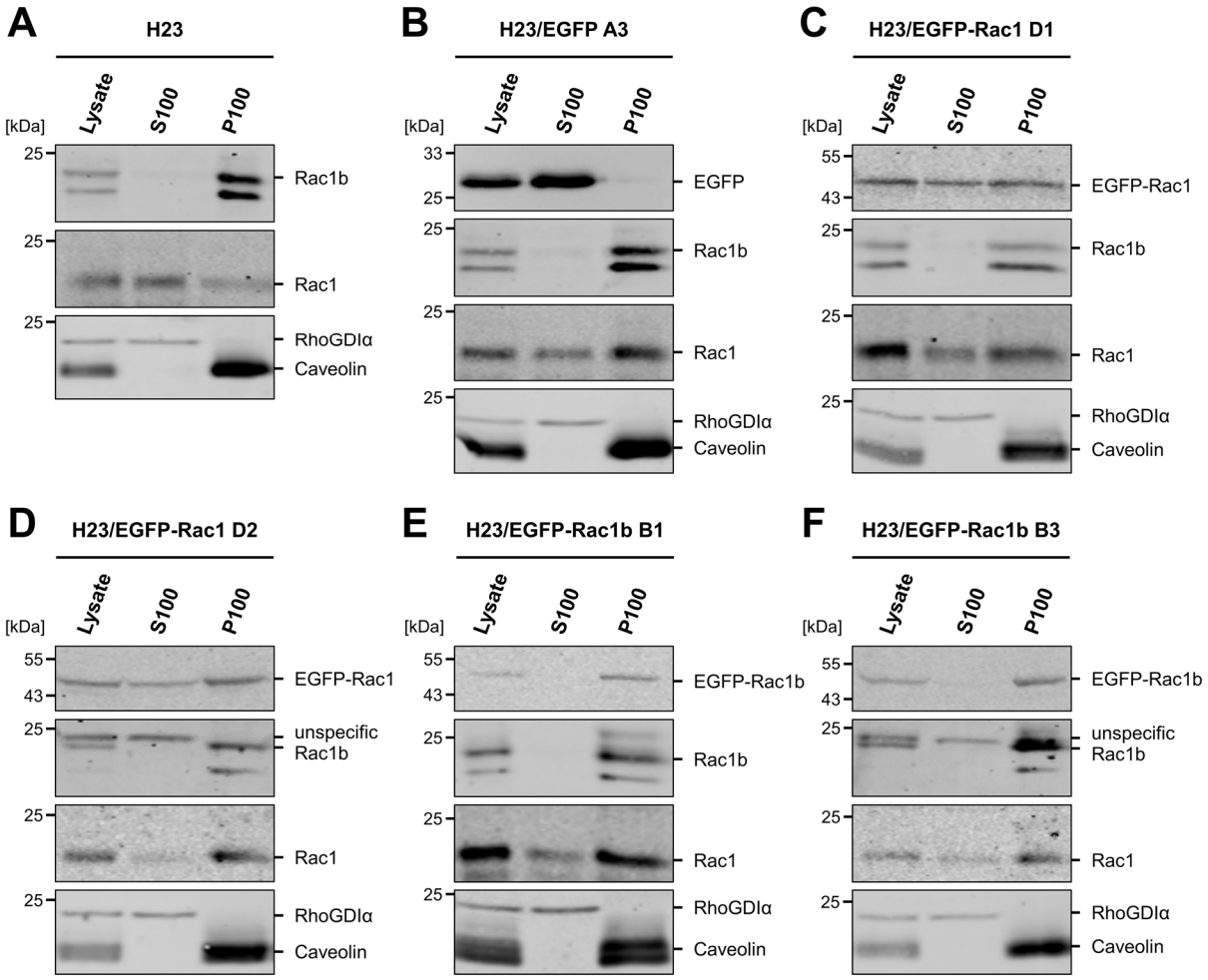

Fig. 3.4: Analysis of the subcellular localization of ectopically expressed EGFP-Rac1 and EGFP-Rac1b stably expressed in H23 cell clones. The insoluble, membrane-containing protein fraction (P100) was separated from the soluble, cytosolic proteins (S100) using centrifugation at 100.000 x g. The fractions and a cell lysate control (Lysate) were separated in 13,5 % SDS polyacrylamide gels and analyzed via western blot procedure. The detection of ectopically expressed EGFP, EGFP-Rac1 and EGFP-Rac1b is shown in the top panels (A: not for parental H23 cells). The subcellular localization of endogenous Rac1b and Rac1 proteins is displayed in the 2nd and 3rd panel (A: top and 2nd panel for parental H23 cells). The purity of the respective fractions was analyzed by detecting the cytosolic marker protein RhoGDIα and the membranous marker protein Caveolin (bottom panel). (**A** and **B**) Parental H23 cells and H23/EGFP clone A3. (**C** and **D**) H23/EGFP-Rac1 clone D1 and D2. (**E** and **F**) H23/EGFP-Rac1b clone B1 and B3. The figure shows representative western blots of two independent experiments.

3.2.3 Subcellular localization of transiently expressed wildtype and mutant Rac1 and Rac1b

The influence of the activity state of Rac1 and Rac1b on their subcellular localization was analyzed by transient expression of HA-tagged constitutive active (G12V) as well as dominant negative (T17N) Rac1 and Rac1b mutants in H1299 cells for 48 h before performing subcellular fractionation assays. The presence of wildtype and mutant HA-tagged Rac1 and Rac1b proteins in the S100 and P100 cellular fractions was elucidated by western blot analyses (see Fig. 3.5). A HRP-coupled anti-HA antibody was used to detect only the ectopically expressed HA-Rac1

and HA-Rac1b fusion proteins. The endogenous Rac1 proteins and also the ectopically expressed wildtype and mutant HA-tagged Rac1 and Rac1b were detected using anti-Rac1 and anti-Rac1b antibodies. These experiments revealed a predominantly membranous localization of wildtype HA-Rac1b and the constitutive active as well as the dominant negative HA-Rac1 and HA-Rac1b mutants. In contrast, wildtype HA-Rac1 was detected in cytoplasmic and membranous cellular fractions.

Interestingly, when the cells were analyzed 24 h after transfection, wildtype Rac1b was present in the cytosolic, rather than the membranous fraction (data not shown). This demonstrated that a minimal incubation time period of 48 h after transfection is necessary for proper subcellular localization of ectopically expressed Rac1 and Rac1b proteins.

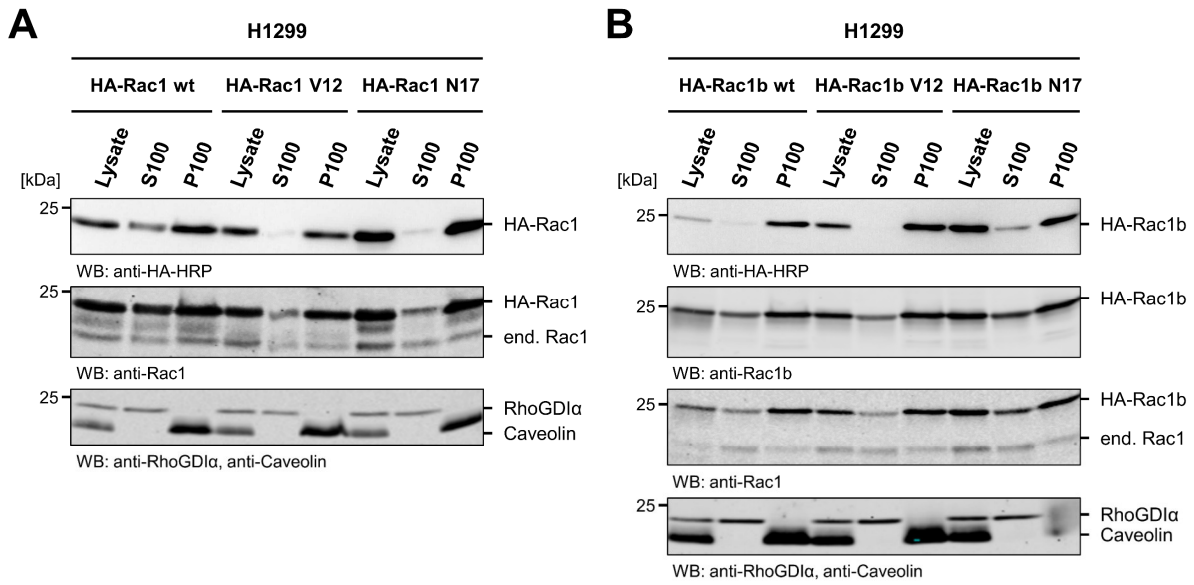

Fig. 3.5: Analysis of the subcellular localization of ectopically expressed wildtype and mutant Rac1 and Rac1b. H1299 lung carcinoma cells were transiently transfected with pCGN expression plasmids, that encoded wildtype (wt), constitutive active (V12), and dominant negative (N17) HA-tagged (**A**) Rac1 and (**B**) Rac1b, respectively. After incubation for 48 h, the insoluble, membrane-containing protein fraction (P100) was separated from the soluble, cytosolic proteins (S100) using ultra-centrifugation at 100.000 x g. The fractions and a cell lysate control (Lysate) were separated in 13,5 % SDS polyacrylamide gels and analyzed via western blot procedure. The top panel shows the subcellular localization of ectopically expressed wildtype and mutant HA-Rac1 and HA-Rac1b fusion proteins as detected by a HRP-coupled anti-HA antibody. The detection of endogenous Rac1 proteins and also the wildtype and mutant HA-tagged Rac1 and Rac1b fusion proteins with specific antibodies is shown in the 2nd and 3rd panel. The detected cytosolic marker protein RhoGDIα and the membranous marker protein Caveolin, which served to verify the purity of the fractions, are displayed in the bottom panel. The figure shows representative western blots of two independent experiments.

3.2.4 Analysis of a nuclear localization of endogenous Rac1 and Rac1b

In addition to the separation of S100 and P100 fractions, nuclear proteins were extracted via ultra-centrifugation and analyzed by western blot procedure. For this, the pancreatic carcinoma cell lines Colo357, PANC-1 Capan-2 and the immortalized human pancreatic duct epithelial cells H6c7 as well as the lung carcinoma cell lines H358, HTB-55, HCC44 and H2122 were used. Lamin A/C confirmed the presence of nuclear proteins within NE.

In PANC-1, Colo357 and HTB-55 cells, but not in H358 cells, Rac1 and Rac1b, were both detected in NE in very small amounts (see Fig. 3.6: NE). Both Rac1 isoforms were very heterogeneously detected within nuclear extracts between different cell lines. Moreover, the endogenous Rac1b isoform was predominantly detected in the P100 fraction for PANC-1 and Colo357 pancreatic carcinoma cells as well as H358 and HTB-55 lung carcinoma cells. In contrast, the endogenous Rac1 proteins were present within the P100 and S100 fraction. These findings were consistent for all the other analyzed pancreatic and lung cell lines (data not shown). Furthermore, the subcellular localization of endogenous Rac1 and Rac1b, elucidated for several pancreatic and lung carcinoma cell lines, were consistent with the localization of stably and transiently expressed wildtype EGFP-Rac1 and EGFP-Rac1b as well as transiently expressed HA-Rac1 and HA-Rac1b fusion proteins as described in the previous two chapters.

Altogether, these analyses revealed differences in the cytoplasmic and membranous subcellular localization between Rac1 isoforms. Specifically, the analyses of functional mutants uncovered, that the subcellular localization depended on the activity state of the small GTPases. The subcellular localization of wildtype Rac1b was comparable to that of constitutive active Rac1 (G12V), where wildtype Rac1 was present in cytoplasmic and membranous cellular fractions. Differences in the nuclear localization of both GTPase isoforms were not identified with the experiments performed in this work.

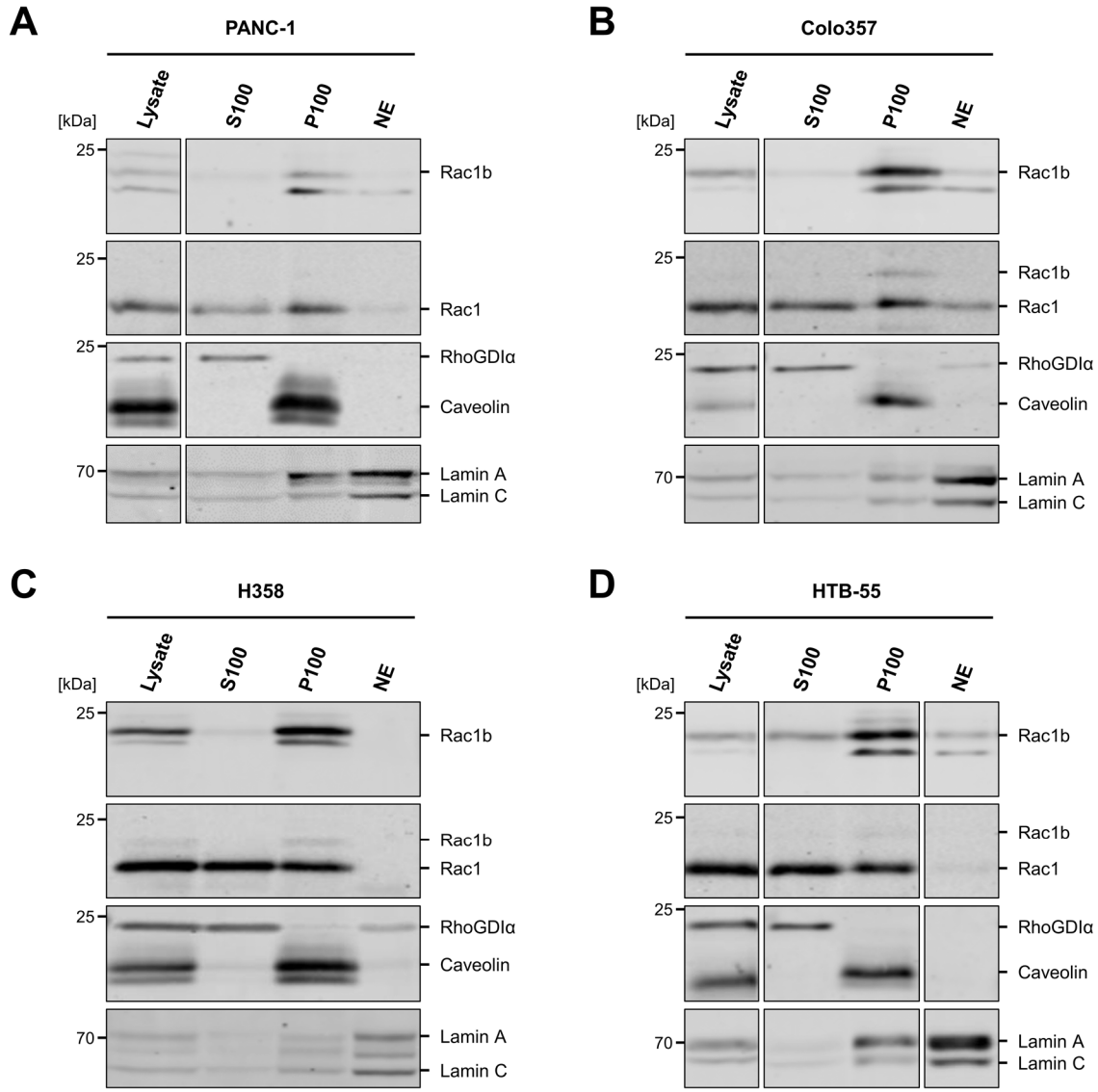

Fig. 3.6: Analysis of the nuclear localization of endogenous Rac1 and Rac1b in pancreatic and lung carcinoma cells. Differences in the subcellular localization of endogenous Rac1 and Rac1b were analyzed in (**A**) PANC-1 and (**B**) Colo357 pancreatic as well as (**C**) H358 and (**D**) HTB-55 lung carcinoma cells. The soluble, nuclear proteins (NE) and the insoluble, membrane-containing protein fraction (P100) as well as the soluble, cytosolic proteins (S100) were isolated by using ultra-centrifugation at 100.000 x g. The fractions and a cell lysate control (Lysate) were separated in 13,5 % and 10 % SDS polyacrylamide gels and analyzed via western blot procedure. The detection of endogenous Rac1b and Rac1 proteins by using an anti-Rac1b and anti-Rac1 antibody is shown in the top and 2nd panel. The cytosolic and membranous marker proteins RhoGDIα and Caveolin verified the purity of the respective fractions (3rd panel). Lamin A/C confirmed the presence of nuclear proteins in NE (bottom panel). The figure shows representative western blots of three or four independent experiments.

3.3 Analysis of cellular invasion with the chorioallantoic membrane invasion model

The chorioallantoic membrane (CAM) invasion model was utilized as an *in vivo* model for analyzing the invasion of carcinoma cells into tissues, in this case the CAM of chick embryos. In the course of this work, possible Rac1- and Rac1b-specific effects on cellular invasion were analyzed. For that, cells were incubated on the CAM for four days and tissue sections prepared as described in detail in Ch. 2.2.5. Additionally, the protocol of the CAM invasion assay is graphically summarized in Fig. 3.7. Hemalum eosin-stained tissue sections were analyzed to assess carcinoma cell invasion into the CAM.

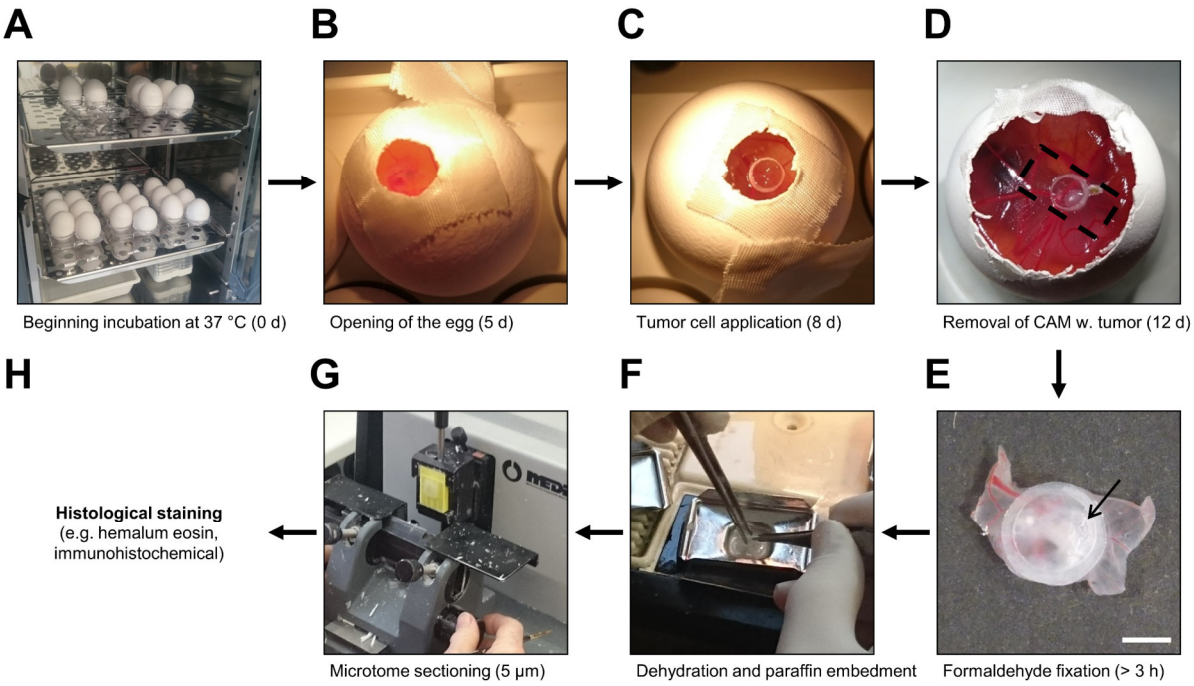

Fig. 3.7: The chorioallantoic membrane invasion assay. (**A-H**) Workflow of the chorioallantoic membrane (CAM) invasion assay. (**E**) Scale bar: 3 mm.

3.3.1 Invasion of Rac1b-expressing pancreatic and lung carcinoma cells into the chorioallantoic membrane of chick embryos

The invasion of the Colo357 pancreatic and H358 as well as HTB-55 lung carcinoma cells with high Rac1b as well as H23 cells with low Rac1b protein amounts was assessed to analyze a possible effect of high endogenous Rac1b protein expression on tumor cell invasion.

The data presented in Fig. 3.8 revealed, that Colo357 cells exhibited weak invasive potential with the majority of cells remaining in a solid tumor cell nest on top of the CAM. In four of eight cases, small cell aggregates disseminated form the primary cell mass and invaded into the mesenchymal layer of the CAM, leading to the thickening of the area around the infiltration (see A-C). The H358 lung carcinoma cells also formed solid cell masses with varying invasive behavior. The cells of seven of eleven H358-derived inoculations, invaded through the outer epithelium of the CAM and formed solid tumors within the mesenchymal layer. The CAM was markedly thickened at the area of cell infiltration (see D-F). For the lung carcinoma cell line HTB-55 no invasion was observed in all nine cases. The cells were completely located on top of the outer epithelium of the CAM (see G-I). The H23 lung carcinoma cell line exhibited a high invasive potential. The cells of all three H23-derived inoculations broke through the outer epithelial layer of the CAM and spread into surrounding regions of the mesenchyme (see J-K). The results of all CAM invasion experiments were summarized in Tab. 3.2. Altogether, the CAM invasion assays did not reveal a conclusive connection between high Rac1b protein expression and tumor cell invasion.

Tab. 3.2: Results of the CAM invasion assays of Colo357 pancreatic as well as H358, HTB-55 and H23 lung carcinoma cells. The numbers of cases, in which the cells displayed invasive and non-invasive behavior, are totals, added up from all the CAM invasion experiments performed. The combined results of two (H23) or three (Colo357, H358, and HTB-55) independent CAM invasion experiments (n) were listed, in which three to eight eggs were used per cell line.

Cell line	Eggs (n)	Cell behavior	
		invasive	non-invasive
Colo357	8 (3)	4	4
H358	11 (3)	7	4
HTB-55	9 (3)	0	9
H23	3 (2)	3	0

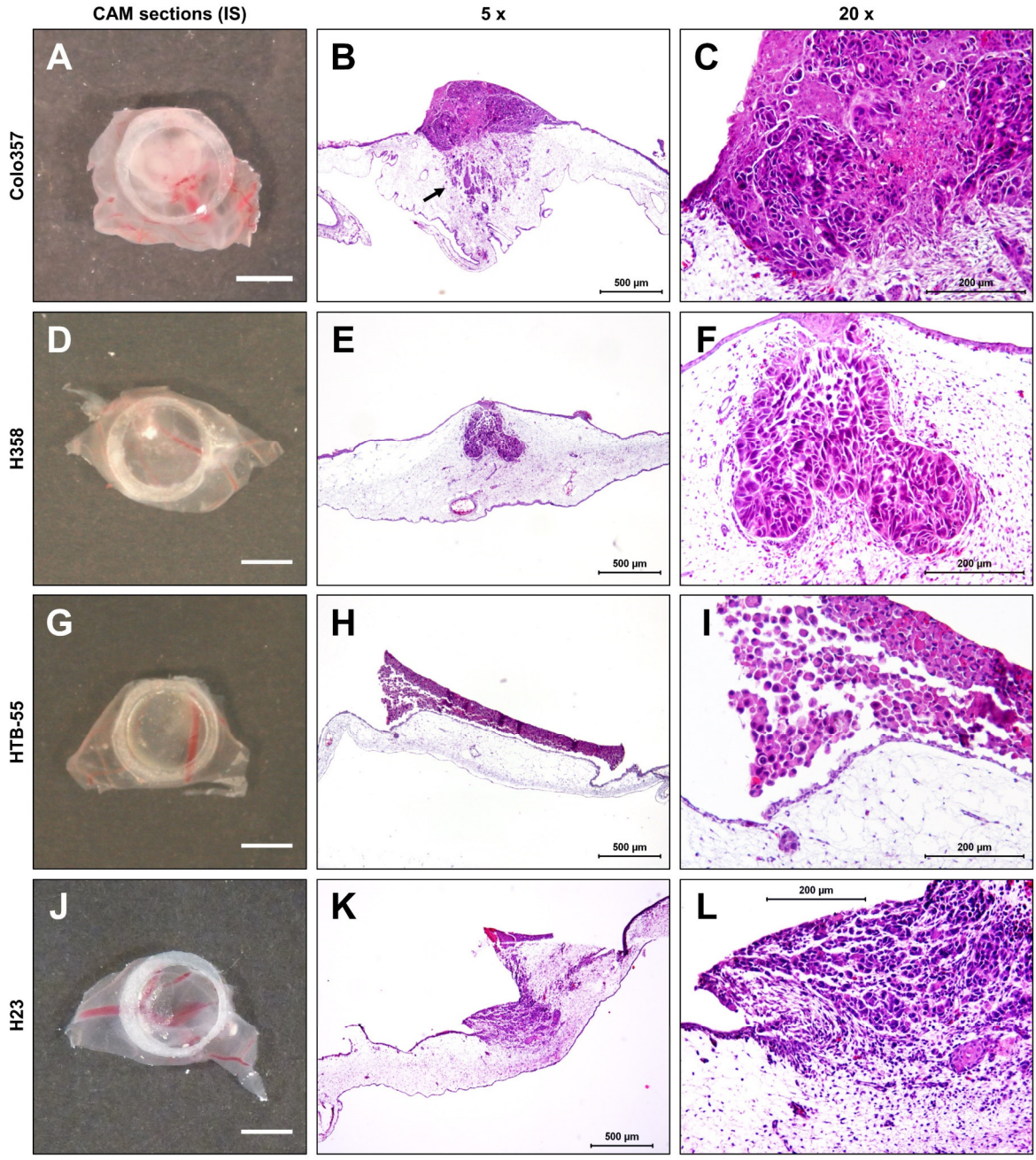

Fig. 3.8: Analysis of the invasion of pancreatic and lung carcinoma cells into the chorioallantoic membrane of chick embryos. The invasion of (**A-C**) Colo357 pancreatic, (**E-F**) H358 and (**G-I**) HTB-55 lung carcinoma cells with high Rac1b protein levels as well as (**J-L**) H23 lung carcinoma cells with a low Rac1b-to-Rac1 ratio was assessed by using the chorioallantoic membrane (CAM) invasion model. Four days after the carcinoma cells (1 x 10^6 cells/egg) were xenografted onto the CAM of fertilized chicken eggs, CAM sections were retrieved at the inoculations sites (IS) and fixed using formaldehyde. A, D, G and J display representative images of CAM sections for each cell line taken directly after CAM retrieval. Scale bar: 3 mm. The embedded CAM sections were cut into 5 µm slices and stained using hemalum eosin. Representative microscopic images of each cell line are shown taken at a 5 x and a 20 x magnification. Scale bars: 500 µm (5 x) and 200 µm (20 x). Arrow: Invading Colo357 cells. The figure shows representative images of two or three independent experiments for each cell line.

3.3.2 Invasion of H23 cell clones stably expressing EGFP, EGFP-Rac1 and EGFP-Rac1b

Additionally, H23/EGFP clone A3, H23/EGFP-Rac1 clone D1 and D2 as well as H23/EGFP-Rac1b clone B1 and B3 cells were xenografted onto the CAM. Representative results are shown in Fig. 3.9.

H23/EGFP A3 cells exhibited a high invasive capacity. In four of five cases the cells broke through the outer epithelium and spread into the underlying mesenchyme tissue of the CAM, leading to the thickening of the area around the infiltration (see A-C). Both EGFP-Rac1 expressing cell clones, H23/EGFP-Rac1 D1 and D2, invaded and spread into the mesenchymal CAM tissue in all cases (see D-I). A strong invasive capacity was also observed for the H23/EGFP-Rac1b B1 and B3 cell clones. In six of eight and four of five cases, the H23/EGFP-Rac1b B1 and B3 cells invaded into mesenchyme of the CAM and formed large tumor cell nests within (see J-O). In contrast to H23/EGFP-Rac1 D1 and D2 cells, single cell dissemination from the primary cell mass was not observed. Rather the presence of multiple tumor nests was identified (see L and O).

The results of the CAM invasion experiments for all five H23 cell clones are summarized in Tab. 3.3. In conclusion, stable ectopic expression of EGFP-Rac1b did not alter the invasive potential of H23 cells, but rather the characteristics of the tumors formed. In contrast to EGFP and EGFP-Rac1 expressing H23 cell clones, cells stably expressing EGFP-Rac1b formed large solid tumor nests without obvious single cells dissemination.

Tab. 3.3: Results of the CAM invasion assays performed with H23 cell clones. The numbers of cases, in which the cells displayed invasive and non-invasive behavior, are totals, added up from all the CAM invasion experiments performed. The combined results of two (H23/EGFP A3, H23/EGFP-Rac1 D2, and H23/EGFP-Rac1b B3) or three (H23/EGFP-Rac1 D2 and H23/EGFP-Rac1b B1) independent CAM invasion experiments (n), in which three to eight eggs were used per cell line are listed.

Cell line	Eggs (n)	Cell behavior	
		invasive	non-invasive
H23/EGFP A3	5 (2)	4	1
H23/EGFP-Rac1 D1	8 (3)	8	0
H23/EGFP-Rac1 D2	5 (2)	5	0
H23/EGFP-Rac1b B1	8 (3)	6	2
H23/EGFP-Rac1b B3	5 (2)	4	1

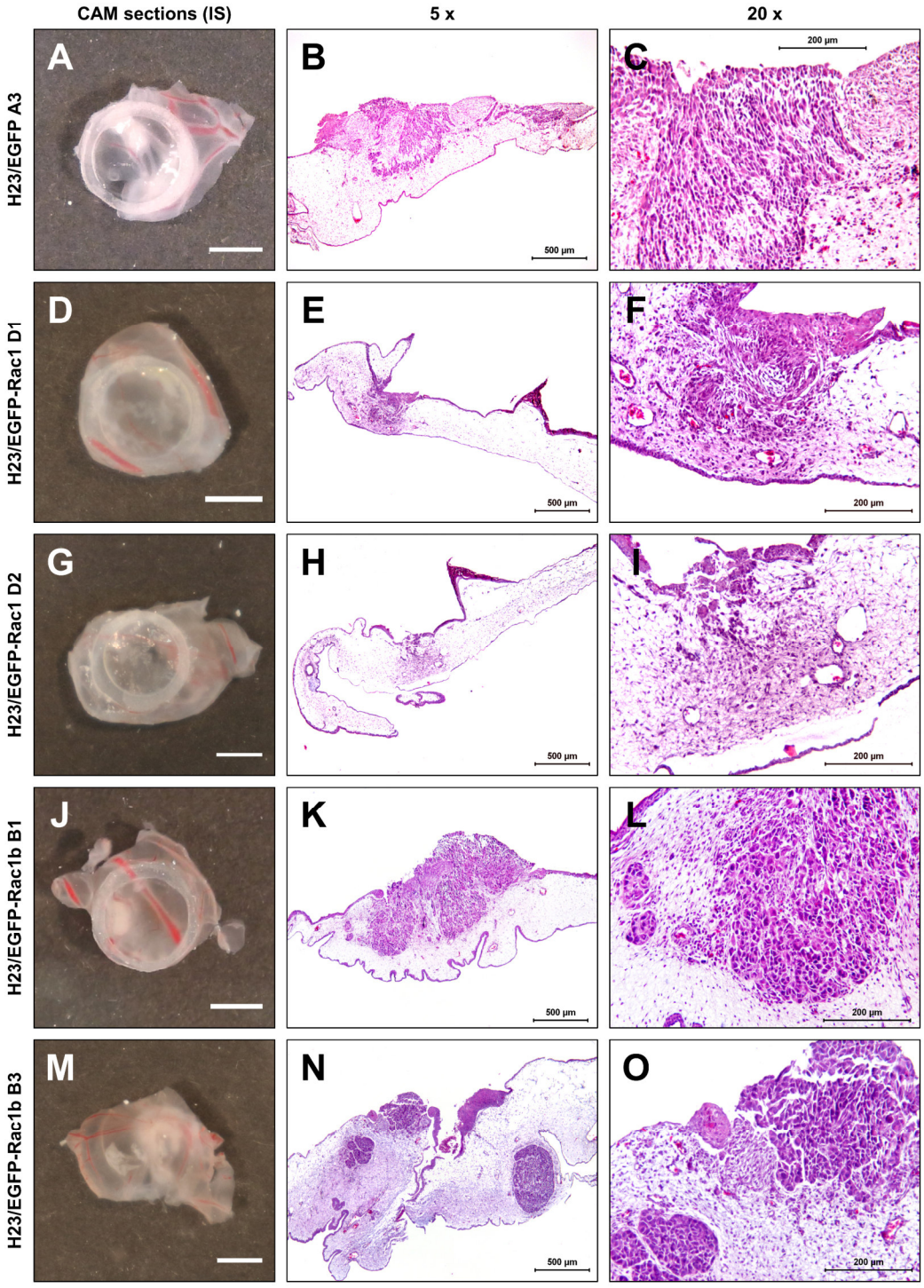

Fig. 3.9: Analysis of the invasion of H23 cell clones into the chorioallantoic membrane of chick embryos. The invasion of H23 cell clones stably expressing EGFP, EGFP-Rac1 and EGFP-Rac1b was analyzed using the chorioallantoic membrane (CAM) invasion model. The figure shows representative results of CAM invasion assays performed with (**A-C**) H23/EGFP A3, (**D-F** and **G-I**) H23/EGFP-Rac1 clone D1 and D2 as well as (**J-L** and **M-O**) H23/EGFP-Rac1b clone B1 and B3. Four days after the carcinoma cells (1 x 10^6 cells/egg) were xenografted onto the CAM of fertilized chicken eggs, CAM sections were retrieved at the inoculations sites (IS) and fixed using formaldehyde. A, D, G, J and M display representative images of CAM sections for each cell clone taken directly after CAM retrieval. Scale bar: 3 mm. The embedded CAM sections were cut into 5 µm slices and stained using hemalum eosin. Microscopic images of each cell clone taken at a 5 x and a 20 x magnification are shown. Scale bars: 500 µm (5 x) and 200 µm (20 x). The figure shows representative images of two or three independent experiments for each cell line.

3.4 The regulation of Rac1 and Rac1b protein and mRNA levels by splicing factors

To analyze factors involved in enhanced Rac1b protein expression in some carcinoma cells, the mRNA and protein expression levels of different splicing factors known to be involved in *RAC1* pre-mRNA maturation were examined and compared to Rac1 and Rac1b amounts. Based on the results, siRNA-mediated depletion experiments were performed to analyze a possible cross talk between the Rac1 isoforms and some of the splicing factors.

3.4.1 Relation of the mRNA and protein expression of Rac1 isoforms and splicing factors involved in *RAC1* pre-mRNA maturation

The mRNA amounts of the different splicing factors involved in *RAC1* pre-mRNA maturation were analyzed by sqRT-PCR in several pancreatic and lung cell lines. The same cDNA samples, as used for analyzing the mRNA levels of *RAC1* and *RAC1B,* were used. Specific primer pairs were used to detect the mRNA amounts of *ESRP1*, *ESRP2*, *SRSF1*, *SRSF3* and *HNRNPA1* in separate sqRT-PCR experiments (see Tab. 2.11). The sqRT-PCR results of the *RAC1* isoforms as well as *ACTB* (as shown in Fig. 3.1) were added to the results displayed in Fig. 3.10.

These sqRT-PCR analyses revealed a positive association of the mRNA levels of *RAC1B* with *ESRP1* and *ESRP2*. High amounts of *ESRP1* and *ESRP2* mRNA were detected in the pancreatic carcinoma cell lines Colo357, Capan-1, Capan-2, BxPC-3 and the duct epithelial cells H6c7, in which relatively high levels of *RAC1B* mRNA were detected (see A: top and 2nd panel). Correspondingly, elevated amounts of *ESRP1* and *ESRP2* mRNA correlated with high *RAC1B* mRNA levels in the lung carcinoma cell lines H358, HTB-55 and H2122 (see B: top and 2nd panel). In contrast, the cell lines with weak or non-detectable *RAC1B* mRNA content displayed weak or non-detectable *ESRP1* and *ESRP2* levels, respectively. This was the case for MIA PaCa-2 pancreatic carcinoma cells as well as HCC44, Colo699, H23, H1299 and A549 lung carcinoma cells. In contrast, PANC-1 cells expressed relatively high amounts of *ESRP2* mRNA. The mRNA levels of *SRSF1* and *SRSF3* did not vary strongly, whereas the amounts of *HNRNPA1* mRNA showed marked differences between all analyzed pancreatic and lung cell lines (see A and B: 3rd, 4th and 5th panel). Nevertheless, a relation between the mRNA amounts of *SRSF1*, *SRSF3* or *HNRNPA1* and *RAC1B* was not observed.

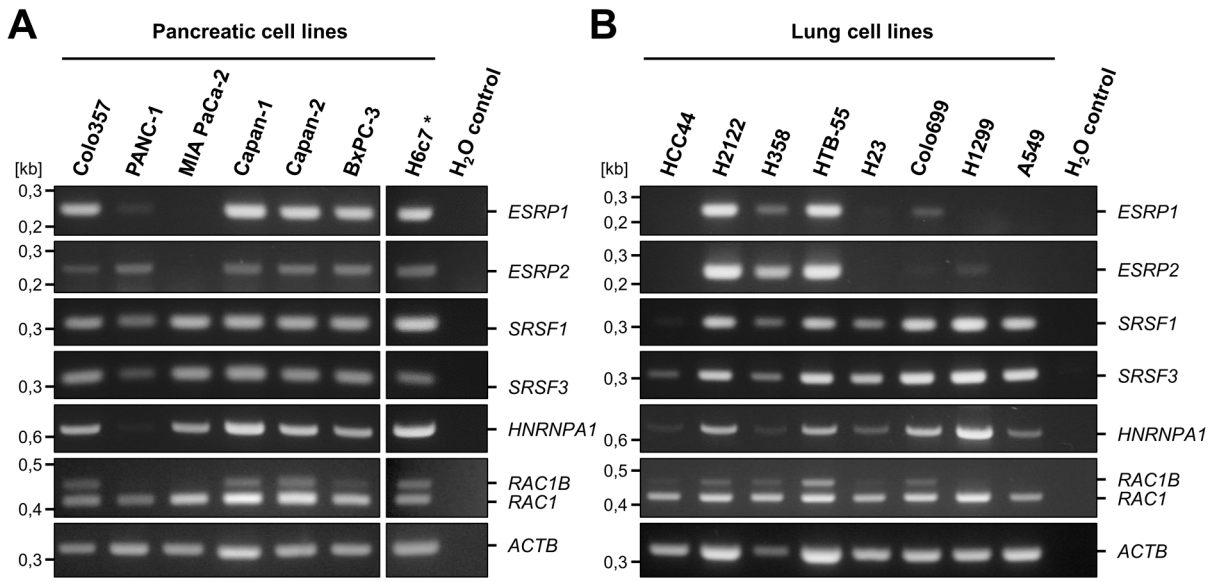

Fig. 3.10: Semi quantitative analyses of the mRNA content of different splicing factors involved in *RAC1* pre-mRNA maturation in pancreatic and lung cell lines. The sqRT-PCR experiments were carried out using cDNA samples of established (**A**) pancreatic and (**B**) lung cell lines. The results of individual sqRT-PCR experiments to detect the mRNA levels of the splicing factors *ESRP1*, *ESRP2*, *SRSF*1, *SRSF3* and *HNRNPA1* are displayed (top to 5th panel). The sqRT-PCR results of the *RAC1* isoforms (6th panel) and *ACTB* (bottom panel) were added to the figure and were already shown in Fig. 3.1. The figure shows representative agarose gels of three independent experiments. (*) One experiment was carried out for H6c7 cells.

In the next set of experiments, a relation between the protein levels of Rac1b and ESRP1 as well as ESRP2 was analyzed. The same cell lysates of pancreatic and lung cell lines were used, which had been analyzed regarding the protein expression of Rac1 and Rac1b beforehand. The results of the Rac1b and β-Actin detection shown in Fig. 3.2 were added to the results displayed in Fig. 3.11. Elevated amounts of ESRP1 proteins were associated with a high protein content of Rac1b in the pancreatic cell lines Colo357, Capan-1, Capan-2, BxPC-3 and H6c7 cells (see A). This is also the case for the lung carcinoma cell lines H358, HTB-55 and H2122, but not for HCC44 cells (as shown in B). ESRP2 proteins were detected in Colo357, PANC-1, Capan-2, BxPC-3 and H6c7, but not in Capan-1 cells. High ESRP2 protein levels were observed in the lung carcinoma cells H358, HTB-55, and H2122, but also in HCC44. Little amounts of ESRP2 protein were detected in H23 and H1299 cells. Protein expression of ESRP1 and ESRP2 was not identified in MIA PaCa-2 pancreatic and A549 lung carcinoma cells (as shown in A and B).

Additionally, the ESRP1 and ESRP2 protein levels were analyzed in RIPA cell lysates of H23 cell clones, which stably expressed EGFP, EGFP-Rac1, and EGFP-Rac1b. In parental H23 cells no protein expression of ESRP1 and only very low amounts of ESRP2 proteins were identified (see B and D). Stable ectopic expression of EGFP-Rac1 and EGFP-Rac1b in H23 cells did not influence the protein expression of neither ESRP1 nor ESRP2 (data not shown).

Altogether, the expression levels of endogenous Rac1b and ESRP1 as well as ESRP2 were positively associated with each other on the mRNA and protein level. This was particularly the case in pancreatic cell lines, but also evident in several lung carcinoma cell lines. To analyze whether this relation was also linked to cooperative effects between Rac1b and the two splicing factors, siRNA-mediated depletion experiments were performed next.

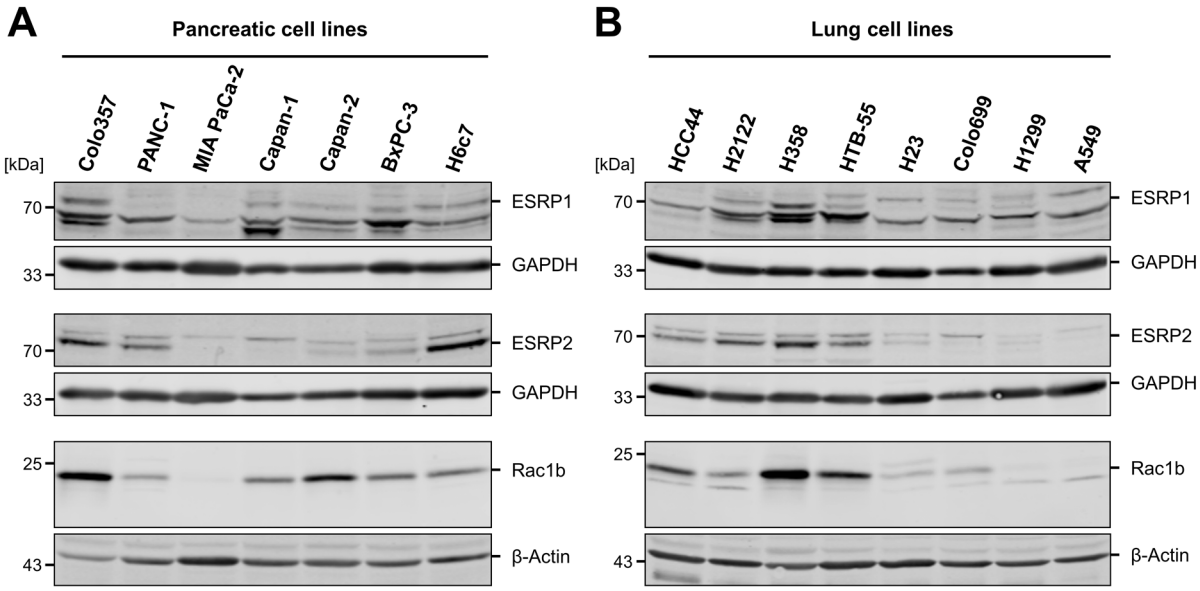

Fig. 3.11: Western blot analysis of ESRP1 and ESRP2 protein levels in pancreatic and lung cell lines. The western blot experiments to compare the protein amounts of Rac1b and ESRP1 as well as ESRP2 were carried out using RIPA cell lysates of (**A**) pancreatic and (**B**) lung cell lines. The detection of ESRP1 is displayed in the top panel and of ESRP2 in the 3rd panel. GAPDH protein levels were detected in each western blot (2nd and 4th panel). The detection of the Rac1b and β-Actin protein levels were already shown in Fig. 3.2 and added to this figure (5th and 6th panel). The figure shows representative western blots of two independent experiments.

3.4.2 Specifying the relation between Rac1b and ESRPs by siRNA-mediated knockdown experiments

To determine a possible cross talk between Rac1b, ESRP1 and ESRP2 siRNA-mediated depletion experiments were performed in the pancreatic carcinoma cell line Colo357 as well as in the two lung carcinoma cell lines H358 and HTB-55. The most efficient knockdown was achieved by performing two consecutive transfections within 24 h and incubating the cells for a total of 96 h after the first transfection (total incubation time: 96 h [1. transfection], 72 h [2. transfection]). A mixture of two Rac1b-specific siRNAs as well as commercially available pools of four ESRP1- and ESRP2-specific siRNAs were used. Additionally, different siRNAs were tested to deplete Rac1 proteins (see Tab. 2.13). Neither the tested transfection conditions, nor the used siRNAs led to a Rac1 knockdown higher than 40 % in comparison to the control (data not shown). Thus, the following experiments were carried out without depleting Rac1.

3.4.2.1 RT-PCR analysis of *RAC1* isoform and *ESRP* mRNA levels after siRNA-mediated silencing

Colo357 pancreatic as well as H358 and HTB-55 lung carcinoma cells were transfected with specific siRNAs to knockdown the *RAC1B*, *ESRP1* and *ESRP2* mRNAs. After generating cDNAs, semi quantitative RT-PCR analyses were performed. To allow quantitative statements, densitometric analyses of two independent experiments were performed and evaluated as described in Ch. 2.2.6.1. The values of the fold change (FC) in relation to siControl (set to 1,0), which are stated below, are means of two independent experiments. The individual values of the two experiments were highlighted by the scatter plots in Fig. 3.12.

These analyses verified the depletion of the *RAC1B*, *ESRP1* and *ESRP2* mRNAs by the respective specific siRNAs. The mRNA levels of *RAC1B* were depleted in Colo357 (FC = 0,48 x), in H358 (FC = 0,13 x) as well as in HTB-55 cells (FC = 0,36 x). The mRNA levels of *ESRP1* were weakly depleted in Colo357 cells (FC = 0,71 x) and reduced by 50 % in H358 (FC = 0,47 x) as well as HTB-55 cells (FC = 0,46 x). *ESRP2* mRNA contents were downregulated strongly in Colo357 (FC = 0,30 x) as well as H358 cells (FC = 0,08 x) and reduced by only 40 % in HTB-55 cells (FC = 0,57 x). Interestingly, *ESRP2* mRNA levels were markedly downregulated in all three analyzed cell lines after siRNA-mediated depletion of *RAC1B*: Colo357 (FC = 0,18 x), H358 (FC = 0,44 x) and HTB-55 (FC = 0,10 x) (see Fig. 3.12 A, B and C: *ESRP2*). Additionally, *RAC1B* mRNA levels were increased after depletion of *ESRP1* in H358 cells (FC = 1,43 x) (see B: *RAC1B*). The siRNA-mediated knockdown of neither *RAC1B*, *ESRP1* nor *ESRP2* had any effect on the mRNA levels of *RAC1*.

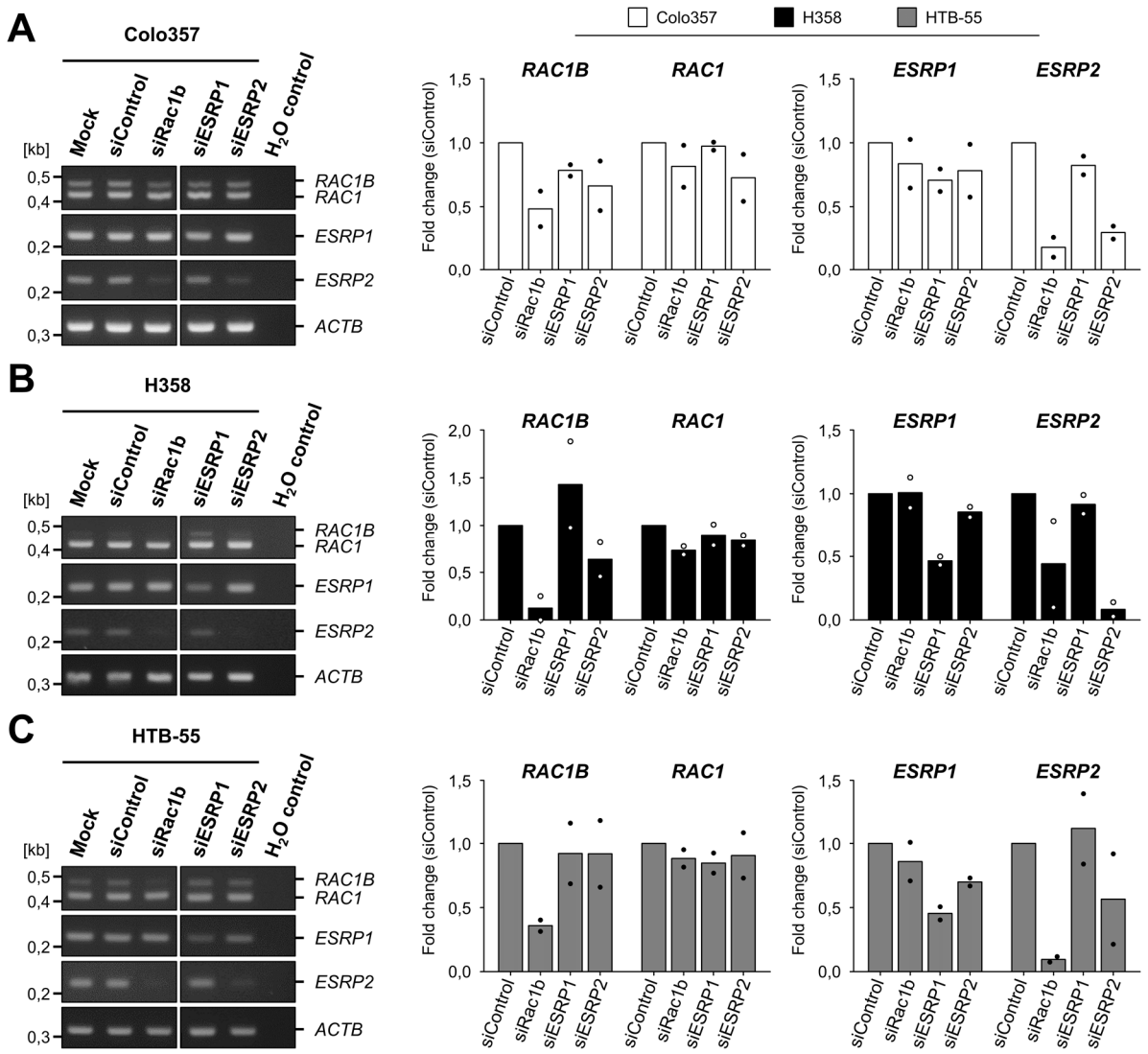

Fig. 3.12: Semi quantitative RT-PCR analysis of *RAC1* isoform and *ESRP* mRNA levels after siRNA-mediated depletion in Colo357, H358 and HTB-55 cells. The (**A**) Colo357 pancreatic as well as (**B**) H358 and (**C**) HTB-55 lung carcinoma cells were transfected twice with specific siRNAs against *RAC1B* (siRac1b), *ESRP1* (siESRP1) and *ESRP2* (siESRP2) mRNAs. Untransfected cells (Mock) and cells transfected with non-targeting siRNA (siControl) served as controls. 72 h after the second transfection RNA was isolated and reversely transcribed into cDNA. The figure shows representative agarose gels of two independent sqRT-PCR experiments, to detect the mRNA levels of *RAC1* and *RAC1B* (top panel) as well as *ESRP1* (2nd panel) and *ESRP2* (3rd panel). *ACTB* mRNA was detected as a loading control (bottom panel). The bar graphs display the means of densitometric analyses of two independent experiments, whereas the individual values of each experiment are depicted as scatter plots. The normalization was performed as described in Ch. 2.2.6.1.

The findings of the semi quantitative analysis were also analyzed by quantitative, SYBR green-based RT-PCR experiments. Therefore, the same two sets of cDNA samples as well as an additional third set of cDNAs were used. The mRNA quantities of *RAC1B* were analyzed by using a specific primer pair designed for qRT-PCR reactions, whereas predesigned, commercially available primers were applied to detect *ESRP1* and *ESRP2* mRNA amounts (see Tab. 2.12). The mRNA levels of the ubiquitously expressed ribosomal protein lateral stalk subunit P0 (*RPLP0*) were detected as a reference. The fold change (FC) of the relative mRNA quantities in relation to siControl, which was set to 1,0, was calculated by the $2^{-\Delta\Delta Ct}$ method as described in Ch. 2.2.6.2. The values stated below are means and standard deviations (± SD) of three independent experiments. The statistical significance in relation to siControl was analyzed by a one sample t-test.

As shown in Fig. 3.13, these qRT-PCR analyses verified the siRNA-mediated depletion of *ESRP1* and *ESRP2* in Colo357, H358 and HTB-55 cells. Additionally, the upregulation of *RAC1B* mRNA amounts upon depletion of *ESRP1* in H358 cells was confirmed (FC = 2,07 ± 0,69 x) (see C: *RAC1B*). In contrast to the results of the sqRT-PCR experiments, the qRT-PCR analyses revealed, that *ESRP1* and *ESRP2* were upregulated in relation to siControl after siRNA-mediated depletion of *RAC1B*. *ESRP1* was upregulated approximately 1,3 to 1,6-fold in H358, HTB-55 and Colo357 cells, whereas *ESRP2* mRNA levels were increased by 1,2 to 1,5-fold (data not shown). These observations were in contrast to the results of the sqRT-PCR experiments, in which knockdown of *RAC1B* resulted in a strong downregulation of *ESRP2*. Closer inspection of the C_t values revealed, that the *RAC1B* knockdown slightly decreased *RPLP0* mRNA levels, which was indicated by a higher C_t value in comparison to siControl (see Tab. 3.4: *RPLP0*). This led to an apparent upregulation of *ESRP1* and *ESRP2* after calculating the relative mRNA quantities using the $2^{-\Delta\Delta Ct}$ method. Three additional primer pairs for *ACTB* (β-Actin), *GAPDH* (Glyceraldehyde-3-phostphate dehydrogenase) and *B2M* (β-2-microglobuline) were tested as reference genes using only the siControl and siRac1b cDNA samples, respectively (data not shown). Comparison of the C_t values revealed, that the siRNA-mediated depletion of *RAC1B* did not alter the C_t values of *ACTB*, *GAPDH* and *B2M* (see Tab. 3.4). All the qRT-PCR experiments described in the following chapters were performed with *ACTB* as a reference gene.

Tab. 3.4: Comparison of the C_t values of different reference genes. The C_t values of the different reference genes *RPLP0*, *ACTB*, *GAPDH* and *B2M* listed below are means of duplicates of three independent qRT-PCR experiments.

Cell line	cDNA	Average C_t values (n = 3)			
		RPLP0	***ACTB***	***GAPDH***	***B2M***
Colo357	siControl	17,99	18,74	18,56	19,42
	siRac1b	18,44	18,86	18,74	19,39
H358	siControl	17,95	18,13	18,46	18,41
	siRac1b	19,05	18,00	18,49	18,30
HTB-55	siControl	18,76	17,83	18,37	19,36
	siRac1b	19,11	17,51	18,20	19,61

The qRT-PCR analyses were repeated using only the siRac1b and siControl cDNA samples and *ACTB* as a reference gene (see Fig. 3.13: *ACTB*). These experiments revealed, that *ESRP1* mRNA levels were not influenced by siRNA-mediated depletion of *RAC1B* as the FC values were comparable to those of siControl. In contrast, the amount of *ESRP2* mRNA was slightly reduced after siRNA-mediated depletion of *RAC1B*. In Colo357 cells, *ESRP2* mRNA amounts were downregulated in two of three cases (individual FC values: 0,693 x, 0,719 x and 1,169 x). In H358 cells, *ESRP2* mRNA levels were downregulated in only one of three experiments (individual FC values: 0,653 x, 0,914 x and 1,042 x). The same was the case in HTB-55 cells, where *ESRP2* mRNA amounts were reduced in only one out of three cases (individual FC values: 0,705 x, 1,007 x and 0,979 x). Furthermore, a significant depletion of *RAC1B* was detected in all three cell lines: Colo357 (FC = 0,37 ± 0,07 x, p = 0,0046), H358 (FC = 0,31 ± 0,21 x, p = 0,0303) and HTB-55 (FC = 0,37 ± 0,07 x, p = 0,0041).

Altogether, the siRNA-mediated depletion experiments and RT-PCR analyses indicate a weak influence of Rac1b on the mRNA levels of *ESRP2* in all three cell lines, whereas a role of ESRP1 in increasing *RAC1B* mRNA levels in H358 cells was also evident.

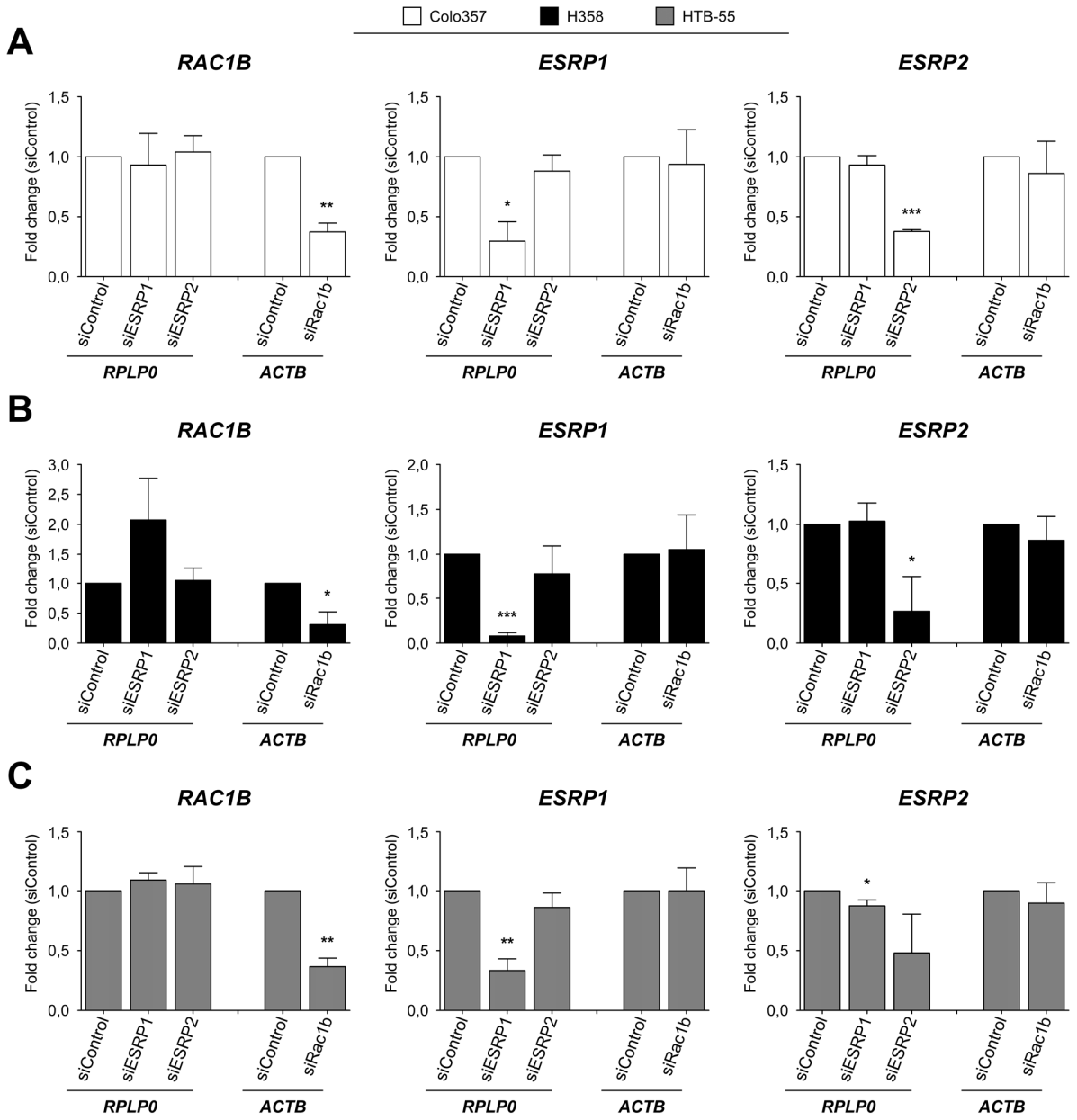

Fig. 3.13: Quantitative RT-PCR analysis of *RAC1B* and *ESRP1* as well as *ESRP2* mRNA levels after siRNA-mediated depletion in Colo357, H358 and HTB-55 cells. The (**A**) Colo357 pancreatic and (**B**) H358 as well as (**C**) HTB-55 lung carcinoma cells were transfected twice with specific siRNAs against *RAC1B* (siRac1b), *ESRP1* (siESRP1) and *ESRP2* (siESRP2). Cells transfected with non-targeting siRNA (siControl) served as controls. 72 h after the second transfection RNA was isolated and reversely transcribed into cDNA. The figure shows the mean ± SD of three independent experiments to detect the mRNA levels of *RAC1B*, *ESRP1* and *ESRP2*. The ribosomal protein lateral stalk subunit P0 (*RPLP0*) mRNA was detected as a reference gene for siESRP1 and siESRP2 cDNA samples, whereas *ACTB* was detected as a reference gene for siRac1b cDNAs. The fold change in relative mRNA quantities ($2^{-\Delta\Delta Ct}$ method) and statistical evaluations (one sample t-test) were calculated in relation to siControl (set to 1,0) as described in Ch. 2.2.6.2 (significance levels: $p < 0{,}05$ = *, $p < 0{,}01$ = **, $p < 0{,}001$ = ***).

3.4.2.2 Analysis of a cross talk of Rac1b, ESRP1 and ESRP2 protein expression after siRNA-mediated knockdown

In the next set of experiments, protein amounts were analyzed in RIPA cell lysates after transfection of Colo357, H358 and HTB-55 cells with specific siRNA against Rac1b, ESRP1 and ESRP2. The changes in protein content were examined by western blot analyses and the intensity of the protein bands was evaluated by densitometric analysis. The statistical significance in relation to siControl (set to 1,0) was assessed as described in Ch. 2.2.6.1.

Representative western blots and the result of the densitometric analyses depicted as the mean ± SD of three independent experiments are shown in Fig. 3.14. These evaluations revealed the following knockdown efficiencies by the corresponding siRNAs: In pancreatic Colo357 carcinoma cells a weak, but significant knockdown of Rac1b (FC = 0,68 ± 0,07 x, p = 0,0152) compared to a distinct depletion of ESRP1 (FC = 0,20 ± 0,12 x, p = 0,007) and a decent knockdown of ESRP2 (FC = 0,46 ± 0,30 x) was observed. In H358 lung carcinoma cells the protein levels of Rac1b (FC = 0,33 ± 0,10 x, p = 0,007), ESRP1 (FC = 0,07 ± 0,17 x, p = 0,011) and ESRP2 (FC = 0,20 ± 0,12 x, p = 0,008) were all reduced significantly. In HTB-55 cells the western blot and densitometric analyses demonstrated an obvious depletion of Rac1b (FC = 0,25 ± 0,04 x, p = 0,001) and of ESRP2 (FC = 0,13 ± 0,09 x, p = 0,004). Due to an overall weak protein detection of ESRP1 in HTB-55 cells, densitometric analyses resulted in strongly varying results. An overall weak depletion of ESRP1 was identified in two of three experiments (individual FC values: 0,295 x, 0,511 x and 1,468 x).

ESRP2 protein levels were slightly, but significantly downregulated after depletion of Rac1b in H358 cells (FC = 0,80 ± 0,06 x, p = 0,030) and in two of three experiments with HTB-55 cells (individual FC values: 0,654 x, 0,300 x and 1,024 x) (see B and C: ESRP2). In Colo357 pancreatic carcinoma cells ESRP2 protein levels were upregulated in one of three experiments (individual FC values: 1,491 x, 1,097 x and 1,045 x). The protein amount of ESRP1 was increased after depletion of Rac1b (FC = 1,74 ± 0,32 x, p = 0,056) and ESRP2 (FC = 1,57 ± 0,16 x, p = 0,026) in H358 cells. These effects were not observed in HTB-55 and Colo357 cells, but Rac1b protein levels of HTB-55 cells were very weakly, but significantly upregulated after the depletion of ESRP1 (FC = 1,17 ± 0,02 x, p = 0,0032).

In conclusion of the siRNA-mediated depletion experiments, a weak influence of Rac1b on the mRNA and protein quantities of ESRP2 was evident in H358 and HTB-55 cells. Furthermore, a role of ESRP1 in regulating the mRNA and protein amounts of Rac1b in H358 cells was observed.

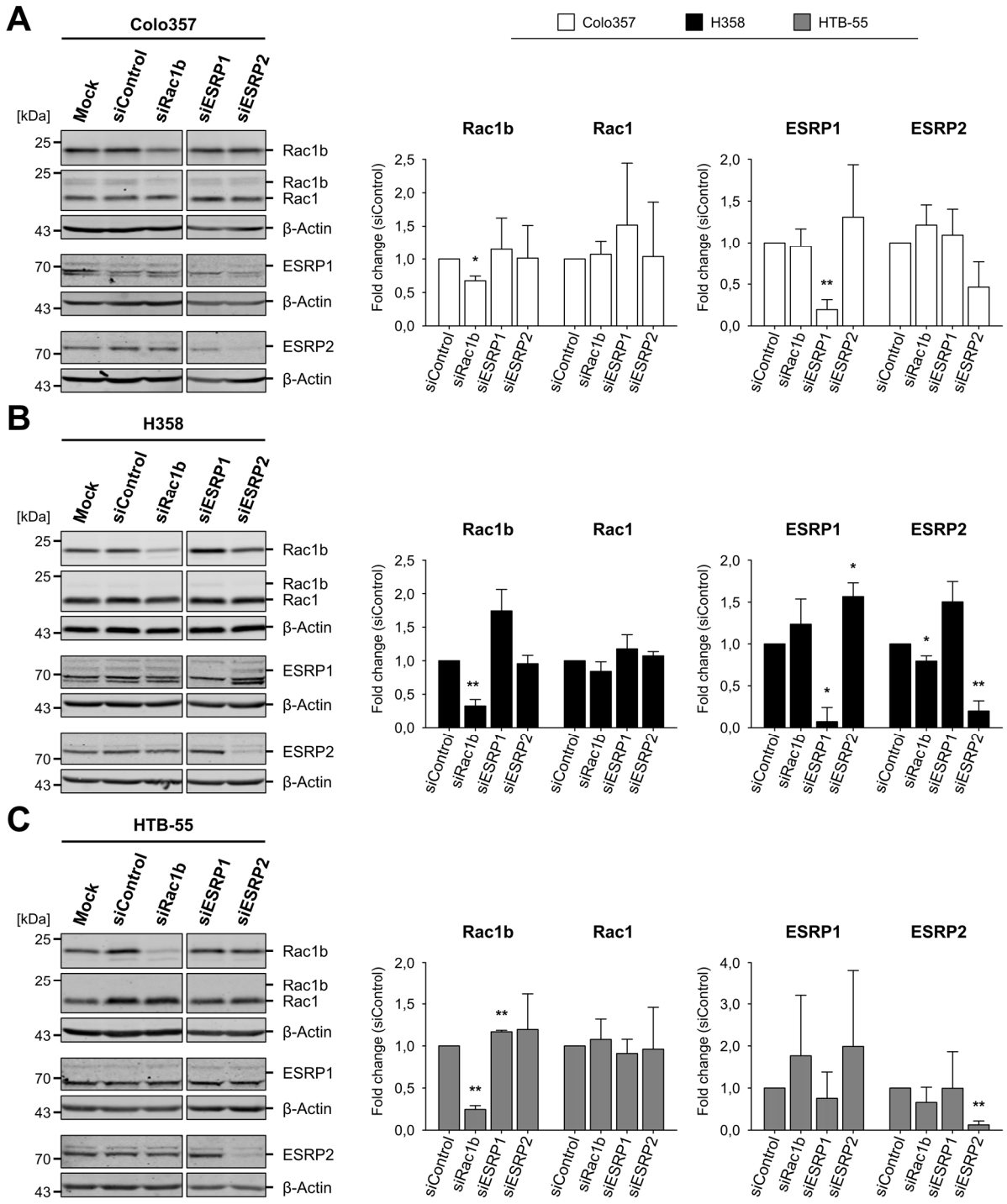

Fig. 3.14: Analysis of Rac1 isoform and ESRP protein levels in Colo357, H358 and HTB-55 cells after siRNA-mediated depletion. The (**A**) Colo357 pancreatic as well as the (**B**) H358 and (**C**) HTB-55 lung carcinoma cell lines were transfected twice with specific siRNAs against Rac1b (siRac1b), ESRP1 (siESRP1) and 2 (siESRP2) and incubated for 72 h. Untransfected cells (Mock) and cells transfected with non-targeting siRNA (siControl) served as controls. RIPA lysates were separated in 13,5 % and 10 % SDS polyacrylamide gels and analyzed via western blot procedure. The figure shows representative western blots of three independent experiments for each cell line, in which Rac1b (top panel), Rac1 and Rac1b (2nd panel), ESRP1 (4th panel) and ESRP2 (6th panel) were detected using specific antibodies. The β-Actin protein levels were detected as a loading control (3rd, 5th and 7th panel). The bar graphs display the means ± SD of densitometric analyses of three independent experiments. The normalization was performed as described in Ch. 2.2.6.1. The statistical differences in relation to siControl (set to 1,0) were analyzed by a one sample t-test (significance levels: $p < 0,05$ = *, $p < 0,01$ = **, $p < 0,001$ = ***).

3.5 The influences of the Rac1b-ESRP2 axis on epithelial-to-mesenchymal transition

In the following experiments, the epithelial-to-mesenchymal transition (EMT) status of different pancreatic and lung cell lines was analyzed by investigating the mRNA and protein amounts of E-Cadherin and Vimentin. Additionally, an effect of the siRNA-mediated silencing of Rac1b, ESRP1 and ESRP2 on the mRNA and protein amounts of these EMT-markers was analyzed in Colo357, H358 and HTB-55 carcinoma cells.

3.5.1 Comparison of the EMT status of pancreatic and lung cell lines with the mRNA and protein expression of Rac1b and ESRPs

The expression levels of E-Cadherin and Vimentin of the pancreatic and lung cell lines were analyzed using sqRT-PCR and western blot analyses and subsequently compared to the mRNA and protein levels of Rac1b and ESRPs. The same cDNA samples and RIPA lysates were used as in the prior analyses described above. Specific primer pairs were used to detect the mRNA amount of the epithelial marker *CDH1* (E-Cadherin) and the mesenchymal marker *VIM* (Vimentin) in individual sqRT-PCR experiments (Tab. 2.11). The sqRT-PCR results of *RAC1B*, *ESRP1* and *ESRP2* were added to Fig. 3.15 to allow a direct comparison of the mRNA expression patterns. These sqRT-PCR analyses revealed a positive relation between the mRNA levels of *CDH1* and *RAC1B*, *ESRP1* as well as *ESRP2*. Reciprocally, the occurrence of *VIM* mRNA correlated negatively with the *RAC1B* mRNA contents. These observations were evident in all the analyzed pancreatic cell lines (shown in A). A similar relation was not as strongly evident in lung carcinoma cells. H2122, H358 and HTB-55 cells, which expressed relatively high amounts of *RAC1B*, *ESRP1* and *ESRP2* mRNA, also displayed high levels of *CDH1* mRNA. But H358 and HTB-55 cells also contained *VIM* mRNA (see B). HCC44 and H23 cells, in which weak mRNA levels of *RAC1B* and no *ESRP1* and *ESRP2* mRNA were detected, also contained *CHD1* and *VIM* mRNA. In contrast, no *CHD1* and high amounts of *VIM* mRNA were detected in Colo699 cells, which were shown to contain weak amounts of *RAC1B*, but no *ESRP1* and *ESRP2* mRNA. A549 cells, in which neither *RAC1B* nor *ESRP1* and *ESRP2* mRNA was detected, exhibited *CDH1* and *VIM* mRNA expression.

In conclusion, the mRNA levels of *RAC1B* correlated positively with the epithelial marker *CDH1* and reciprocally with *VIM* mRNA in pancreatic cells. Moreover, high *RAC1B* mRNA levels also correlated with *CDH1* in some lung carcinoma cells, whereas the expression patterns

of *VIM* mRNA did not seem to be associated with the occurrence of high amounts of *RAC1B* mRNA.

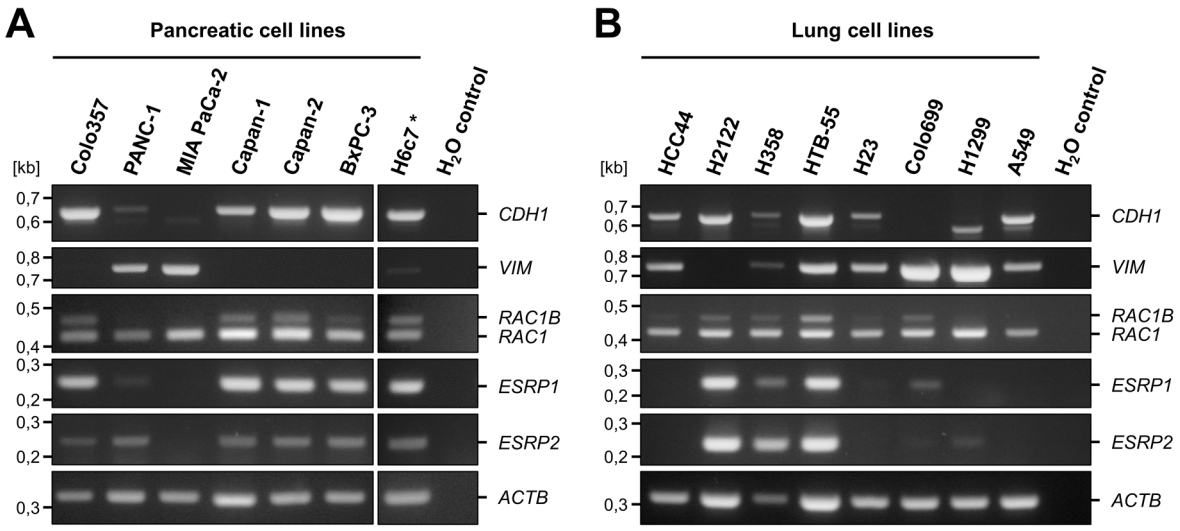

Fig. 3.15: Semi quantitative analysis of the EMT-markers *CDH1* and *VIM* in comparison to the mRNA levels of *RAC1* isoforms as well as *ESRP1* and *ESRP2* in pancreatic and lung cell lines. The sqRT-PCR analyses were carried out using the same cDNA samples of (**A**) pancreatic and (**B**) lung cell lines, which previously had been analyzed regarding the *RAC1*, *RAC1B*, *ESRP1* and *ESRP2* mRNA contents. The figure shows representative agarose gels of three independent sqRT-PCR experiments to detect the mRNA levels of *CDH1* (E-Cadherin) and *VIM* (Vimentin) displayed in the top and 2nd panels. The sqRT-PCR results of the *RAC1* isoforms (3rd panel), *ESRP1* (4th panel), *ESRP2* (5th panel) and *ACTB* (bottom panel) are the same ones shown in Fig 3.10. (*) For H6c7 cells only one experiment was performed.

Next, the protein levels of E-Cadherin and Vimentin were analyzed by performing western blot experiments. The protein expression patterns of both EMT-related marker proteins were compared to the Rac1b protein amounts shown in previous chapters. The results shown in Fig. 3.16 correspond to the results of the sqRT-PCR experiments described above. A correlation in the protein levels of E-Cadherin and Rac1b was detected in the Colo357, Capan-1, Capan-2, BxPC-3 and H6c7 pancreatic cells. PANC-1 and MIA PaCa-2, in which weak or no Rac1b protein contents were observed, contained Vimentin proteins (shown in A). Again, no relationship between Rac1b and E-Cadherin or Vimentin protein amounts were evident in most lung carcinoma cells (see B).

Altogether, the mRNA and protein levels of the epithelial marker E-Cadherin were positively associated with Rac1b mRNA and protein expression particularly in pancreatic cell lines. This was also the case in some lung carcinoma cell lines with high amounts of Rac1b protein and mRNA.

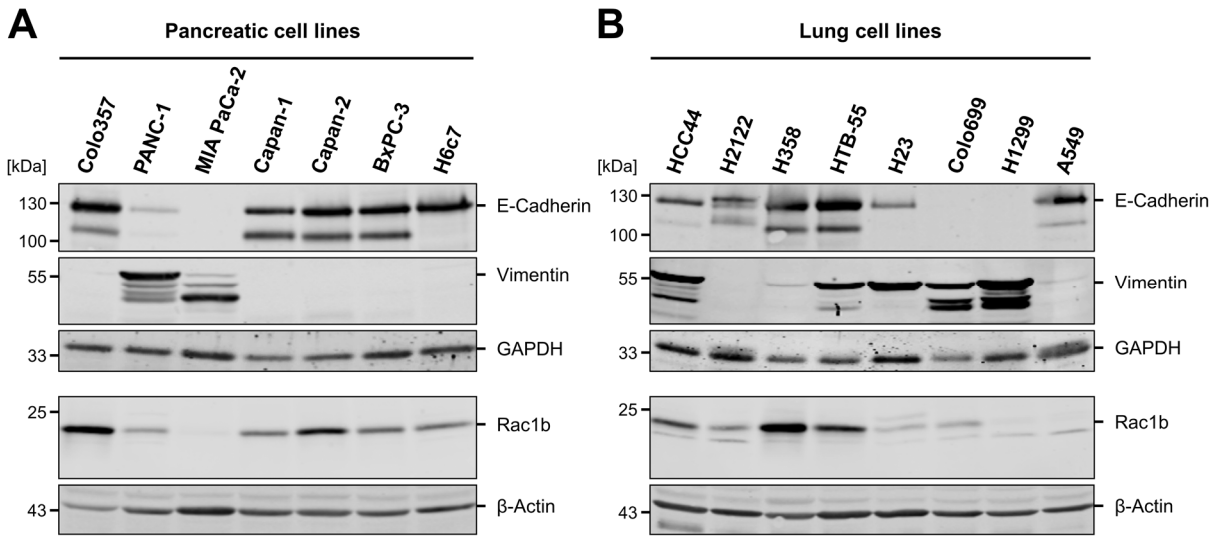

Fig. 3.16: Analysis of the protein amounts of E-Cadherin and Vimentin in comparison to Rac1b in different pancreatic and lung cell lines. The western blot experiments were performed with RIPA lysates of (**A**) pancreatic and (**B**) lung cell lines. The figure shows representative western blots of two independent experiments, in which E-Cadherin (top panel) and Vimentin proteins (2nd panel) were detected using specific antibodies. The detection of GAPDH is also displayed (3rd panel). The detection of the Rac1b and β-Actin proteins was already shown in Fig. 3.2 and added to this figure (4th and bottom panel).

3.5.2 Analysis of a Rac1b-ESRP-dependent influence on EMT markers after siRNA-mediated knockdown

Next, the effects of siRNA-mediated depletion of Rac1b, ESRP1 or ESRP2 on the EMT markers E-Cadherin and Vimentin of Colo357, H358 and HTB-55 cells were analyzed on mRNA and protein level. Therefore, sqRT-PCR analyses, western blot experiments and qRT-PCR analyses were conducted. To directly compare the results with the Rac1b-ESRP2 effect described above, the same cDNA and protein preparations were used.

Neither the sqRT-PCR analyses nor the western blot experiments revealed marked changes in the mRNA and protein expression of E-Cadherin and Vimentin upon siRNA-mediated depletion of Rac1b, ESRP1 and ESRP2 (see Fig. 3.17). Of note is, that Vimentin mRNA and protein content was not detected in untransfected Colo357 cells, which was neither altered by knockdown of Rac1b, ESRP1 nor ESRP2 (see A). Therefore, Vimentin was not further analyzed in Colo357 cells.

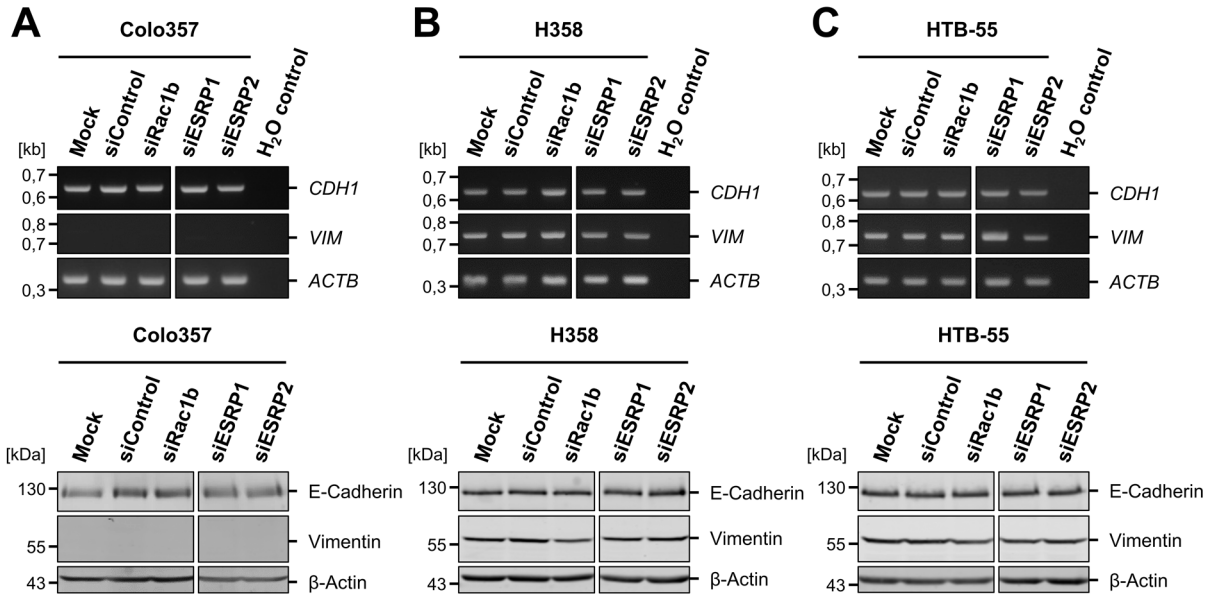

Fig. 3.17: Analysis of Rac1b or ESRP-dependent changes in EMT markers of Colo357, H358 and HTB-55 cells after siRNA-mediated depletion. The (**A**) Colo357 pancreatic as well as (**B**) H358 and (**C**) HTB-55 lung carcinoma cells were transfected twice with specific siRNAs against Rac1b (siRac1b), ESRP1 (siESRP1) and ESRP2 (siESRP2). Untransfected cells (Mock) and cells transfected with non-targeting siRNA (siControl) served as controls. The cDNAs and RIPA lysates were prepared 72 h after siRNA transfection, respectively. The figure shows representative agarose gels of two independent sqRT-PCR experiments, in which the mRNA levels of *CDH1* and *VIM* were detected (top and 2nd panel). *ACTB* detection is displayed in the bottom panel (same as shown in Fig. 3.12). The lower panels show representative western blots of three independent experiments, in which corresponding RIPA lysates of siRNA transfected cells were used. Specific antibodies were used to detect E-Cadherin (top panel) and Vimentin (2nd panel) as well as β-Actin, which served as a loading control (same as shown in Fig. 3.14).

The sqRT-PCR experiments did not reveal any obvious differences in mRNA levels of *CDH1* and *VIM* after siRNA-mediated depletion of *RAC1B*, *ESRP1* and *ESRP2*. Due to the weak sensitivity of the sqRT-PCR procedure, possible slight differences in mRNA amounts might not have been detected.

Therefore, mRNA quantities of *CDH1* and *VIM* were analyzed more extensively by quantitative, SYBR green-based RT-PCR experiments and evaluated as described in Ch. 2.2.6.2. *ACTB* mRNA was detected as a reference gene. The results of the qRT-PCR analyses are shown in Fig. 3.18. In Colo357 cells *CDH1* was slightly downregulated after the depletion of *ESRP2* (FC = 0,76 ± 0,09 x, p = 0,049) (as shown in A). This was also the case in H358 cells after knockdown of *ESRP1* (FC = 0,69 ± 0,10 x, p = 0,032) and *ESRP2* (FC = 0,76 ± 0,08 x, p = 0,031). In HTB-55 cells *CDH1* mRNA levels were also decreased significantly after siRNA-mediated silencing of *ESRP1* (FC = 0,76 ± 0,02 x, p = 0,0017) and marginally upon knockdown of *ESRP2* (FC = 0,63 ± 0,18 x). Interestingly, *CDH1* mRNA levels were slightly, but not significantly altered through depletion of *RAC1B*. In HTB-55 cells *CDH1* mRNA amounts were slightly reduced (FC = 0,84 ± 0,09 x), whereas the same was

upregulated in H358 cells (FC = 1,17 ± 0,09 x) (see B and C). In H358 cells *VIM* mRNA amounts were upregulated as a result of siRNA-mediated knockdown of *ESRP2* in two out of three experiments (individual FC values: 2,69 x, 1,82 x and 0,82 x). Interestingly, *VIM* mRNA quantities were decreased in HTB-55 cells upon depletion of *ESRP1* (FC = 0,59 ± 0,12 x, p = 0,028) and very weakly after knockdown of *ESRP2* (FC = 0,85 ± 0,002 x, p < 0,0001).

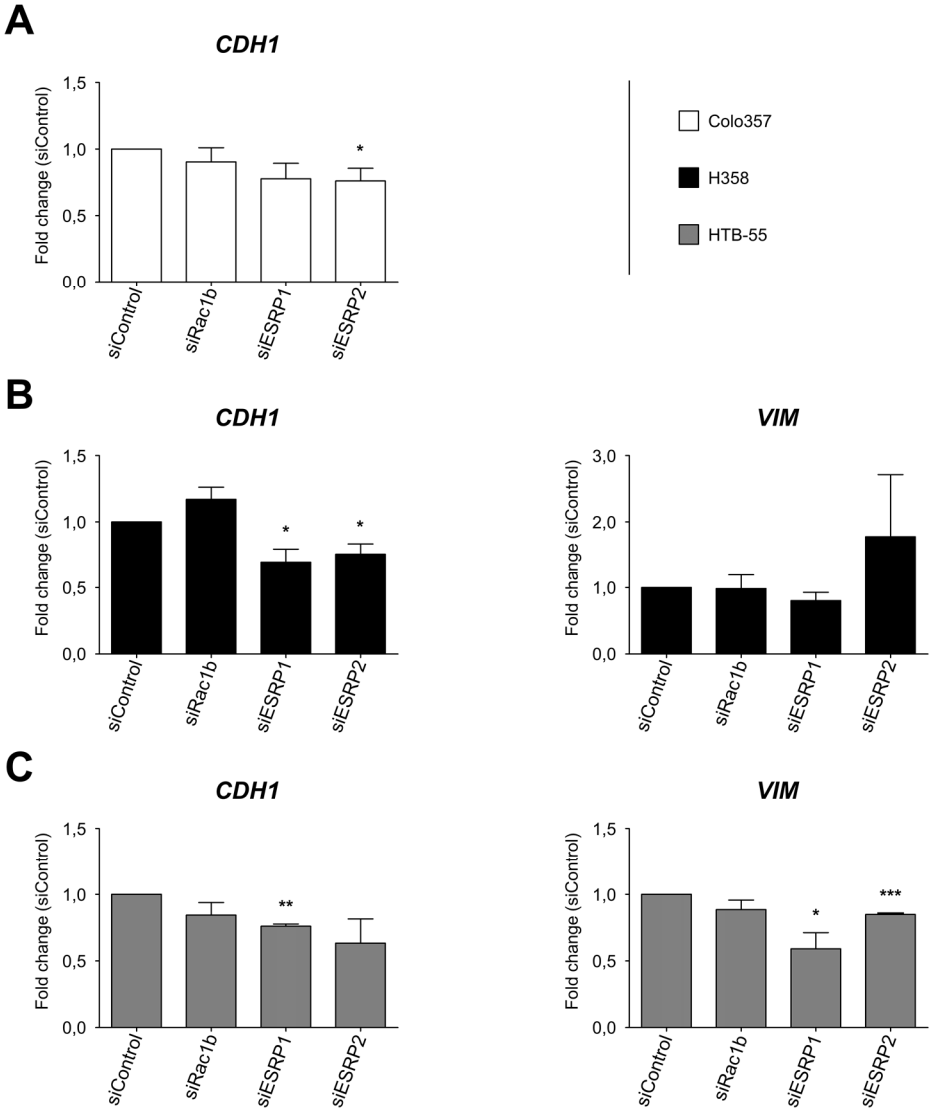

Fig. 3.18: Quantitative RT-PCR analysis of changes in *CDH1* and *VIM* mRNA quantities after siRNA-mediated depletion in Colo357, H358 and HTB-55 cells. (**A**) Colo357, (**B**) H358 and (**C**) HTB-55 carcinoma cells were transfected twice with specific siRNAs against *RAC1B* (siRac1b), *ESRP1* (siESRP1) and *ESRP2* (siESRP2). Cells transfected with non-targeting siRNA (siControl) served as controls. cDNA was prepared 72 h after the second transfection. The bar graphs show the mean ± SD of three independent qRT-PCR experiments, in which the mRNA quantities of *CDH1* (E-Cadherin) and *VIM* (Vimentin) were detected. The mRNA levels of *ACTB* were detected as a reference gene. The fold change in relative mRNA quantities ($2^{-\Delta\Delta Ct}$ method) and statistical evaluations (one sample t-test) were calculated in relation to siControl (set to 1,0) as described in Ch. 2.2.6.2 (significance levels: p < 0,05 = *, p < 0,01 = **, p < 0,001 = ***).

Since the siRNA-mediated knockdown of *RAC1B*, *ESRP1* and *ESRP2* for 96 h revealed only slight changes in *CDH1* and *VIM* mRNA levels, the effect on different EMT-specific transcription factors was assessed in the next set of qRT-PCR experiments. Therefore, the mRNA quantities of *SNAI1* (henceforth referred to as "*SNAIL*"), *SNAI2* (henceforth termed "*SLUG*") and *TWIST1* were analyzed. As shown in Fig. 3.19 the siRNA-mediated depletion of *RAC1B*, *ESRP1* or *ESRP2* had no major effects on the mRNA amounts of *SNAIL* in Colo357, H358 and HTB-55 cells. Interestingly, the *SLUG* mRNA quantities were significantly reduced after depletion of *ESRP1* (FC = 0,69 ± 0,06 x, p = 0,011) and marginally upon *ESRP2* knockdown (FC = 0,79 ± 0,12 x) in H358 cells. Furthermore, a slight tendency toward an upregulation of *SLUG* mRNA quantities was observed after depletion of *RAC1B* in H358 cells, whereas *SLUG* mRNA was decreased significantly in HTB-55 cells (FC = 0,67 ± 0,13 x, p = 0,046). *TWIST1* mRNA quantities were downregulated after depletion of *RAC1B* in Colo357 cells (FC = 0,85 ± 0,04 x, p = 0,027) and markedly downregulated in two of three experiments after knockdown of *ESRP2* (individual FC values: 0,28 x, 0,32 x and 1,19 x). In contrast, *TWIST1* mRNA was increased markedly, but not significantly by depletion of *ESRP2* in H358 cells (FC = 2,62 ± 0,80 x).

The zinc-finger E-box binding transcription factors *ZEB1* and *ZEB2* are also involved in EMT, thus these factors were also examined via qRT-PCR analyses. The results shown in Fig. 3.20 revealed no changes in *ZEB1* mRNA amounts after the siRNA-mediated depletion of *RAC1B*, *ESRP1* and *ESRP2* in Colo357 cells and HTB-55 cells. *ZEB1* mRNA was downregulated after silencing of *ESRP1* in H358 cells only (FC = 0,65 ± 0,14 x, p = 0,048) (see B). Due to the heterogeneous results for *ZEB2* observed in Colo357 and H358 cells in three independent experiments, it was not possible to make a valid statement. In contrast, *ZEB2* mRNA levels were observed to be downregulated in HTB-55 cells after siRNA-mediated depletion of *RAC1B* (FC = 0,66 ± 0,24 x) as well as *ESRP1* (FC = 0,57 ± 0,19 x) marginally and significantly after *ESRP2* silencing (FC = 0,50 ± 0,16 x, p = 0,030) (see C).

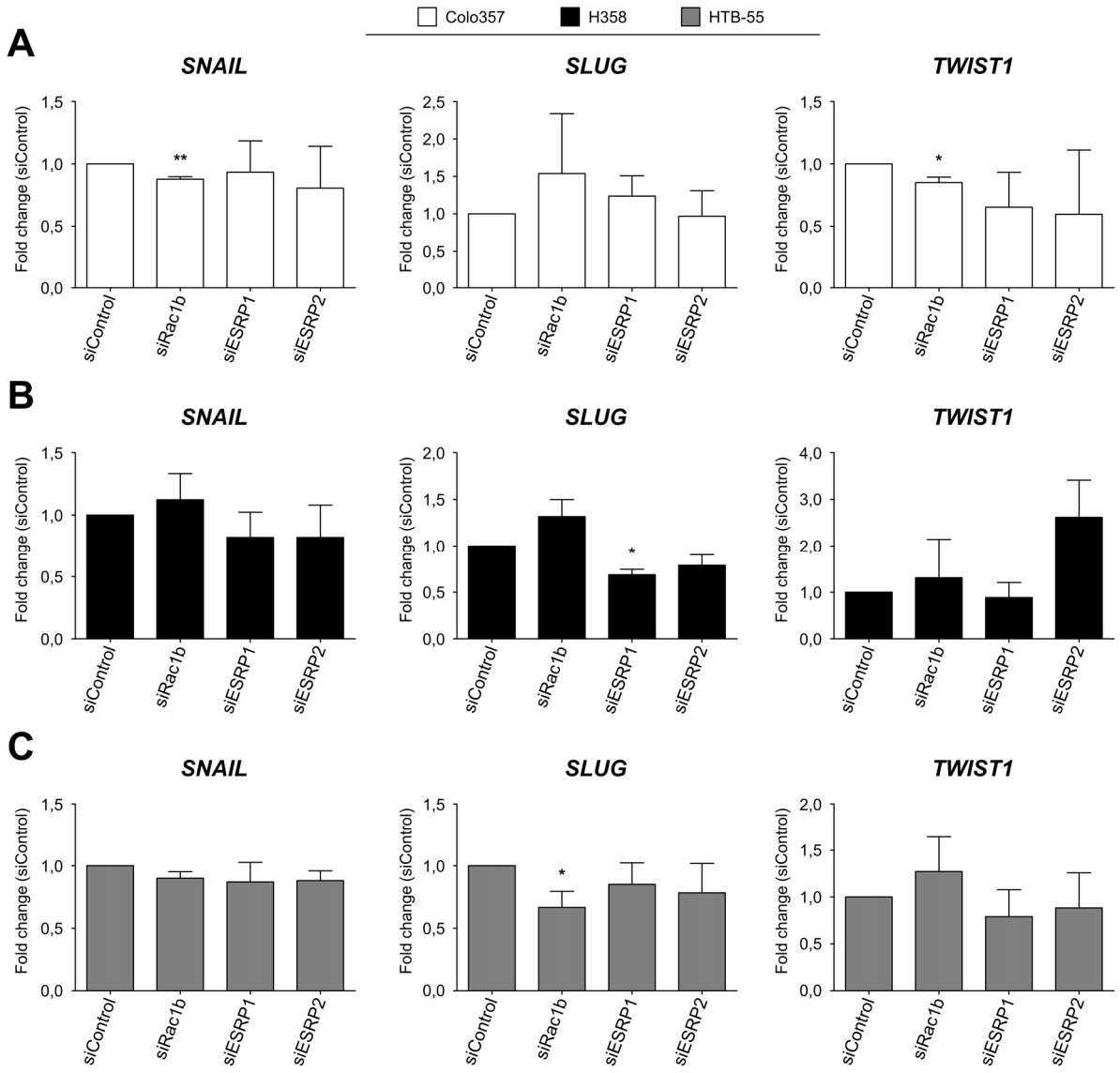

Fig. 3.19: Quantitative RT-PCR analysis of *SNAIL*, *SLUG* and *TWIST1* mRNA quantities after siRNA-mediated depletion in Colo357, H358 and HTB-55 cells. (**A**) Colo357, (**B**) H358 and (**C**) HTB-55 carcinoma cells were transfected twice with siRac1b-, siESRP1- and siESRP2-siRNAs, whereas cells transfected with non-targeting siRNA (siControl) served as controls. After 72 h following the second transfection cDNA was prepared. The figure shows the mean ± SD of three independent qRT-PCR experiments, in which mRNA quantities of *SNAIL*, *SLUG* and *TWIST1* were detected. *ACTB* mRNA was detected as a reference gene. The fold change in relative mRNA quantities ($2^{-\Delta\Delta Ct}$ method) and statistical evaluations (one sample t-test) were calculated in relation to siControl (set to 1,0) as described in Ch. 2.2.6.2 (significance levels: $p < 0,05$ = *, $p < 0,01$ = **, $p < 0,001$ = ***).

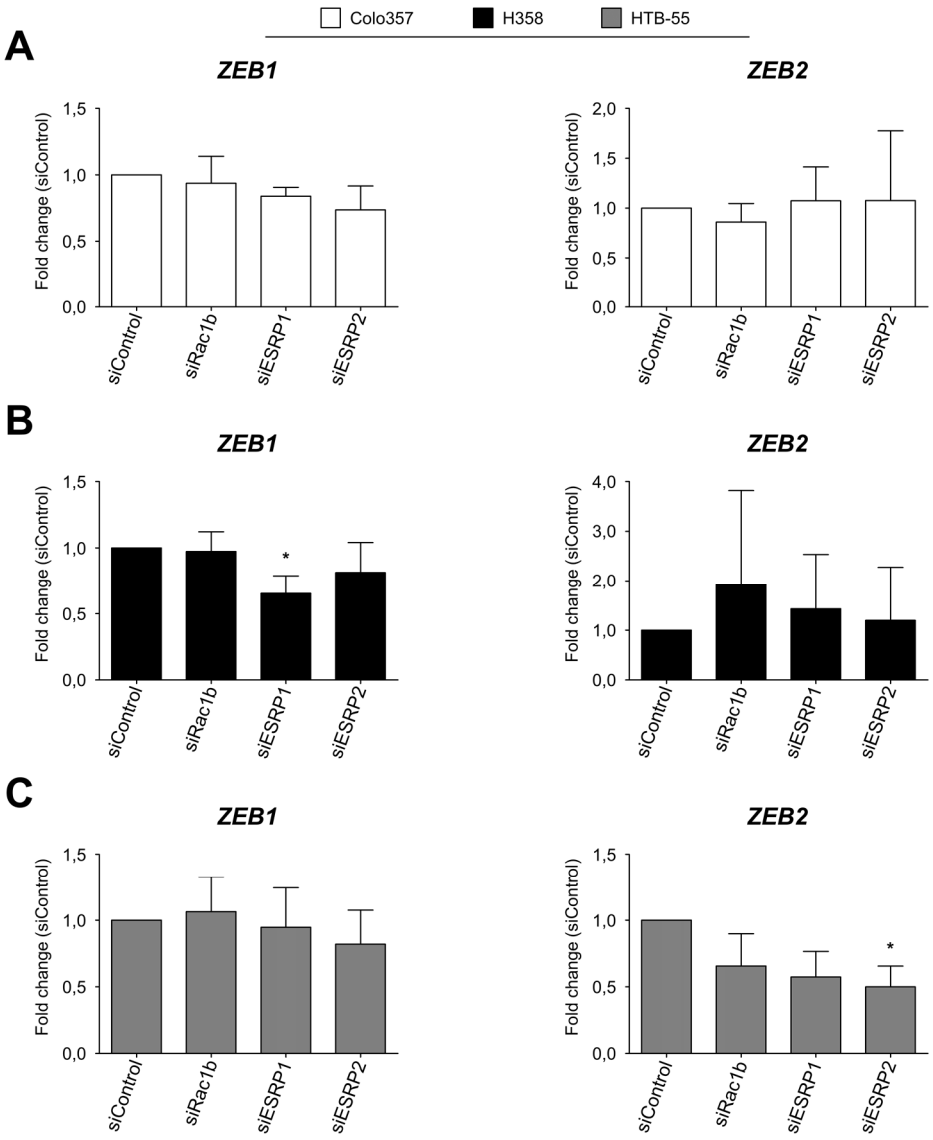

Fig. 3.20: Quantitative RT-PCR analysis of *ZEB1* and *ZEB2* mRNA amounts after siRNA-mediated depletion in Colo357, H358 and HTB-55 cells. (**A**) Colo357 pancreatic and (**B**) H358 as well as (**C**) HTB-55 lung carcinoma cells were transfected twice with specific siRac1b-, siESRP1- and siESRP2-siRNAs. Cells transfected with non-targeting siRNA (siControl) served as controls. cDNA was generated 72 h after the second transfection. The bar graphs display the mean ± SD of three independent qRT-PCR experiments to detect the mRNA quantities of *ZEB1* and *ZEB2*. *ACTB* mRNA was detected as a reference gene. The fold change in relative mRNA quantities ($2^{-\Delta\Delta Ct}$ method) and statistical evaluations (one sample t-test) were calculated in relation to siControl (set to 1,0) as described in Ch. 2.2.6.2 (significance levels: $p < 0,05$ = *, $p < 0,01$ = **, $p < 0,001$ = ***).

In conclusion of the siRNA-mediated depletion experiments, sqRT-PCR and western blot experiments as well as subsequent densitometric evaluations (data not shown) did not reveal any changes in the mRNA and protein levels of E-Cadherin and Vimentin in Colo357, H358 and HTB-55 cells. More sensitive qRT-PCR analyses revealed, that the siRNA-mediated depletion of *ESRP1* and *ESRP2* affected the mRNA levels of *CDH1* negatively in all three cell lines and influenced *VIM* mRNA differently in a cell line-specific context, whereas depletion of *RAC1B* had no significant effect on the mRNA expression of the two EMT markers.

Additionally to *CDH1* and *VIM*, the mRNA levels of EMT-specific transcription factors *SNAIL*, *SLUG*, *TWIST1* and *ZEB1* as well as *ZEB2* were quantified via qRT-PCR procedure. Altogether, the heterogeneous results of the qRT-PCR experiments after depletion of *RAC1B*, *ESRP1* and *ESRP2* described above, indicate a diverse and cell line-specific role of the three proteins in affecting mRNA levels of the EMT-specific transcriptions factors *SLUG*, *TWIST1, ZEB1* and *ZEB2*, but not *SNAIL*. In summary, the *SLUG* mRNA levels were affected differently as they were decreased in HTB-55 cells and slightly increased in H358 cells upon *RAC1B* silencing. Furthermore, *SLUG* was downregulated by knockdown of *ESRP1* and *ESRP2* only in H358 cells. The mRNA amounts of *TWIST1* were negatively affected in Colo357 cells after knockdown of *RAC1B* and upregulated in H358 cells after depletion of *ESRP2*. Furthermore, depletion of *ESRP1* negatively affected *ZEB1* mRNA levels in H358 cells, whereas a knockdown of *ESRP2* downregulated *ZEB2* mRNA in HTB-55 cells. Therefore, a generalized cell line-independent statement on specific effects of neither Rac1b, ESRP1 nor ESRP2 on the mRNA expression of *SLUG*, *TWIST1, ZEB1* and *ZEB2* and their role involvement in the observed changes in *CDH1* and *VIM* mRNA amounts is not possible.

3.6 The effects of transient expression of HA-ESRP1 and HA-ESRP2 on Rac1 isoform and EMT marker protein expression

In the next set of experiments, the effects of an ectopic upregulation of ESRP1 and ESRP2 on the protein amounts of Rac1 isoforms and EMT marker proteins were analyzed. PANC-1 pancreatic carcinoma cells, which were shown to contain low protein amounts of Rac1b as well as ESRP1 and ESRP2, were transiently transfected with plasmids for ectopic expression of HA-tagged ESRP1 and ESRP2 fusion proteins. Analogous to the siRNA-mediated depletion experiments in Colo357, H358 and HTB-55 cells, the PANC-1 cells were incubated for a total of 96 h after plasmid transfection. Western blot experiments were performed to identify effects of the ectopic expression of HA-ESRP1 and HA-ESRP2 fusion proteins in comparison to untransfected cells.

Representative results shown in Fig. 3.21 revealed a marginal reduction of E-Cadherin protein levels (see A) and a very weak increase of Rac1b and Snail protein amounts (as shown in B). Changes in the protein levels of Vimentin, N-Cadherin and $p120^{ctn}$ were not identified (see A and C). The expression of HA-ESRP1 and HA-ESRP2 fusion proteins was verified, although the transfection efficiency was not determined due to a missing fluorescent tag. Additionally, the cellular morphologies were assessed by light microscopy 96 h after transient transfection, but did not reveal any striking differences (see D).

In conclusion, the ectopic expression of HA-ESRP1 and HA-ESRP2 for four days in PANC-1 cells did not affect protein expression patterns of Rac1 isoforms and EMT marker proteins strikingly.

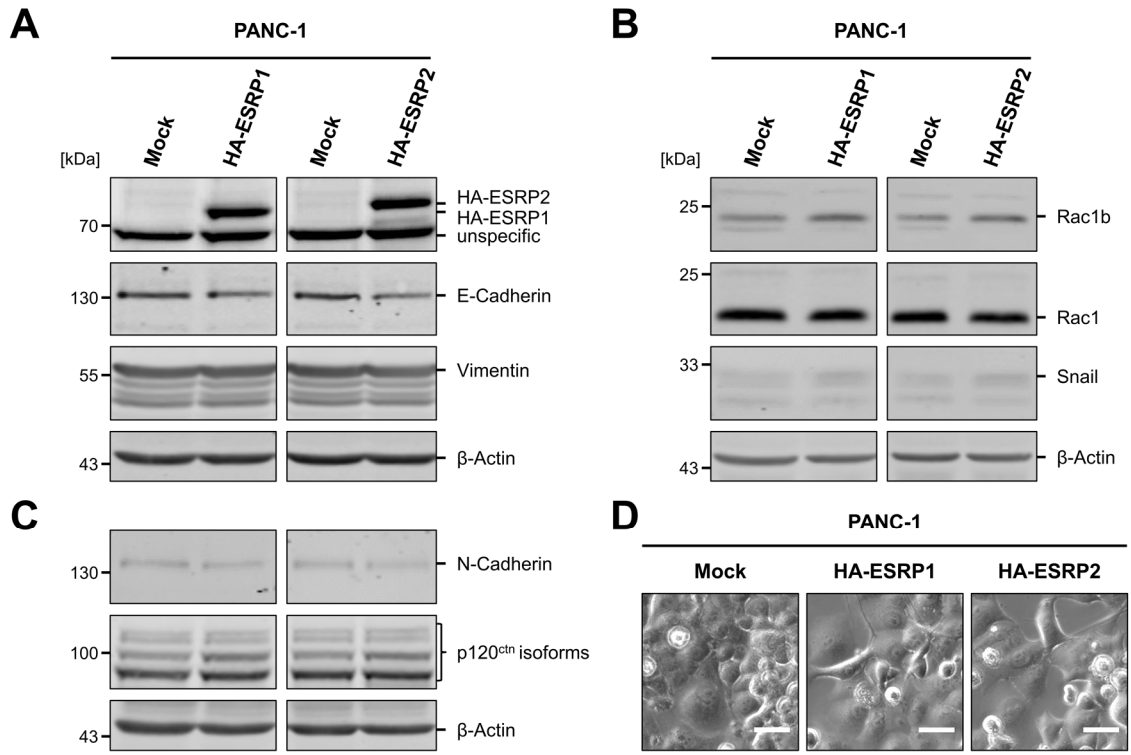

Fig. 3.21: Analysis of the transient expression of HA-ESRP1 and HA-ESRP2 on the protein amounts of Rac1 isoforms and EMT marker proteins in PANC-1 cells. PANC-1 cells were transiently transfected with pcDNA3.1(+) plasmids encoding HA-tagged ESRP1 and ESRP2, respectively. Untransfected cells (Mock) served as controls. After 96 h, whole cell lysates were generated, separated in SDS polyacrylamide gels and analyzed via western blot procedure. (**A**) The detection of ectopically expressed HA-ESRP1 and HA-ERSP2 fusion proteins is shown as detected by a HRP-coupled anti-HA antibody (top panel). The detection of E-Cadherin and Vimentin is displayed in the 2nd and 3rd panel. (**B**) The top and 2nd panel show the detection of Rac1b and Rac1 proteins, whereas the detected protein amounts of Snail are shown in the 3rd panel. (**C**) The detections of N-Cadherin and p120ctn isoforms are displayed in the top and 2nd panel. The protein amounts of β-Actin were detected as loading control and are displayed in the bottom panels. The figure shows representative western blots of three independent experiments (**D**) Representative phase contrast images are shown. Scale bar: 40 µm.

3.7 Characterizing specific roles of Rac1b, ESRP1 and ESRP2 in TGFβ1-induced EMT

In the previous chapters, different effects of Rac1b, ESRP1 and ESRP2 on the mRNA and protein amounts of EMT-related factors were analyzed after four days of depletion or transient overexpression. In the following experiments, different long-term effects were analyzed. First, the protein contents of Rac1 isoforms, ESRP1 and ESRP2 as well as different EMT-specific proteins were examined after a twelve-day stimulation of H358 and HTB-55 cells with TGFβ1.

Next, protein amounts of Rac1b, ESRP1 and ESRP2 were depleted over a time course of fourteen days by siRNA-mediated knockdown experiments. Finally, HA-ESRP1 and HA-ESRP2 were ectopically expressed in H358 cells, which had been stimulated with TGFβ1 for six to eight days prior to transient plasmid transfection. Thereby, the rescue of the TGFβ1-induced downregulation of ESRP1 and ESRP2 was analyzed.

3.7.1 Analysis of EMT markers in H358 and HTB-55 cells after long-term TGFβ1 stimulation

H358 and HTB-55 cells were treated with 10 ng/ml TGFβ1 every two days for a twelve-day period to induce EMT. Untreated cells and cells treated with 0,2 mM citrate served as controls. The lysates were provided by Prof. Dr. Andre Menke. The changes in the protein expression patterns of Rac1 isoforms, ESRPs and EMT-specific proteins were examined via western blot procedure.

These analyses revealed substantial TGFβ1-induced changes in the protein expression pattern of H358 cells. As shown in Fig. 3.22 a twelve-day treatment of H358 cells with TGFβ1 led to a downregulation of E-Cadherin, whereas the protein contents of Vimentin and Snail were markedly increased. N-Cadherin was not detected in H358 cells neither in untreated nor in TGFβ1 treated cells in these experiments. The ESRP1 and ESRP2 protein levels were strongly downregulated (see B and C). Furthermore, the splicing pattern of $p120^{ctn}$ was altered upon TGFβ1 treatment, facilitating the presence of a longer isoform in comparison to unstimulated H358 cells (see C). In parallel, the protein amounts of Rac1b, but not Rac1, were markedly downregulated after long-term stimulation with TGFβ1 (see A). An upregulation of β-Actin protein content was also detected. The long-term treatment of HTB-55 cells with TGFβ1 did not alter the protein expression pattern as markedly as seen for the H358 cells. Only Vimentin and weakly N-Cadherin protein levels were increased after TGFβ1 treatment (see E and F).

These changes in the protein expression patterns in H358 and HTB-55 cells were also analyzed in a time course experiment, in which RIPA cell lysates were generated every two days during the twelve-day TGFβ1 stimulation period. These analyses revealed, that the protein expression changes in the H358 cells were first detectable on the eighth day of TGFβ1 treatment (data not shown). Additionally, a long-term TGFβ1 stimulation experiment was carried out in Colo357 pancreatic carcinoma cells. But alterations in the protein expression pattern similar to that observed for H358 cells were not detected in Colo357 cells (data not shown).

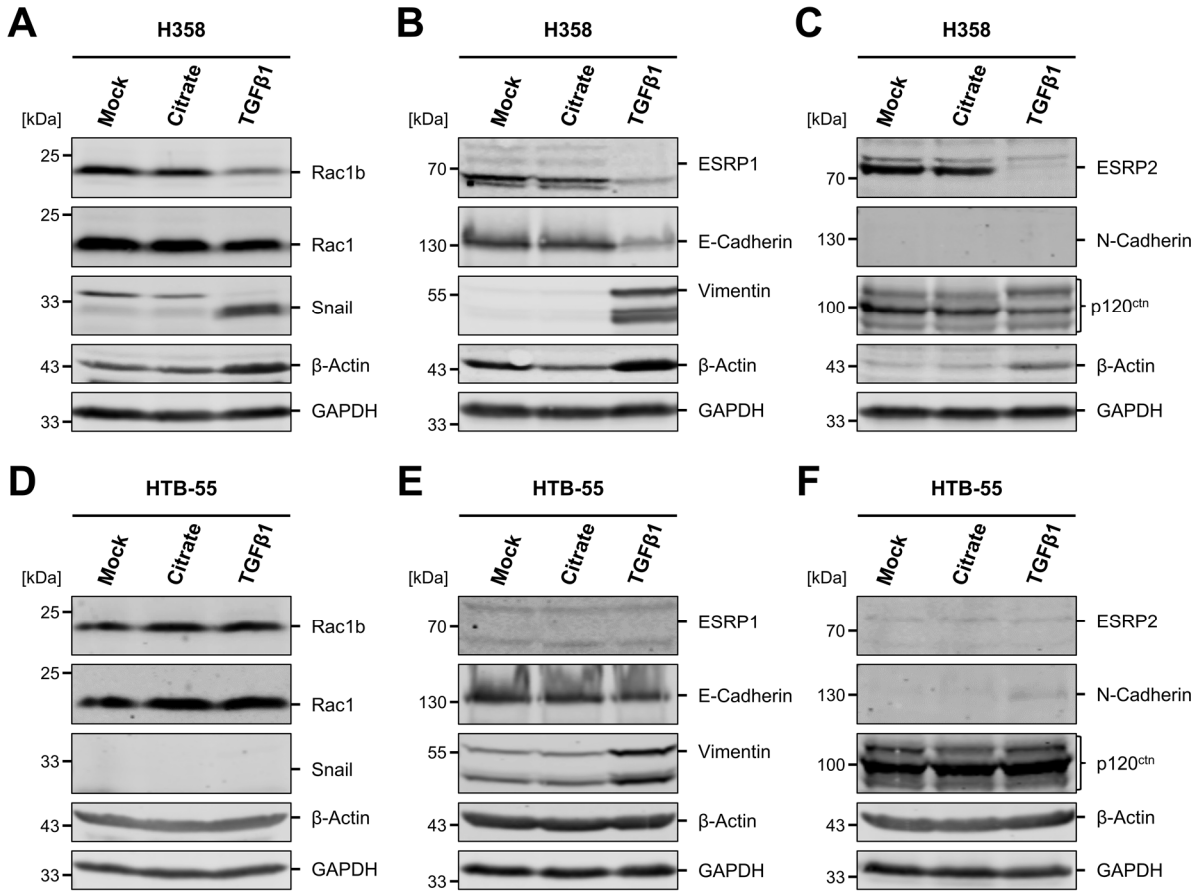

Fig. 3.22: Analysis of Rac1 isoforms, ESRPs and EMT marker proteins in H358 and HTB-55 cells after long-term stimulation with TGFβ1 for twelve days. (**A-C**) H358 and (**D-F**) HTB-55 cells were stimulated with TGFβ1 for 12 days to induce EMT. The cells were treated with 10 ng/ml TGFβ1 every two days for up to twelve days. Untreated cells (Mock) and cells treated with 0,2 mM citrate (Citrate) served as controls. The TGFβ1-induced changes in the protein expression patterns were examined via western blot procedure. (**A** and **D**) The top and the 2nd panel show the detection of Rac1b and Rac1 proteins, whereas detected Snail proteins are shown in the 3rd panel. (**B** and **E**) The detection of ESRP1 (top panel), E-Cadherin (2nd panel) and Vimentin proteins (3rd panel) is displayed. (**C** and **F**) Representative western blots are shown, in which ESRP2 (top panel), N-Cadherin (2nd panel) and p120ctn isoforms (3rd panel) were detected. β-Actin and GAPDH were detected as loading controls and are displayed in the 4th and the bottom panels, respectively. The figure shows representative western blots of three independent experiments.

Altogether, the stimulation of H358 cells with TGFβ1 for twelve days led to protein expression changes consistent with EMT. Epithelial marker proteins like E-Cadherin, ESPR1 and ESRP2 were markedly downregulated, whereas the protein amounts of mesenchymal proteins like Vimentin and the EMT-specific transcription factor Snail were strongly increased. Interestingly, the long-term treatment of H358 cells with TGFβ1 also led to a downregulation of Rac1b, but not Rac1. Due to the fact, that these TGFβ1 effects were only weakly detected in HTB-55 cells and non-evident Colo357 cells, the following experiments were carried out in H358 cells only.

3.7.2 Simulation of the EMT-related downregulation of Rac1b, ESRP1 and ESRP2 by long-term siRNA-mediated protein knockdown

The downregulation of ESRP1 and ESRP2 as well as Rac1b after twelve days of TGFβ1 treatment was an interesting observation in H358 cells. In the next set of experiments, the protein levels of Rac1b, ESRP1 and ESRP2 were depleted by sequential siRNA transfections and the effects analyzed after fourteen days. Additionally, a mixture of the ESRP1 and ESRP2 siRNAs was used allowing the simultaneous knockdown of both splicing factors. The H358 cells were transfected with the specific siRNAs, detached from the 6-well tissue plates after four days, re-seeded and transfected again with the specific siRNAs. After four further days the procedure was repeated resulting in a protein depletion for a total of fourteen days. The knockdown efficiency and protein expression changes were assessed by densitometric analyses of three independent western blot experiments and the fold change (FC) of relative up- or downregulation calculated as described (see Ch. 2.2.6.1).

The long-term siRNA-mediated depletion experiments displayed in Fig. 3.23 revealed a marked protein knockdown of Rac1b, ESRP1 and ESRP2 by the respective siRNAs. The mixture of the ESRP1 and ESRP2 siRNA also resulted in distinct silencing of both, ESRP1 and of ESRP2. Additionally, several changes in protein levels were elucidated after siRNA-mediated depletion of Rac1b. Rac1 (FC = 0,64 ± 0,09 x, p = 0,022) and ESRP1 (FC = 0,71 ± 0,09 x, p = 0,029) were downregulated significantly after knockdown of Rac1b. Vimentin (FC = 0,45 ± 0,11 x, p = 0,013) and N-Cadherin (FC = 0,46 ± 0,12 x, p = 0,016) protein levels were also decreased. ESRP2 protein content was downregulated weakly in only two of three experiments after Rac1b silencing (individual FC values: 0,82 x, 0,86 x and 1,18 x).

Rac1b protein levels were upregulated after the depletion of ESRP1 in two of three cases (individual FC values: 1,91 x, 1,42 x and 1,06 x). The E-Cadherin protein amounts were weakly, but significantly downregulated after siRNA-mediated depletion of ESRP1 (FC = 0,87 ± 0,04 x, p = 0,027). ESRP2 depletion and silencing of both splicing factors lead to a very weak and non-significant decrease of E-Cadherin. Another effect of ESRP1 silencing was an altered splicing pattern of $p120^{ctn}$ leading to the presence of a longer isoform. This was also observed, when a mixture of both ESRP siRNAs was used. The depletion of ESRP2 had no effect on the amounts of the analyzed proteins. Additionally, the knockdown of none of the three proteins had an effect on Snail.

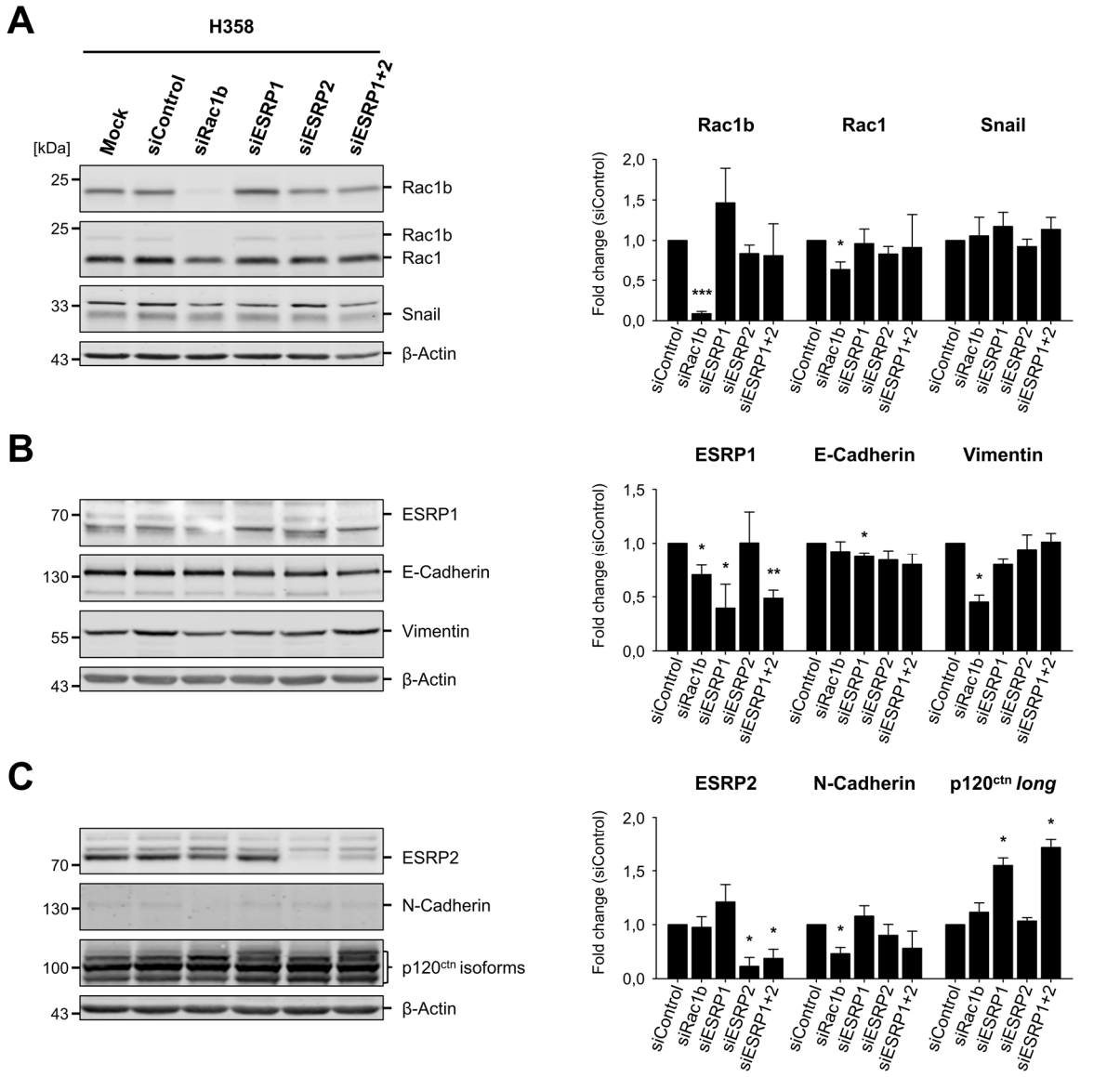

Fig. 3.23: Analysis of long-term siRNA-mediated depletion of Rac1b, ESRP1 and ESRP2 in H358 cells. H358 lung carcinoma cells were transfected with specific siRNAs against Rac1b (siRac1b), ESRP1 (siESRP1) and 2 (siESRP2) as well as a mixture of both ESRP siRNAs (siESRP1+2). Untransfected cells (Mock) and cells transfected with non-targeting siRNA (siControl) served as controls. Long-term silencing was achieved by sequentially transfecting the cells three times within a fourteen day time period before preparing RIPA lysates. The panels on the left show representative western blots of three independent experiments. (**A**) Rac1b detection is shown in the top panel, whereas the detection of Rac1 and Rac1b are displayed in the 2nd panel and Snail detection is shown in the 3rd panel. (**B**) The detected ESRP1 (top panel), E-Cadherin (2nd panel) and Vimentin (3rd panel) protein amounts are displayed. (**C**) The detection of ESRP2 (top panel), N-Cadherin (2nd panel) and p120ctn (3rd panel) is shown. β-Actin was detected as a loading control (bottom panels). The bar graphs on the right display the means ± SD of densitometric analyses of three independent experiments. The normalization was performed as described in Ch. 2.2.6.1. The statistical significance of protein amount differences in relation to siControl (set to 1,0) was analyzed by a one sample t-test (significance levels: $p < 0,05$ = *, $p < 0,01$ = **, $p < 0,001$ = ***).

Altogether, the knockdown of ESRP1 and ESRP2 weakly downregulated E-Cadherin protein levels, whereas Rac1b depletion reduced ESRP1 protein levels. Interestingly, the depletion of Rac1b also led to a downregulation of Vimentin and N-Cadherin. Parallel to the upregulation

of the Rac1b protein amount, an ESRP1 knockdown altered the splicing pattern of $p120^{ctn}$. Overall, the marked EMT-related changes in protein expression patterns, which were observed after a twelve-day TGFβ1 treatment of H358 cells, were not identified after long-term siRNA-mediated depletion of neither Rac1b, ESRP1 nor ESRP2. Nevertheless, all three proteins seem to be partly involved in regulating the expression of some EMT-related proteins.

3.7.3 Transient expression of HA-ERSP1 and HA-ESRP2 after long-term TGFβ1-stimulation of H358 cells

Finally, H358 cells were transiently transfected with expression plasmids encoding HA-tagged ESRP1 and ESRP2 after a six to eight day stimulation with TGFβ1. Thereby, the effects of a reversal of the TGFβ1-induced downregulation of ESRP1 and ESRP2 were analyzed. Two days after transfection, RIPA cell lysates were prepared and the specific roles of the two splicing factors in EMT analyzed via western blot procedure.

As shown in Fig. 3.24 (see A-C), the TGFβ1 treatment of H358 cells transfected only with EGFP expression plasmids (Control) led to the EMT-related changes in the protein expression patters already described in Ch. 3.7.1. The transient expression of HA- ESRP1 and HA-ESRP2 for two days did not alter the expression patterns of none of the analyzed proteins. Densitometric analyses of four independent experiments confirmed this observation (data not shown). Additionally, fluorescence microscopic images were taken to analyze the changes in the cellular morphology and to assess the transfection efficiency. H358 cells treated with citrate exhibited an epithelial-specific cobblestone-like morphology and formed uniform cell layers. The ten-day stimulation of the cells with TGFβ1 led to drastic changes in cell morphology. The cells formed small islets of spindle-shaped cells. The transient expression of HA-ESRP1 and HA-ESRP2 did not alter the respective morphologies of neither the citrate- nor the TGFβ1-treated transfected H358 cells. Furthermore, the H358 cells were co-transfected with EGFP expression plasmids to allow a quantification of the transfection efficiency. Thereby, a transfection efficiency of approximately 30 % was detected for cells treated with citrate. H358 cells stimulated with TGFβ1 exhibited a higher transfection efficiency of approximately 50 % (as shown in D). A similar discrepancy was also observed in the western blot analyses as TGFβ1-stimulated H358 cells contained much higher HA-ESRP1 and HA-ESRP2 protein amounts than cells treated with citrate.

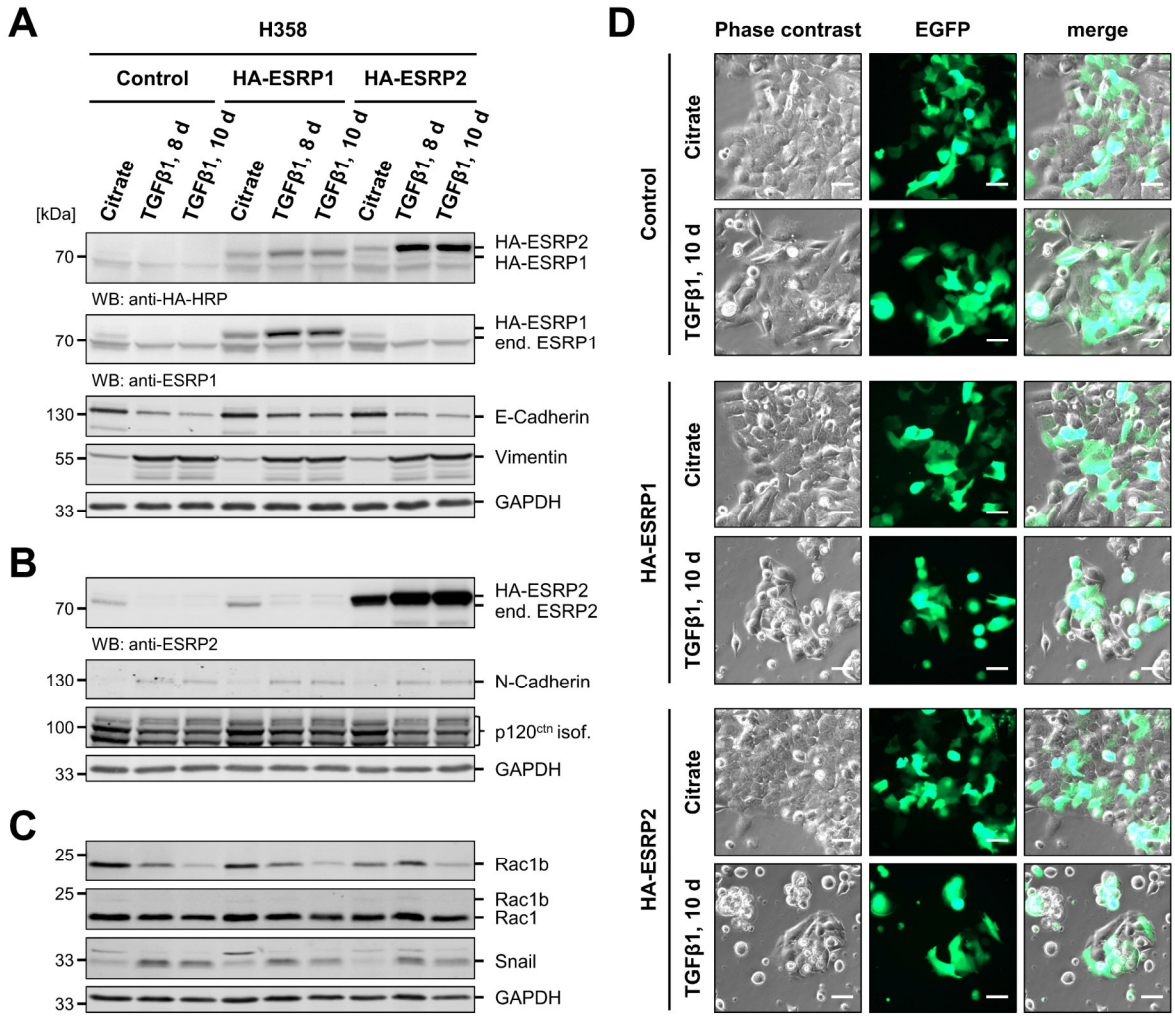

Fig. 3.24: Analysis of the transient expression of HA-ESRP1 and HA-ESRP2 in H358 cells after a long-term treatment with TGFβ1. H358 cells were treated with 10 ng/ml TGFβ1 every two days for eight and ten days to induce EMT. Untreated cells (Mock) and cells treated with 0,2 mM citrate (Citrate) served as controls. On the sixth and eighth day, the H358 cells were transiently transfected with expression plasmids encoding HA-tagged ESRP1 and ESRP2. The cells were co-transfected with EGFP plasmids to allow quantification of the transfection efficiency. The changes in the protein expression patterns were analyzed via western blot procedure. (**A**) The detection of HA-ESRP1 and HA-ESRP2 with a HRP-coupled anti-HA antibody is shown in the top panel. Additionally, endogenous ESRP1 and HA-ESRP1 (2nd panel) as well as E-Cadherin (3rd panel) and Vimentin (4th panel) were detected. (**B**) The top panel shows the detection of endogenous ESRP2 and HA-ESRP2 proteins, whereas the detections of N-Cadherin and p120^{ctn} are displayed in the 2nd and 3rd panels. (**C**) The detected protein amounts of Rac1b (top panel), Rac1 and Rac1b (2nd panel) as well as Snail (3rd panel) are shown. GAPDH was detected as a loading control and is displayed in the bottom panels. (**D**) Representative phase contrast, EGFP and merged fluorescence microscopic images are shown to exemplify morphological changes after the ten-day TGFβ1 stimulation as well as the ectopic expression of HA-ESRP1 and HA-ESRP2. Scale bar: 40 µm. The figure shows representative western blots and fluorescence microscopic images of four independent experiments.

Altogether, the long-term stimulation of H358 cells with TGFβ1 led to protein expression changes consistent with EMT. Epithelial marker proteins were markedly downregulated, whereas the protein expression of the mesenchymal proteins were strongly increased. Interestingly, the protein amounts of Rac1b, but not Rac1, and ESRP1 as well as ESRP2 were downregulated upon TGFβ1 stimulation. Long-term siRNA-mediated depletion experiments for a period of fourteen days resulted in a weak downregulation of E-Cadherin after ESRP1 and ESRP2 knockdown and slightly reduced ESRP1 protein levels after Rac1b silencing. Strikingly, an ESRP1 knockdown altered the splicing pattern of $p120^{ctn}$ as seen after long-term TGFβ1 stimulation. But altogether, the marked TGFβ1-related changes in protein expression patterns could not be simulated by long-term depletion of Rac1b, ESRP1 and ESRP2 in H358 cells. Furthermore, the transient expression of HA-ESRP1 and HA-ESRP2 for two days after long-term TGFβ1 stimulation of H358 cells did not alter the TGFβ1-induced changes in the protein expression patterns of different EMT-related factors.

4 Discussion

The experiments performed in the course of this work elucidated differences between the two GTPase isoforms Rac1 and alternatively spliced Rac1b regarding their expression levels and subcellular localization. Additionally, an influence of different Rac1 and Rac1b protein expression ratios on tumor cell invasion was elucidated. Furthermore, a relation between high Rac1b protein amounts and the presence of epithelial-specific splicing factors as well as EMT markers was uncovered. The roles of both GTPase isoforms in tumorigenesis and metastasis are still controversially debated and remain to be fully understood. The results presented in this work provide new insights into the functions of Rac1 and Rac1b in these processes.

4.1 Rac1 and Rac1b differ in expression levels, subcellular localization and activity

4.1.1 Differences in expression patterns and subcellular localization of Rac1 and Rac1b

The mRNA and protein expression analyses revealed variations in the Rac1b mRNA and protein levels between the examined pancreatic and lung cell lines, whereas the amounts of Rac1 were comparable in all analyzed cell lines (see Fig. 3.1 and Fig. 3.2). Subcellular fractionation assays revealed, that endogenous Rac1b proteins were predominantly located in the membrane-containing P100 fraction in different pancreatic and lung carcinoma cells, whereas endogenous Rac1 proteins were present in both the P100 and cytoplasmic S100 fractions (see Fig. 3.6). Moreover, live-cell images of stably transfected H23 cells showed, that EGFP-Rac1 fusion proteins were localized in the cytoplasm, but also in the plasma membrane, whereas EGFP-Rac1b was predominantly found associated to the plasma membrane (see Fig. 3.3). This was also confirmed by subcellular fractionation experiments with the H23 cell clones (see Fig. 3.4). More extensive subcellular localization analyses, which included functional mutants of Rac1 and Rac1b, revealed differences in the cytoplasmic and membranous localization between Rac1 isoforms and their constitutive active as well as dominant negative mutants. Specifically, the subcellular localization of wildtype HA-Rac1b was comparable to that of constitutive active HA-Rac1 (G12V) mutants, whereas wildtype HA-Rac1 was again present in cytoplasmic and membranous cellular fractions (see Fig. 3.5).

At the end of the last century, Jordan *et al.* (1999) identified the *RAC1B* cDNA after RT-PCR amplification of the entire *RAC1* coding sequence from a series of colorectal cancer tissues. Since then Rac1b was also shown to be expressed in breast, thyroid and pancreatic as well as

lung carcinomas cells (Faria *et al.*, 2016; Jordan *et al.*, 1999; Mehner *et al.*, 2014; Schnelzer *et al.*, 2000; Zhou *et al.*, 2013a). But many earlier studies, which were set to analyze the role of Rac1 in tumor progression and metastasis, did not take the possible presence of the Rac1b proteins into consideration. This is due to the circumstance, that Rac1b proteins are generally expressed in significantly lesser amounts than Rac1. This observation is based on the fact, that both isoforms only differ by the presence of an in-frame insertion of a small 19 amino acid exon 3b (Jordan *et al.*, 1999) and all antibodies used for detection of Rac1 proteins recognize both isoforms. This is also the case for the mouse monoclonal anti-Rac1 antibody used in the course of this work due to lack of suitable alternatives (see Fig. 3.2. C). The analyses of this work confirmed an overall low Rac1b-to-Rac1 protein expression ratio. This was even the case in cell lines, in which relatively high Rac1b protein levels were observed, like Colo357, Capan-2, H358 or HTB-55 cells (see Fig. 3.2. A and B: middle panel). Sahu *et al.* (2016) also observed, that Rac1 protein levels significantly exceeded those of Rac1b in different NSCLC cells. The sqRT-PCR analysis performed in this work also confirmed low Rac1b-to-Rac1 expression ratios on mRNA level (see Fig. 3.1). The results were consistent with a study, in which only approximately 10 % of *RAC1* pre-mRNA were shown to be spliced into the *RAC1B* transcript variant in the colorectal carcinoma cell line HT29 (Gonçalves *et al.*, 2009).

The studies to analyze differences in the subcellular localization of Rac1 and Rac1b conducted in this work came to the common result, that Rac1b is predominantly located within the membrane, whereas Rac1 proteins were present in both the membrane and the cytoplasm. As described before, inactive, GDP-loaded Rac1 proteins interact with RhoGDIs and are sequestered in the cytosol. The dissolution of this complex is essential for subsequent membrane association, GDP-GTP nucleotide exchange and activation of Rac1 proteins (Garcia-Mata *et al.*, 2011). It was shown, that Rac1b proteins are unable to be bound by RhoGDI and subsequently sequestered in the cytosol (Matos *et al.*, 2003; Singh *et al.*, 2004). The subcellular localization of Rac1b observed in this work is in line with its inability to interact with RhoGDI and is consistent with the results of Matos *et al.* (2003) and Singh *et al.* (2004). Additionally, Rac1b was characterized as a self-activating, constitutively GTP-bound GTPase (Fiegen *et al.*, 2004). Although Rac1b protein amounts are present in considerably smaller amounts in comparison to Rac1, the levels of active, GTP-loaded Rac1b proteins were shown to exceed that of activated Rac1 by a factor of three (Gonçalves *et al.*, 2009; Matos *et al.*, 2003). This was also confirmed by affinity precipitation assays to specifically identify GTP-bound Rac1 and Rac1b proteins performed in our group. Thereby, we could show, that endogenous as well as ectopically expressed Rac1b proteins were present in a predominantly GTP-bound state,

whereas Rac1 proteins were identified in a GDP- and GTP-loaded state to a similar extent (Ungefroren *et al.*, 2013).

The subcellular fractionation analyses of functional mutants of Rac1 and Rac1b confirmed the influence of their activity state on the subcellular localization of the respective GTPase (see Fig. 3.5). Gandhi *et al.* (2004) analyzed membrane ruffling in COS-7 cells expressing constitutively active Rac1 (G12V) and double mutants, which harbored an additional R66E mutation, that inhibited Rac1-RhoGDI interaction. Both, Rac1 (G12V) and Rac1 (G12V/R66E), were shown to be unable to bind to RhoGDI and were present at the plasma membrane where they induced membrane ruffling (Gandhi *et al.*, 2004). The fact, that constitutive active Rac1 (G12V) proteins are unable to be bound and sequestered in the cytosol by RhoGDI, is one explanation, why HA-Rac1 (G12V) was predominantly located within the P100 fractions in the experiments carried out in this work. Moreover, the identified comparable subcellular localization of wildtype HA-Rac1b and HA-Rac1 (G12V) mutants further establishes Rac1b as a constitutive active isoform of Rac1. The subcellular fractionation assays of this work also revealed, that both dominant negative mutants, HA-Rac1 (T17N) and HA-Rac1b (T17N), were mainly detected in the membranous P100 fractions (see Fig. 3.5). It has long been known, that dominant negative GTPase mutants bind to different GEFs more tightly than their wildtype counterparts and sequester these GEFs from interacting with and activating the endogenous proteins (Feig, 1999). In a recent study, Peurois *et al.* (2017) observed, that GEFs are mainly active at the membrane interface. They used artificial membrane tethering to demonstrate, that the RhoGEF-mediated nucleotide exchange rates were strongly enhanced at the membrane interface *in vitro*, whereas a nucleotide exchange was undetectable in solution. Peurois and colleagues explained this observation by the fact, that GEFs are activated through different transmembrane receptors by either binding directly to them or by interacting with adaptor proteins bound to activated receptors. They also proposed, that GEFs themselves are associated with plasma membranes. Either possibility is sufficient to explain the observed presence of dominant negative HA-Rac1 (T17N) and HA-Rac1b (T17N) proteins in membranous P100 fractions in this work as they could be tightly bound to GEFs present at the plasma membrane. This hypothesis can be underlined by the interesting findings of Remorino *et al.* (2017), who used optogenetic tools to track single Rac1 molecules and analyze the activity-dependent nanoclustering and immobilization of Rac1 proteins at the plasma membrane of migrating cells. They could show, that constitutive active Rac1 (Q61L) and dominant negative Rac1 (T17N) formed larger membrane-associated nanoclusters than wildtype Rac1. Additionally, they observed, that nanocluster size depended on the interaction

with GEFs, GAPS and effector proteins (Remorino *et al.*, 2017). Although GEF and GAP functions were shown to be redundant for Rac1b GTP-GDP cycling and activity, Fiegen *et al.* (2004) proposed, that an even faster GEF-mediated GDP-GTP exchange rate may occur in Rac1b proteins. Therefore, it is possible, that dominant negative HA-Rac1b (T17N), like HA-Rac1 (T17N), was mainly identified in P100 fractions in this work through its interactions with different membrane-located GEFs. In conclusion, the activity states of Rac1 and Rac1b as well as their differential ability to interact with RhoGDI explain the observed variations in their subcellular localization. Rac1 proteins, which cycle between a GDP- and a GTP-loaded state are present in both the cytoplasm and at the membranes, whereas the predominantly GTP-bound Rac1b is mainly found associated to membranes.

Another interesting observation of the subcellular localization experiments was, that the fluorescence signals of both, EGFP-Rac1 and EGFP-Rac1b, were strongly enhanced in areas of cell-cell contacts between H23 cell clones (see Fig. 3.3 K and N). Rac1 was shown to be involved in the early formation of novel Cadherin-dependent cell-cell adhesion sites in breast epithelial MCF10A cells, which was observed to coincide with extensive Rac1-dependent Actin-cytoskeleton rearrangements at these contact sites (Grobe *et al.*, 2018). This was also observed in MDCK cells, where the formation and strengthening of Cadherin-mediated cell-cell contacts depended on the spatio-temporal recruitment of Rac1 (Ehrlich *et al.*, 2002). Both studies provide explanations for the enhanced fluorescence signals of EGFP-Rac1 at areas of cell-cell contacts of H23/EGFP-Rac1 cells observed in this work. Interestingly, Ehrlich *et al.* (2002) also observed, that constitutively active Rac1 mutants were recruited to areas of cell-cell contacts, where they altered the kinetics and strength of these cell-cell adhesions, but not the generation of such contacts. This could be one explanation, why presumably constitutive-active EGFP-Rac1b proteins were also found in areas of cell-cell contacts in H23/EGFP-Rac1b cells in the live-cell imaging analyses conducted in this work (see Fig. 3.3 K and N). Additionally, it was observed, that Rac1b interacts more efficiently with the ARM-containing proteins $p120^{ctn}$ and β-Catenin than Rac1 (Orlichenko *et al.*, 2010; Pethe *et al.*, 2011). Both of these proteins are components of Cadherin-mediated adhesion complexes and are involved in the regulation of cell-cell adhesion (Hartsock and Nelson, 2008). $p120^{ctn}$ interacts with and stabilizes Cadherins on the intracellular transmembrane domain where it inhibits endocytoses and promotes cell adhesion (Kourtidis *et al.*, 2013). β-Catenin is an integral component of adherens junctions and connects Cadherins to the Actin cytoskeleton (Hartsock and Nelson, 2008). The enhanced interaction of Rac1b with both types of molecules could also explain the identified presence of EGFP-Rac1b at cell-cell contacts of H23/EGFP-Rac1b cells.

4.1.2 Nuclear localization of Rac1 and Rac1b

Since Rac1 and Rac1b only differ by the presence of the alternative exon 3b, both proteins contain a NLS within the C-terminal PBR (Lam and Hordijk, 2013; Pethe *et al.*, 2011). In this work, Rac1 and Rac1b were both detected in nuclear extracts (NE) in very small amounts in PANC-1, Colo357 and HTB-55 cells, but not in H358 cells (see Fig. 3.6). Several factors were identified to drive nuclear accumulation of Rac1 proteins through direct interaction with the small GTPase, including the ARM-containing small GTPase GDP dissociation stimulator (SmgGDS) and the nuclear import receptor Karyopherin α2 (Lanning *et al.*, 2003; Sandrock *et al.*, 2010). Interestingly, Rac1b was shown to interact with the atypical RhoGEF SmgGDS more efficiently than Rac1 (Lanning *et al.*, 2003; Orlichenko *et al.*, 2010). Therefore, SmgGDS might be involved in nuclear translocation of both Rac1 and Rac1b. Different expression patterns of these and other proteins involved in nuclear import should be analyzed in future experiments and might explain the observed variations in the presence of Rac1 and Rac1b proteins in the nucleus of the different cell lines.

Both, Rac1 and Rac1b, were shown affect gene expression. Luciferase reporter gene assays performed in our group revealed, that ectopically expressed wildtype Rac1 and Rac1b differentially affected the activity of several promotors (Seiz *et al.*, 2019). TGFβ/Smad2/Smad3-sensitive constructs were solely activated by Rac1, which is consistent with the findings of Ungefroren *et al.* (2013), that Rac1 is also directly involved in regulating Smad proteins in addition to its involvement in non-canonical TGFβ signaling in pancreatic carcinoma cells. The luciferase assays of our group also revealed, that Rac1b activated NF-κB-binding and LEF1/TCF-responsive promoter constructs more efficiently than Rac1 (Seiz *et al.*, 2019). These luciferase reporter gene assays did confirm the role of Rac1 and Rac1b in affecting gene expression, but the identified promoter activity alterations did not necessarily have to emanate from direct nuclear localization and promotor binding of both isoforms. But different studies confirmed a direct nuclear localization and functions of both proteins within the nucleus. Rac1 was shown to interact directly with STAT (signal transducer and activator of transcription) proteins and regulate their nuclear translocation (Kawashima *et al.*, 2006). Additionally, it was shown, that nuclear Rac1 proteins drive cell division during late G2 phase of the cell cycle (Michaelson *et al.*, 2008). On the other hand, Pethe and colleagues showed, that nuclear Rac1b binds directly to Wnt target gene promotors independent of Wnt3A stimulation, thereby acting as a transcriptional co-activator in β-Catenin/transcription factor 4 (TCF4)-mediated transcription (Pethe *et al.*, 2011). Furthermore, Rac1b functionally

interacts with and recruits Dishevelled-3 (Dvl-3) to these promotors and thereby drives the expression of Wnt target genes including *CCND1* (cyclin-D1) (Esufali *et al.*, 2007).
The studies performed in this work solely identified the presence of Rac1 and Rac1b proteins within nuclear extracts. To further evaluate possible divergent functions of Rac1 and Rac1b in the nucleus, Chromatin immunoprecipitation (ChIP) experiments followed by analyses of genomic DNA fragments (qRT-PCR, high throughput sequencing or micro array analyses) as well as the interacting proteins (western blot experiments or mass spectrometry) could be performed (Bhatia *et al.*, 2019). Furthermore, Rac1 and Rac1b mutants lacking the NLS could be generated as described in Esufali *et al.* (2007) and Lanning *et al.* (2004) and subsequently analyzed via the above mentioned luciferase reporter gene assays or ChIP experiments.

4.2 The chick embryonic chorioallantoic membrane assay as a tool to analyze Rac1 isoform-specific carcinoma cell invasion

The chick embryonic chorioallantoic membrane (CAM) is an extra embryonic excavation of the chorion and allantois, which develops at day 3 after fertilization and initiation of breeding. It functions as a respiratory organ of the chick embryo. The CAM is of mesodermal origin and consists of three layers, the outer chorionic epithelium, the intermediate, highly vascularized mesenchyme and the inner allantoic epithelium. The vascular network of the CAM is connected to the embryonic circulation allowing respiratory exchanges of oxygen and carbon dioxide, respectively (Cimpean *et al.*, 2008). The CAM invasion assay is an *in vivo* model to study carcinoma cell invasion and metastatic processes (Lokman *et al.*, 2012). As part of this work, the CAM assay was re-established in the group according to Hofer *et al.* (2004) and Veit *et al.* (2004) with slight modifications to analyze functional differences between Rac1 and Rac1b in carcinoma cell invasion.
The CAM assays revealed very heterogeneous invasive behaviors of the different analyzed cell lines (see Fig. 3.8 and Tab. 3.2). The parental H23 cells with low Rac1b-to-Rac1 protein ratios exhibited a high invasive potential with cells spreading into surrounding regions of the mesenchyme. HTB-55 cells, which were shown to express high levels of Rac1b proteins, exhibited no invasive potential and remained on top of the outer CAM epithelium. These observations are in line with the before mentioned findings in breast and pancreatic carcinoma cells, that an increased Rac1b protein expression reduces carcinoma cell migration, whereas low Rac1b-to-Rac1 protein ratios are linked to increased motility and TGFβ1-induced EMT (Melzer *et al.*, 2017; Ungefroren *et al.*, 2013). The comparison of the invasive behaviors of H23 and HTB-55 cells in regard to their Rac1b protein levels point towards antagonistic roles of

Rac1 and Rac1b in carcinoma cell invasion as well as a role of Rac1b as a negative regulator of this process. But the results of the CAM invasion assays of this work did not confirm this hypothesis thoroughly in all the analyzed cell lines. The picture was more heterogeneous for Colo357 and H358 cells. H358-derived tumors, invaded through the outer epithelium of the CAM and formed solid tumor cell nests within the mesenchymal layer, whereas Colo357 cells exhibited weak invasive potential with only a few small cell aggregates invading into the mesenchymal layer of the CAM. Both, H358 and Colo357 cells, were shown to exhibit high levels of ESRP1 and ESRP2 proteins next to the high protein amounts of Rac1b. Fagoonee *et al.* (2017) demonstrated, that an increased ESRP1 and ESRP2 protein expression promoted the formation of liver macrometastases. The increased formation of macrometastases due to high ESRP protein expression levels could be one explanation for the formation of solid tumor nests and multicellular aggregates within the mesenchymal layer of the CAM. Additionally, different studies linked Rac1b to an elevated cancer cell invasion, as MMP-dependent Rac1b protein expression was shown to enhance EMT in breast, lung and pancreatic cancer cells (Cichon *et al.*, 2015; Mehner *et al.*, 2014; Stallings-Mann *et al.*, 2012). These findings could explain the observed invasive behaviors of H358 and Colo357 cells of this work.

The stable ectopic expression of EGFP-Rac1b did not alter the invasive potential of H23 cells, but rather the characteristics of the tumors formed (see Fig. 3.9 and Tab. 3.3). EGFP-Rac1b expressing cell clones formed large solid tumor nests within the mesenchyme of the CAM without obvious single cells dissemination. This is consistent with the invasive behavior of H358 cells mentioned above and further strengthens the hypothesis, that high Rac1b protein levels correlate with less aggressive tumor cell invasion and more importantly abrogates single cell dissemination. On the other hand, the invasion of EGFP-Rac1-expressing H23 cells was comparable to that of H23/EGFP cells as both cell clones exhibited strong CAM invasion and single cell spreading throughout the mesenchyme of the CAM. Different studies showed, that an increased Rac1 expression accelerated tumorigenic processes and promoted cell motility in colorectal adenocarcinoma cells, whereas Rac1 hyperactivation was shown to drive alveolar EMT in lung cancer (Espina *et al.*, 2008; Shen *et al.*, 2014). Furthermore, a previous study of our group provided evidence, that an increased Rac1 activity inhibited E-Cadherin-mediated adherens junctions in pancreatic carcinoma cells leading to enhanced carcinoma cell migration (Hage *et al.*, 2009). More recently, our group could show, that EGFP-Rac1-expressing H23 cell clones exhibited clearly diminished E-Cadherin protein levels, whereas the mesenchymal marker Vimentin was upregulated in comparison to H23/EGFP (Seiz *et al.*, 2019). This indicated an EMT-related de-differentiation of H23/EGFP-Rac1 cells and provides another

explanation for the extensive CAM invasion of these cell clones. But due to the high invasive potential of parental H23 cells, an enhanced invasion of the EGFP-Rac1 expressing cells was not evident within the four days of incubation on the CAM.

The results of CAM invasion assays performed in this work gave some hints on potential antagonistic functions of Rac1 and Rac1b in carcinoma cell invasion, but did not reveal a conclusive link between high Rac1b protein expression and reduced tumor cell invasion. To further address this matter, the protein expression ratios and activities of Rac1 and Rac1b should be altered in different pancreatic and lung carcinoma cells before applying them to the CAM. Next to analyzing the carcinoma cell invasion after stable ectopic expression of EGFP-Rac1 and EGFP-Rac1b as performed for H23 cell clones in this work, changes in the invasive capacity after siRNA-mediated silencing of the Rac1 and Rac1b proteins could be analyzed in future experiments. Additionally a knockout of *RAC1* or *RAC1B* by utilizing the CRISPR-Cas9 gene editing system could provide additional promising insights into the role of both proteins in carcinoma cell invasion (Cong *et al.*, 2013; Mali *et al.*, 2013). Possible effects of an abrogated Rac1 or Rac1b activity on carcinoma cell invasion could be examined by treating the pancreatic and lung carcinoma cells with Rac1- or Rac1b specific inhibitors while being incubated on the CAM (Akbar *et al.*, 2006; Arnst *et al.*, 2017; Beausoleil *et al.*, 2009; Ying *et al.*, 2015).

4.3 Rac1b is a potential epithelial-specific Rac1 isoform

4.3.1 Rac1b expression is associated with epithelial-specific splicing factors and EMT markers

The splicing factors ESRP1, SRSF1, SRSF3 and hnRNP A1 were shown to regulate alternative splicing of *RAC1* pre-mRNA differently, whereas no influence of ESRP2 on exon 3b splicing was described (Gonçalves *et al.*, 2009; Ishii *et al.*, 2014; Pelisch *et al.*, 2012) (see also Fig. 1.5). Determination of mRNA amounts of all five splicing factors in various pancreatic and lung carcinoma cell lines and comparison to the mRNA levels of both *RAC1* isoforms revealed an interesting positive association between high *RAC1B* mRNA amounts and the presence of *ESRP1* and *ESRP2* mRNA. This was observed in Colo357, Capan-2 and BxPC-3 pancreatic as well as HTB-55, H358 and H2122 lung carcinoma cells (see Fig. 3.10). These expression patterns were also observed on protein level (see Fig. 3.11). ESRP1 was shown to drive the exclusion of the alternative exon 3b, thereby shifting the splicing outcome toward the *RAC1* transcript variant (Ishii *et al.*, 2014). The observed positive relation in the mRNA and protein levels of the Rac1b isoform and ESRP1 differs from the described function of this splicing factor in *RAC1* pre-mRNA maturation, since high ESRP1 expression should coincide with

enhanced exon 3b out-splicing and therefore reduced amounts of the *RAC1B* transcript variant. This novel observation was subsequently investigated in more detail by altering the mRNA and protein levels through siRNA-mediated depletion of Rac1b, ESRP1 and ESRP2 and will be addressed in more detail in the following chapters. The RT-PCR analyses conducted in this work elucidated only slight differences in *HNRNPA1*, *SRSF1* and *SRSF3* mRNA amounts between several pancreatic and lung carcinoma cell lines (see Fig. 3.10). Several studies revealed an overexpression of SRSF1, SRSF3 and hnRNP A1 in various tumor entities, thereby affecting alternative splicing in pro-tumorigenic fashion and promoting tumor-relevant processes like EMT, cancer cell invasion and increased cell survival (Anczuków *et al.*, 2012; Chen *et al.*, 2018b; Cogoi *et al.*, 2017; Corbo *et al.*, 2012; Gout *et al.*, 2012; Jia *et al.*, 2010). This might explain the slight differences in the mRNA amounts of the three splicing factors observed between the analyzed cell lines as the expression of them might be increased in some of them. But since a Rac1b-dependent relation in the mRNA amounts of *HNRNPA1*, *SRSF1* and *SRSF3* was not observed, as seen for *ESRP1* and *ESRP2,* these splicing factors were excluded from further analyses.

In the following experiments, the EMT-status of several pancreatic and lung cell lines was analyzed by investigating the expression levels of E-Cadherin and Vimentin (see Fig. 3.15 and Fig. 3.16). The results were compared to the detected mRNA and protein levels of Rac1b and ESRPs and revealed a positive association with mRNA and protein levels of the epithelial marker E-Cadherin. Reciprocally, the mRNA and protein levels of Vimentin correlated negatively with high Rac1b and ESRP amounts. This was particularly evident in pancreatic cell lines, whereas the picture was not as clear in lung carcinoma cells. But the lung cell lines, that expressed high amounts of Rac1b, also exhibited E-Cadherin mRNA and protein expression. Warzecha and colleagues could show, that ESRP1 and ESRP2 are expressed exclusively in epithelial cells (Warzecha *et al.*, 2009b). It is not surprising, that cell lines expressing both epithelial splicing factors also exhibit high mRNA and protein levels of the epithelial marker E-Cadherin.

4.3.2 A novel cooperation of Rac1b and ESRP2

The observation, that high ESRP and E-Cadherin mRNA and protein levels were related to high amounts of Rac1b was very interesting. A possible cooperation of Rac1b and ESRP1 as well as ESRP2 was subsequently analyzed by siRNA-mediated depletion experiments. Additionally, Rac1-specific effects were supposed to be elucidated by siRNA-mediated silencing of Rac1. Different siRNAs were tested, one of which was complementary to the exon 3-exon 4 junction

of mature *RAC1* mRNA (Melzer *et al.*, 2017). But none of the tested transfection conditions nor the different siRNAs led to a Rac1 protein knockdown efficiency higher than 40 % in the experiments performed in this work (data not shown). The ubiquitously expressed Rac1 protein was shown to be an essential player in cytoskeletal rearrangements, cell migration, focal adhesion complex formation and several other cellular processes (Raftopoulou and Hall, 2004; Wertheimer *et al.*, 2012). Additionally, the western blot experiments of this work revealed high overall Rac1 protein expression levels in comparison to Rac1b (see Fig. 3.2). Both, the essential role in cellular processes and the high protein expression levels of Rac1, could serve as possible explanations for the weak knockdown efficiencies observed in this work. But since Melzer *et al.* (2017) achieved strong and specific silencing of Rac1 using a Rac1-specific siRNA, further testing is needed to deplete Rac1 sufficiently in future experiments.

In contrast, siRNAs complementary to the alternative exon 3b of Rac1b were shown to strongly and specifically deplete the Rac1b isoform without affecting Rac1 mRNA and protein levels (Melzer *et al.*, 2017; Ungefroren *et al.*, 2013; Witte *et al.*, 2017). This was also observed in the siRNA-mediated depletion experiments performed in the course of this work (see Fig. 3.12, Fig. 3.13 and Fig. 3.14). These experiments revealed, that a knockdown of Rac1b had an influence on the mRNA and protein expression of ESRP2. This observation was particularly evident in sqRT-PCR analyses, where the *RAC1B* knockdown resulted in a strong downregulation of *ESRP2* in all three analyzed cell lines. When performing qRT-PCR and western blot analyses the Rac1b-dependent downregulation of ESRP2 was also observed, but not as strong. The observed discrepancy between the *ESRP2* mRNA levels after *RAC1B* depletion detected in semi quantitative in comparison to quantitative RT-PCR analyses might be explained by methodical differences between these two experimental setups, like different primers, reaction conditions and PCR devices (Livak and Schmittgen, 2001; Marone *et al.*, 2001). Nevertheless, results of the qRT-PCR analyses are to be considered more reliable and the results also reflect the changes on the protein level more consistently, which were observed in the western blot experiments (compare Fig. 3.13 and Fig. 3.14). Horiguchi *et al.* (2012) could show that ESRP2 was downregulated by the transcription factors delta-crystallin enhancer binding protein 1 (δEF1) and Smad-interacting protein 1 (SIP1, also known as ZEB2). By performing ChIP experiments and luciferase reporter assays, they could show, that δEF1 and SIP1 not only bind to E-box promoter elements upstream of the *ESRP2* gene, but also suppress *ESRP2* gene expression. Similar experimental approaches could provide insights whether nuclear Rac1b proteins could either directly interact with E-box promotor elements and drive the transcription of the *ESRP2* gene or act as a transcriptional co-activator in the process. As

described before, Rac1b was shown to influence Wnt target genes by acting as a transcriptional co-activator and binding to these promotors via interaction with β-Catenin and Dishevelled-3 (Esufali *et al.*, 2007; Pethe *et al.*, 2011). Rac1b could act similarly in regulating *ESRP2* gene expression.

Another observation, which was consistently made in H358 cells in the course of this work was the upregulation of Rac1b mRNA and protein levels upon siRNA-mediated knockdown of ESRP1. This is consistent with the observation of Ishii *et al.* (2014), that ESRP1 regulates the out-splicing of the alternative exon 3b during *RAC1* pre-mRNA maturation. The results of this work confirm the findings of Ishii and colleagues and show, that the knockdown of ESRP1 shifts the balance of alternative splicing towards exon 3b inclusion and therefore the generation of *RAC1B* mRNA. Interestingly, this effect was neither observed in HTB-55 nor in Colo357 cells after depletion of ESRP1 in the course of this work. It is known, that the ratio and relative abundance of multiple splicing factors influence the splicing outcome. Moreover, the balance of an alternative splicing event can be shifted through expression changes, re-localization and altered activity states of different splicing factors (Warzecha and Carstens, 2012). It is therefore possible, that *RAC1* pre-mRNA splicing patterns could be compensated by other splicing factors after the RNA interference-mediated loss of ESRP1 in HTB-55 and Colo357 cells. As mentioned before, SRSF3 and hnRNP A1 were both shown to regulate alternative exon 3b out-splicing (Gonçalves *et al.*, 2009; Pelisch *et al.*, 2012). Additionally, both splicing factors were shown to shuttle between the cytoplasm and nucleus, depending on prior activation (Gonçalves *et al.*, 2014; Wang *et al.*, 2017a). It would be interesting to analyze, whether the depletion of ESRP1 altered the expression levels or the subcellular localization of SRSF1 and hnRNP A1, which could explain the unchanged mRNA and protein levels of Rac1b in HTB-55 and Colo357 cells.

As mentioned before, Rac1b was previously connected to enhanced cancer cell motility and EMT in several cancer types, including lung, pancreatic, breast, thyroid and colorectal cancer (Cichon *et al.*, 2015; Esufali *et al.*, 2007; Faria *et al.*, 2017; Mehner *et al.*, 2014; Stallings-Mann *et al.*, 2012). On the other hand, ESRPs were shown to regulate the protein expression of isoforms involved the maintenance of cell-cell and cell-matrix adhesion as well as epithelial cell polarity (Warzecha *et al.*, 2009b; Warzecha *et al.*, 2010; Yang *et al.*, 2016). High protein expression levels of ESRP1 and ESRP2 were shown to attenuate metastases in pancreatic cancer mouse xenografts (Ueda *et al.*, 2014). The identified novel link between Rac1b and the epithelial-specific splicing factor ESRP2 points towards a previously unknown role of Rac1b in regulating an epithelial phenotype.

4.3.3 The connection between the Rac1b-ESRP2 axis and EMT-related factors

The mRNA and protein amounts of Rac1b, ESRP1 and ESRP2 were positively associated to the presence of the epithelial marker E-Cadherin and negatively linked to the mesenchymal marker Vimentin (see Fig. 3.15 and Fig. 3.16). In further experiments, the mRNA and protein amounts of E-Cadherin and Vimentin were analyzed after silencing Rac1b, ESRP1 and ESRP2 in Colo357 pancreatic as well as H358 and HTB-55 lung carcinoma cells. The qPCR analyses revealed, that silencing of *ESRP1* and *ESRP2* weakly, but consistently downregulated *CDH1* mRNA levels in Colo357, H358 and HTB-55 cells. Downregulation of ESRP1 and ESRP2 were highlighted as obligate and general events at the onset of EMT during early cancer progression and correlated with a higher risk of metastasis during early breast and oral squamous cancer tumorigenesis (Fici *et al.*, 2017; Ishii *et al.*, 2014). The downregulation of E-Cadherin was extensively analyzed as a hallmark event during EMT and different regulators, transcription factors and micro RNAs (miRNA) were shown to be involved in this process (Wang *et al.*, 2017b; Zhao *et al.*, 2016). Ishii *et al.* (2014) identified distinct mechanisms by which ESRP1 and ESRP2 suppressed cancer cell motility. A knockdown of ESRP2 in head and neck squamous cell cancer cell lines led to the attenuation of cell-cell adhesion through downregulation of E-Cadherin, whereas the knockdown or overexpression of ESRP1 did not alter E-Cadherin protein levels. Ishii and his colleagues could also show, that ESRP2 was not as potent of a splicing factor as ESRP1 and postulated, that it might affect the protein levels of epithelial-specific proteins indirectly through regulating the gene expression of miRNAs and different transcription factors. Horiguchi *et al.* (2012) showed, that ectopic lentiviral expression of ESRP2 in TGFβ-treated human breast cancer cells resulted in restored E-Cadherin protein expression, but failed to downregulate mesenchymal markers and was not accompanied by a de-repression of EMT transcription factors. Again it was hypothesized, that ESRP2 might affect expression of other E-Cadherin inducers and different epithelial-specific regulators. Jeong *et al.* (2017) observed that overexpression of ESRP1 in ovarian cancer cells promoted switching from a mesenchymal to an epithelial phenotype. Although an upregulation of E-Cadherin and downregulation of Vimentin was observed, Jeong and his colleagues postulated, that this was due to the downregulation of ZEB2 and other EMT-specific transcription factors. Nevertheless, the combined results of the studies described above are consistent with the observation of this work, that *ESRP1* and *ESRP2* both are somehow involved in regulating the *CDH1* mRNA amounts positively. Furthermore, the qPCR analyses of this work demonstrated an upregulation of *VIM* mRNA after an *ESRP2* knockdown in H358 cells, which might be another indirect target

of ESRP2, comparably to the described results after ESRP1 depletion of Jeong *et al.* (2017). Surprisingly, *VIM* mRNA levels were downregulated in HTB-55 cells after an *ESRP2* knockdown and depletion of *ESRP1* in both cell lines, H358 and HTB-55. These results are different from the previously described roles of the two epithelial-specific splicing factors in maintaining an epithelial phenotype. It is important to note, that the precise role of ESRP1 and ESRP2 in carcinogenesis remain to be fully elucidated. Different studies have linked high ESRP1 and ESRP2 expression profiles to enhanced tumor progression and cancer cell proliferation (Fagoonee *et al.*, 2017; Gökmen-Polar *et al.*, 2019). Therefore, further research is necessary to fully understand the role of ESRPs in cancer and EMT. Another interesting observation was, that the siRNA-mediated silencing of *RAC1B* resulted in a weak upregulation of *CDH1* in H358 cells, but not in Colo357 and HTB-55 cells. This observation is consistent with the results of Esufali *et al.* (2007), who demonstrated that RNA interference-mediated suppression of Rac1b resulted in an increase of E-Cadherin protein levels due to downregulation of Slug, which resulted in a decreased colorectal cancer cell adhesion. This result differs from the previously described finding of this work, that Rac1b is a positive regulator of ESRP2, which in turn is involved in maintaining E-Cadherin protein expression (Horiguchi *et al.*, 2012; Ishii *et al.*, 2014; Jeong *et al.*, 2017).

Since the siRNA-mediated knockdown of *RAC1B*, *ESRP1* and *ESRP2* for 96 h revealed only slight changes in *CDH1* and *VIM* mRNA levels, *SNAIL, SLUG*, *TWIST1* and *ZEB1* as well as *ZEB2* were analyzed (see Fig. 3.19 and Fig. 3.20). The EMT-specific transcription factors Snail, Slug and Twist1 as well as ZEB1 and ZEB2 were shown to downregulate a vast array of epithelial-specific proteins, e.g. E-Cadherin, and upregulate the protein expression of mesenchymal proteins, e.g. N-Cadherin. Furthermore, these transcription factors also influence the protein levels of each other in a positive feedback manner, thereby amplifying the EMT response (Lamouille *et al.*, 2014; Tran *et al.*, 2011). The qRT-PCR experiments performed in this work revealed very diverse and cell line-dependent mRNA expression changes. The knockdown of neither splicing factor nor the GTPase had a major effect on the mRNA amounts of *SNAIL* in Colo357, H358 and HTB-55 cells. *SLUG* mRNA quantities were weakly decreased upon depletion of *ESRP1* and *ESRP2* only in H358 cells, whereas the knockdowns of the splicing factors did not alter the mRNA amounts of *SLUG* in HTB-55 and Colo357 cells. Snail was shown to regulate ESRP1 protein expression negatively in lung, ovarian and breast cancer cells by directly binding to E-box promoter elements in close proximity to the *ESRP1* gene, thereby enhancing cancer cell invasion and promoting EMT (Chen *et al.*, 2017b; Reinke *et al.*, 2012; Walser *et al.*, 2018). Slug was also shown to repress a broad range of genes responsible

for a differentiated epithelial morphology, including ESRPs (Chen *et al.*, 2017b; Dhasarathy *et al.*, 2011). But ESRP1 and ESRP2 do not seem to play a major role in regulating the amounts of Snail and Slug, since the siRNA-mediated knockdown experiments of this work did not alter the mRNA levels of both transcription factors markedly. This is consistent with the observations made by Horiguchi *et al.* (2012) and Jeong *et al.* (2017), who could demonstrate that ectopic expression of neither ESRP1 nor ESRP2 had an effect on the expression ratios of Slug and Snail. Interestingly, *SLUG* mRNA levels were upregulated in Colo357 and H358 cells upon knockdown of *RAC1B*. This differs from the observations made by Esufali *et al.* (2007) already described above, but matches the results of Ungefroren *et al.* (2013), who could show, that a knockdown of Rac1b led to an increased transcription of the endogenous *SLUG* gene. Additionally, it fits to the role of Rac1b as a putative positive regulator of ESRP2 postulated in this work. Rac1b might repress the protein expression of Slug in H358 cells, thereby abolishing its inhibitory effects on the expression of the *ESRP2* gene.

The third transcription factor, that was analyzed in this work was Twist1, which was also shown to be involved in the downregulation of ESRP1 and ESRP2 (Warzecha *et al.*, 2009a). In this work, it was observed, that *TWIST1* mRNA amounts were upregulated in H358 cells after depletion of *ESRP2*. As mentioned before, Ishii *et al.* (2014) postulated, that ESRP2 might affect the protein levels of epithelial-specific proteins indirectly through regulating the expression of miRNAs and different transcription factors. The repression of the *TWIST1* mRNA expression could be one mechanism by which ESRP2 indirectly influences epithelial protein expression patterns. Jeong *et al.* (2017) could show, that ectopic expression of ESRP1 strongly downregulated *TWIST1* mRNA levels. Similar findings were not evident after depleting *ESRP1* in H358, HTB-55 and Colo357 cells in the course of this work. However, Jeong and colleagues did not analyze the effects of ectopic expression of ESRP2 on *TWIST1* mRNA amounts, which might validate a role of this splicing factor in repressing the mRNA expression of this transcription factor as observed in this work.

Altogether, the qRT-PCR analyses performed in this work revealed very diverse and cell line-dependent mRNA expression changes of EMT-specific transcription factors with regard to the analyzed time point of 96 h after siRNA transfection. EMT is a complex multistep process, that involves extensive and transient changes on the transcriptional, post-transcriptional, translational and post-translational level (see Ch. 1.1 and Ch. 1.2). This process takes time, which was also demonstrated in this work by the necessity of treating H358 cells with TGFβ1 for up to twelve days to induce EMT (see Ch. 3.7.1). It is possible, that the knockdown of Rac1b, ESRP1 and ESRP2 for a duration of only 96 h was not long enough to induce striking

changes in the mRNA and protein levels of the different EMT markers and transcription factors. Nevertheless, a cautious statement can be drawn from the results described above. At least in H358 cells, Rac1b might repress Slug protein expression, which subsequently cannot inhibit transcription of the *ESRP2* gene. ESRP2 subsequently represses the protein expression of Twist1, thereby promoting E-Cadherin protein expression. This could be one mechanism by which Rac1b and ESRP2 might cooperate in maintaining an epithelial phenotype. Further experiments are needed to confirm this hypothesis and possibly identify other factors involved. The short incubating time could also explain the observations made after the transient expression HA-ERSP1 and HA-ESRP2 in PANC-1 cells. Only very weak changes in the protein levels of E-Cadherin, Rac1b and Snail were detected, whereas the protein amounts of Vimentin and p120^{ctn}, a known target of ESRP1 (Warzecha *et al.*, 2009b), were not affected (see Fig. 3.21). As described above, Jeong *et al.* (2017) and Horiguchi *et al.* (2012) observed that overexpression of ESRP1 and ESRP2 promoted the switching from a mesenchymal to an epithelial phenotype. Both studies analyzed long-term effects of stable overexpression of ESRP1 and ESRP2 protein levels. The western blot analyses conducted in this work, were performed after only 96 h of transient overexpression of HA-ESRP1 and HA-ESRP2. It would be interesting to not only analyze the expression patterns of EMT markers and transcription factors, but also the connection between Rac1b and ESRP2, after permanently altering the mRNA and protein levels of Rac1b, ESRP1 and ESRP2. These issues should be addressed in the future experiments as a logical consequence of the observations made in this work.

4.3.4 The role of Rac1b and ESRPs in TGFβ1-induced EMT

H358, Colo357 and HTB-55 cells were stimulated with TGFβ1 for up to twelve days to induce EMT and examine protein expression changes of Rac1 isoforms, ESRP1 and ESRP2 as well as different EMT-related proteins. Only the stimulation of H358 cells with TGFβ1 for twelve days led to obvious protein expression changes consistent with EMT. Epithelial marker proteins like E-Cadherin, ESPR1 and ESRP2 were markedly downregulated, whereas the protein expression of mesenchymal proteins like Vimentin and the EMT-specific transcription factor Snail were strongly increased (see Fig. 3.22). Increased TGFβ1 expression, secretion and activation were shown to induce EMT in a wide variety of cancers. The prolonged treatment of NSCLC cells with TGFβ1 correlated with cancer cell stemness, induced changes in the protein expression patterns consistent with EMT and increased metastatic potential (Gemmill *et al.*, 2011; Pirozzi *et al.*, 2011; Vázquez *et al.*, 2013). Furthermore, it was shown, that TGFβ1 drives cell migration as well as EMT in pancreatic ductal adenocarcinoma cells (Ungefroren *et al.*, 2011). The results

of this work were consistent with the observations made by Gemmill *et al.* (2011) and Pirozzi *et al.* (2011), who analyzed TGFβ1-induced EMT in several NSCLC cell lines including H358 cells. They observed downregulated E-Cadherin, Cytokeratin, ESRP1 and ESRP2 protein levels among many others, whereas the protein expressions of Vimentin, N-Cadherin, Snail, Slug and Twist1 were markedly upregulated (Gemmill *et al.*, 2011; Pirozzi *et al.*, 2011). The results of this work also matched the findings of Horiguchi *et al.* (2012), who observed, that TGFβ1 treatment promoted EMT by downregulating ESRP1 and ESRP2, which depended on the increased expression of the transcription factors δEF1 and SIP1 (also known as ZEB2). A reversal of the TGFβ1-induced downregulation of ESRP1 and ESRP2 was analyzed in this work by a transient expression of HA-ESRP1 and HA-ESRP2 for two days after long-term TGFβ1 stimulation of H358 cells (see Fig. 3.24). But these experiments did not reveal an alteration of the TGFβ1-induced changes in the protein expression patterns of the Rac1 isoforms, EMT-related proteins and transcription factors. Two days of transient overexpression of both splicing factors might be insufficient to reverse the drastic protein expression changes induced by prolonged TGFβ1 stimulation of H358 cells and the subsequent downregulation of ESRP1 and ESRP2.

Another interesting observation was an altered splicing pattern of $p120^{ctn}$ upon TGFβ1 treatment. A longer $p120^{ctn}$ isoform was present in H358 cells, which were stimulated with TGFβ1 in comparison to unstimulated cells (see Fig 3.22). Additionally, the results of long-term siRNA-mediated silencing experiments elucidated a role of ESRP1 in alternative splicing of the *CTNND1* pre-mRNA. A knockdown of ESRP1, but not ESRP2, led to the presence of a longer $p120^{ctn}$ isoform (presumably isoform A1) (see Fig, 3.23). The results of this work confirm the observations of previous studies, that ESRP1 regulates alternative splicing of *CTNND1* pre-mRNA (Warzecha *et al.*, 2009a; Warzecha *et al.*, 2009b). Furthermore, it was shown, that a $p120^{ctn}$ isoform switch plays an important role during EMT. $p120^{ctn}$ isoforms 3A and 4A were shown to promote cell-cell adhesion and stabilize the E-Cadherin juxtamembrane complex, whereas isoform 1A was shown to induce cancer cell motility by decreasing RhoA and stimulating Rac1 activity (Ishiyama *et al.*, 2010; Yanagisawa *et al.*, 2008). Concomitant to the results of long-term TGFβ1 stimulation experiments performed in this work, Zhang *et al.* (2014) also observed a change in the isoform ratio of $p120^{ctn}$ during EMT. Moreover, they showed, that the expression of a shorter $p120^{ctn}$-3A isoform inhibited EMT and decreased cell invasion of different NSCLC cell lines, whereas the longer $p120^{ctn}$-1A promoted these effects. The results of this work support the role of shorter $p120^{ctn}$ isoforms (presumably isoform 3A or 4A) as epithelial-specific isoforms. Nevertheless, further experiments are necessary to identify

the precise $p120^{ctn}$ isoforms, which are generated through ESRP1-mediated alternative splicing, and to elucidate EMT-related functional differences between the various isoforms.

A surprising observation of this work was, that the long-term TGFβ1 treatment of H358 cells also led to a downregulation of Rac1b, but not Rac1, which coincided with a downregulation of ESRP1 (see Fig. 3.22 and Fig. 3.24). Downregulation of ESRP1 protein levels should result in increased Rac1b protein amounts, since the results of this work and of Ishii *et al.* (2014) demonstrated, that ESRP1 regulates exon 3b out-splicing during *RAC1* pre-mRNA maturation. Interestingly, the long-term TGFβ1 treatment of H358 cells revealed a concomitant downregulation of ESRP1 and Rac1b in this work. Additionally, the lab of our collaboration partner Hendrik Ungefroren characterized a novel role of Rac1b as a negative regulator of canonical and also Smad-independent TGFβ1 signaling and carcinoma cell motility in pancreatic ductal and breast adenocarcinoma cells. They observed, that the siRNA-mediated silencing of Rac1b strongly enhanced cancer cell motility in a TGFβ1-dependent manner (Ungefroren *et al.*, 2013; Witte *et al.*, 2017). Furthermore, they could show, that Rac1 on the other hand drives EMT and cancer cell migration by inhibiting TGFβ1-mediated growth inhibition and antagonistically regulating Smad2 and Smad3 (Ungefroren *et al.*, 2011). Altogether, they postulated, that a high Rac1b-to-Rac1 protein expression ratio counteracts TGFβ1-induced EMT and pancreatic carcinoma cell migration. The interesting observation of this work, that TGFβ1-induced EMT and the coherent downregulation of epithelial marker proteins is accompanied by decreased protein levels of Rac1b, underscores the observations of Ungefroren and colleagues, who described Rac1b as an inhibitor of TGFβ1-dependent EMT and pancreatic carcinoma cell migration. Whether or not this downregulation of Rac1b is due to an altered splicing pattern of *RAC1* pre-mRNA or enhanced Rac1b protein degradation requires further investigation. Nevertheless, the results of this work strengthens the postulated role of Rac1b as an epithelial-specific Rac1 isoform.

4.4 Therapeutic significance and outlook

The precise role Rac1b in carcinogenesis and its functional differences to Rac1 are controversially debated and remain to be fully elucidated. The overexpression and hyperactivation of Rac1 proteins were shown to promote carcinoma cell motility as well as EMT in several tumor types (Espina *et al.*, 2008; Hage *et al.*, 2009; Shen *et al.*, 2014). Overexpression of Rac1b was identified as a driving-force during K-Ras-induced lung tumorigenesis and linked to MMP-induced EMT in breast, lung and pancreatic cancer (Cichon *et al.*, 2015; Mehner *et al.*, 2014; Stallings-Mann *et al.*, 2012; Zhou *et al.*, 2013a). In metastatic

colorectal cancer patients, Rac1b overexpression correlated with a poor prognosis (Alonso-Espinaco *et al.*, 2014; Henriques *et al.*, 2015; Matos *et al.*, 2008). In these cases, high Rac1b protein expression could serve as prognostic marker and negatively altering the protein levels or activity of Rac1b could provide therapeutic benefits. But as mentioned before, Rac1b was also shown to act antagonistically to Rac1 in TGFβ1-induced EMT in breast and pancreatic carcinoma cells. Thereby, a putative role of Rac1b as an inhibitor of TGFβ1-driven EMT was described (Ungefroren *et al.*, 2013; Witte *et al.*, 2017). The results of this work indicate, that Rac1b is associated to an epithelial-specific splicing network as well as a more differentiated and epithelial phenotype in selected pancreatic and lung carcinoma cells. This might attribute high Rac1b protein expression to positive prognostic features.

ESRP1 and ESRP2 were identified as master regulators of an epithelial-specific splicing network and the downregulation of these splicing regulators was shown to be obligate for EMT induction (Fici *et al.*, 2017; Ishii *et al.*, 2014). Nevertheless, the precise role of ESRP1 and ESRP2 in carcinogenesis remains the topic of many controversial debates. The protein levels of ESRPs were described to be plastic during cancer progression as they were shown to be upregulated during early oral squamous cell carcinogenesis, but downregulated in invasive fronts. Subsequently, they were re-expressed in metastatic cancer cell nests that colonized lymph nodes (Ishii *et al.*, 2014). Although high ESRP1 and ESRP2 protein expression levels were shown to drive early tumorigenesis in colorectal and breast cancer cells (Fagoonee *et al.*, 2017; Gökmen-Polar *et al.*, 2019), the presence of these splicing factors was also correlated to a better overall survival in colorectal cancer patients and attenuated metastasis in pancreatic cancer mouse xenografts (Deloria *et al.*, 2016; Ueda *et al.*, 2014). Carvalho *et al.* (2017) demonstrated, that pharmacological manipulation of splicing could prove to be beneficial for developing new anti-cancer drugs. Pharmacological alteration of ESRP expression or activity could therefore provide novel approaches in targeting metastatic cancers.

Altogether, the results of this work indicate a highly complex and diverse role of Rac1b in regulating carcinoma cell motility and EMT. Several findings connect Rac1b to epithelial-specific protein expression patterns, whereas other results contradict this hypothesis. Next to assessing differences in the subcellular localization of Rac1 and Rac1b and their influence on carcinoma cell invasion, this work provides novel insights into a connection between the protein and mRNA expression of Rac1b and the epithelial-specific splicing factor ESRP2. Nevertheless, further research is of the essence to gain a deeper knowledge of the role of Rac1 isoforms in EMT and further characterize the Rac1b-ESRP2 axis identified in this work, which might provide novel targets in treating metastatic pancreatic and lung cancers.

5 Abstract

The small Rho family GTPase Rac1 plays an important role in pre-metastatic events like cell scattering, migration and invasion in several tumor types. Alternative splicing leads to the generation of the splice variant Rac1b, which includes the alternative exon 3b and was characterized as a constitutive active Rac1 isoform. Previous work of our group and collaboration partners revealed antagonistic activities of Rac1 and Rac1b in transforming growth factor β (TGFβ)-induced epithelial-to-mesenchymal transition (EMT) and tumor cell motility in pancreatic carcinoma cell lines. The studies of other groups have shown, that EMT is also fine-tuned by various splicing factors. Especially, the epithelial splicing regulatory proteins 1 (ESRP1) and 2 (ESRP2) were shown to regulate the alternative splicing of epithelial-specific proteins and were observed to be downregulated at the onset of EMT.

In the course of this work, functional differences between the two GTPase isoforms Rac1 and Rac1b and their differential role in tumor cell invasion as well as EMT were analyzed. Initial experiments revealed substantial differences in Rac1b mRNA and protein amounts between various pancreatic and lung carcinoma cell lines, whereas Rac1 mRNA and proteins were expressed in comparable amounts. Subcellular fractionation and fluorescence microscopy analyses to determine the subcellular localization of Rac1 and Rac1b wildtype and mutant proteins revealed a predominantly membranous localization of wildtype Rac1b, which was comparable to constitutive active Rac1. In contrast, wildtype Rac1 showed a comparable cytoplasmic and membranous distribution. By applying the chorioallantoic membrane (CAM) model to study carcinoma cell invasion, a high heterogeneity in the invasive behaviors between all analyzed cell lines with different Rac1 and Rac1b protein expression levels was observed, indicating a more complex network of proteins and factors involved. Furthermore, CAM assays with H23 cell clones stably expressing EGFP-Rac1 and EGFP-Rac1b revealed an enhanced tumor cell scattering of invading H23/EGFP-Rac1 in comparison to H23/EGFP-Rac1b cells.

Analysis of the mRNA and protein levels of different putative *RAC1* splicing factors, both Rac1 isoforms and EMT-related factors revealed a relation in the mRNA and protein expression of Rac1b and ESRP1, a factor shown to be involved in exon 3b out-splicing, as well as ESRP2 and epithelial marker proteins. Furthermore, the siRNA-mediated depletion of Rac1b, ESRP1 and ESRP2 pointed toward a cooperation in the expression of ESRP2 and Rac1b. The TGFβ1 stimulation of H358 lung carcinoma cells to induce EMT revealed a concomitant downregulation of Rac1b, ESRP1 and ESRP2 protein levels, thereby indicating a possible role of these factors in maintaining an epithelial phenotype.

6 Zusammenfassung

Die kleine GTPase Rac1 wurde in verschiedenen Tumorentitäten mit prä-metastatischen Ereignissen wie dem Zell-*Scattering* und einer erhöhten Tumorzellmigration sowie -invasion assoziiert. Durch alternatives Spleißen der *RAC1* prä-mRNA wird Rac1b generiert, welches ein alternatives Exon 3b enthält und als konstitutiv aktive Rac1-Isoform charakterisiert wurde. Die bisherigen Studien der Arbeitsgruppe sowie ihrer Kollaborationspartner deckten antagonistische Aktivitäten von Rac1 und Rac1b in der transformierenden Wachstumsfaktor β (TGFβ)-induzierten epithelialen-zu-mesenchymalen Transition (EMT) und Tumorzellmotilität von Pankreaskarzinomzelllinien auf. Andere Gruppen zeigten auch eine wichtige Rolle verschiedener Spleißfaktoren in der Regulation der EMT auf. Dabei konnte eine Runterregulierung der epithelial-spezifischen Spleißfaktoren ESRP1 und ESPR2 in der frühen Phase der EMT beobachtet werden.

Im Rahmen dieser Arbeit wurden funktionale Unterschiede zwischen den beiden RhoGTPase-Isoformen Rac1 und Rac1b sowie deren differentielle Rolle in der Tumorzellinvasion und EMT analysiert. Dabei wurden zunächst starke Unterschiede in der Menge an Rac1b mRNA und Proteinen zwischen den analysierten Pankreas- und Lungenkarzinomzelllinien festgestellt, wogegen Rac1 in vergleichbaren Mengen exprimiert wurde. Im Rahmen von Studien zur subzellulären Lokalisation mithilfe subzellulärer Fraktionierungs- und Fluoreszenz-mikroskopischer Analysen konnte eine überwiegende Membranlokalisation von Rac1b festgestellt werden, welche mit der von konstitutiv-aktiven Rac1-Mutanten übereinstimmte. Wildtypisches Rac1 wies hingegen eine ausgeglichene cytosolische und membranöse Lokalisation auf. Das Chorionallantois-Membran (CAM)-Modells zur Untersuchung der Karzinomzellinvasion zeigte eine starke Heterogenität in dem invasiven Verhalten der analysierten Zelllinien mit unterschiedlichen Rac1- und Rac1b-Proteinexpressionsmusters auf. Dies spricht für ein komplexeres Netzwerk an beteiligten Faktoren. Die stabile Expression von EGFP-Rac1 in H23-Zellen führte zu einer erhöhten Zellstreuung der eingewanderten Zellen im CAM-Gewebe im Vergleich zu EGFP-Rac1b-expriemierenden H23-Zellen.

Expressionsstudien zeigten eine Verbindung der Protein- und mRNA-Mengen von Rac1b mit der von ESRP1, einem bekannten Exon 3b Spleiß-Aktivator, sowie ESRP2 und einem epithelialen Expressionsmuster. Die siRNA-vermittelte-Depletion von Rac1b, ESRP1 und ESRP2 deckte eine mögliche Kooperation zwischen der Expression von Rac1b und ESRP2 auf. Zusätzlich führte die Induktion der EMT durch die TGFβ1-Stimulation von H358-Zellen zu einer Reduzierung der Rac1b-, ESRP1- und ESRP2-Proteinmengen. Die Ergebnisse deuten auf eine mögliche Assoziation dieser Proteine mit einem epithelialen Phänotyp hin.

7 References

Akbar, H., Cancelas, J., Williams, D.A., Zheng, J. and Zheng, Y. (2006): Rational Design and Applications of a Rac GTPase–Specific Small Molecule Inhibitor. *Methods in enzymology*, **406**, 554–565.

Alonso-Espinaco, V., Cuatrecasas, M., Alonso, V., Escudero, P., Marmol, M., Horndler, C., Ortego, J., Gallego, R., Codony-Servat, J., Garcia-Albeniz, X., Jares, P., Castells, A., Lozano, J.J., Rosell, R. and Maurel, J. (2014): RAC1b overexpression correlates with poor prognosis in KRAS/BRAF WT metastatic colorectal cancer patients treated with first-line FOLFOX/XELOX chemotherapy. *European journal of cancer*, **50**, 1973–1981.

American Cancer Society (2018): Global Cancer Facts and Figures 4th Edition, Atlanta. *American Cancer Society, Atlanta*, 1–76.

Anczuków, O., Rosenberg, A.Z., Akerman, M., Das, S., Zhan, L., Karni, R., Muthuswamy, S.K. and Krainer, A.R. (2012): The splicing factor SRSF1 regulates apoptosis and proliferation to promote mammary epithelial cell transformation. *Nature structural & molecular biology*, **19**, 220–228.

Arnst, J.L., Hein, A.L., Taylor, M.A., Palermo, N.Y., Contreras, J.I., Sonawane, Y.A., Wahl, A.O., Ouellette, M.M., Natarajan, A. and Yan, Y. (2017): Discovery and characterization of small molecule Rac1 inhibitors. *Oncotarget*, **8**, 34586–34600.

Baker, N.M., Yee Chow, H., Chernoff, J. and Der, C.J. (2014): Molecular pathways: targeting RAC-p21-activated serine-threonine kinase signaling in RAS-driven cancers. *Clinical cancer research*, **20**, 4740–4746.

Barros, P., Jordan, P. and Matos, P. (2009): Rac1 signaling modulates BCL-6-mediated repression of gene transcription. *Molecular and cellular biology*, **29**, 4156–4166.

Beausoleil, E., Chauvignac, C., Taverne, T., Lacombe, S., Pognante, L., Leblond, B., Pallares, D., Oliveira, C.D., Bachelot, F., Carton, R., Peillon, H., Coutadeur, S., Picard, V., Lambeng, N., Désiré, L. and Schweighoffer, F. (2009): Structure-activity relationship of isoform selective inhibitors of Rac1/1b GTPase nucleotide binding. *Bioorganic & medicinal chemistry letters*, **19**, 5594–5598.

Bebee, T.W., Park, J.W., Sheridan, K.I., Warzecha, C.C., Cieply, B.W., Rohacek, A.M., Xing, Y. and Carstens, R.P. (2015): The splicing regulators Esrp1 and Esrp2 direct an epithelial splicing program essential for mammalian development. *eLife*, **4**, 1-27.

Bhatia, S., Matthews, J. and Wells, P.G. (2019): Characterization of Epigenetic Histone Activation/Repression Marks in Sequences of Genes by Chromatin Immunoprecipitation-Quantitative Polymerase Chain Reaction (ChIP-qPCR). *Methods in molecular biology*, **1965**, 389–403.

Braeutigam, C., Rago, L., Rolke, A., Waldmeier, L., Christofori, G. and Winter, J. (2014): The RNA-binding protein Rbfox2: an essential regulator of EMT-driven alternative splicing and a mediator of cellular invasion. *Oncogene*, **33**, 1082–1092.

Bustelo, X.R., Ojeda, V., Barreira, M., Sauzeau, V. and Castro-Castro, A. (2012): Rac-ing to the plasma membrane: the long and complex work commute of Rac1 during cell signaling. *Small GTPases*, **3**, 60–66.

Carvalho, T., Martins, S., Rino, J., Marinho, S. and Carmo-Fonseca, M. (2017): Pharmacological inhibition of the spliceosome subunit SF3b triggers exon junction complex-independent nonsense-mediated decay. *Journal of cell science*, **130**, 1519–1531.

Casas, E., Kim, J., Bendesky, A., Ohno-Machado, L., Wolfe, C.J. and Yang, J. (2011): Snail2 is an essential mediator of Twist1-induced epithelial mesenchymal transition and metastasis. *Cancer research*, **71**, 245–254.

Chen, B., Chou, H.T., Brautigam, C.A., Xing, W., Yang, S., Henry, L., Doolittle, L.K., Walz, T. and Rosen, M.K. (2017a): Rac1 GTPase activates the WAVE regulatory complex through two distinct binding sites. *eLife*, **6**, 1-22.

Chen, H., Guo, S., Xia, Y., Yuan, L., Lu, M., Zhou, M., Fang, M., Meng, L., Xiao, Z. and Ma, J. (2018a): The role of Rho-GEF Trio in regulating tooth root development through the p38 MAPK pathway. *Experimental cell research*, **372**, 158–167.

Chen, J., Xu, H., Zou, X., Wang, J., Zhu, Y., Chen, H., Shen, B., Deng, X., Zhou, A., Chin, Y.E., Rauscher, F.J., Peng, C. and Hou, Z. (2014): Snail recruits Ring1B to mediate transcriptional repression and cell migration in pancreatic cancer cells. *Cancer research*, **74**, 4353–4363.

Chen, L., Yao, Y., Sun, L., Zhou, J., Miao, M., Luo, S., Deng, G., Li, J., Wang, J. and Tang, J. (2017b): Snail Driving Alternative Splicing of CD44 by ESRP1 Enhances Invasion and Migration in Epithelial Ovarian Cancer. *Cellular physiology and biochemistry*, **43**, 2489–2504.

Chen, Q.K., Lee, K., Radisky, D.C. and Nelson, C.M. (2013): Extracellular matrix proteins regulate epithelial-mesenchymal transition in mammary epithelial cells. *Differentiation; research in biological diversity*, **86**, 126–132.

Chen, Y., Liu, J., Wang, W., Xiang, L., Wang, J., Liu, S., Zhou, H. and Guo, Z. (2018b): High expression of hnRNPA1 promotes cell invasion by inducing EMT in gastric cancer. *Oncology reports*, **39**, 1693–1701.

Cichon, M.A., Nelson, C.M. and Radisky, D.C. (2015): Regulation of epithelial-mesenchymal transition in breast cancer cells by cell contact and adhesion. *Cancer informatics*, **14**, 1–13.

Cimpean, A.M., Ribatti, D. and Raica, M. (2008): The chick embryo chorioallantoic membrane as a model to study tumor metastasis. *Angiogenesis*, **11**, 311–319.

Cogoi, S., Rapozzi, V., Cauci, S. and Xodo, L.E. (2017): Critical role of hnRNP A1 in activating KRAS transcription in pancreatic cancer cells: A molecular mechanism involving G4 DNA. *Biochimica et biophysica acta.*, **1861**, 1389–1398.

Cong, L., Ran, F.A., Cox, D., Lin, S., Barretto, R., Habib, N., Hsu, P.D., Wu, X., Jiang, W., Marraffini, L.A. and Zhang, F. (2013): Multiplex genome enginieering using CRISPR/Cas systems. *Science*, **339**, 819–823.

Corbo, C., Orrù, S., Gemei, M., Di Noto, R., Mirabelli, P., Imperlini, E., Ruoppolo, M., Vecchio, L.D. and Salvatore, F. (2012): Protein cross-talk in CD133+ colon cancer cells indicates activation of the Wnt pathway and upregulation of SRp20 that is potentially involved in tumorigenicity. *Proteomics*, **12**, 2045–2059.

Corbo, C., Orrù, S. and Salvatore, F. (2013): SRp20: an overview of its role in human diseases. *Biochemical and biophysical research communications*, **436**, 1–5.

Das, S. and Krainer, A.R. (2014): Emerging functions of SRSF1, splicing factor and oncoprotein, in RNA metabolism and cancer. *Molecular cancer research*, **12**, 1195–1204.

Deloria, A.J., Höflmayer, D., Kienzl, P., Lopatecka, J., Sampl, S., Klimpfinger, M., Braunschmid, T., Bastian, F., Lu, L., Marian, B., Stättner, S. and Holzmann, K. (2016): Epithelial splicing regulatory protein 1 and 2 paralogues correlate with splice signatures and favorable outcome in human colorectal cancer. *Oncotarget*, **7**, 73800-73816.

Dhasarathy, A., Phadke, D., Mav, D., Shah, R.R. and Wade, P.A. (2011): The transcription factors Snail and Slug activate the transforming growth factor-beta signaling pathway in breast cancer. *PloS one*, **6**, 1-11.

Dittmar, K.A., Jiang, P., Park, J.W., Amirikian, K., Wan, J., Shen, S., Xing, Y. and Carstens, R.P. (2012): Genome-wide determination of a broad ESRP-regulated posttranscriptional network by high-throughput sequencing. *Molecular and cellular biology*, **32**, 1468–1482.

Dominguez, C., Fisette, J.-F., Chabot, B. and Allain, F.H.-T. (2010): Structural basis of G-tract recognition and encaging by hnRNP F quasi-RRMs. *Nature structural & molecular biology*, **17**, 853–861.

Dong, C., Wu, Y., Yao, J., Wang, Y., Yu, Y., Rychahou, P.G., Evers, B.M. and Zhou, B.P. (2012): G9a interacts with Snail and is critical for Snail-mediated E-cadherin repression in human breast cancer. *The Journal of clinical investigation*, **122**, 1469–1486.

Dreissigacker, U., Mueller, M.S., Unger, M., Siegert, P., Genze, F., Gierschik, P. and Giehl, K. (2006): Oncogenic K-Ras down-regulates Rac1 and RhoA activity and enhances migration and invasion of pancreatic carcinoma cells through activation of p38. *Cellular signalling*, **18**, 1156–1168.

Ehrlich, J.S., Hansen, M.D.H. and Nelson, W.J. (2002): Spatio-temporal regulation of Rac1 localization and lamellipodia dynamics during epithelial cell-cell adhesion. *Developmental Cell*, **3**, 259–270.

Espina, C., Céspedes, M.V., García-Cabezas, M.A., Gómez del Pulgar, M.T., Boluda, A., Oroz, L.G., Benitah, S.A., Cejas, P., Nistal, M., Mangues, R. and Lacal, J.C. (2008): A critical role for Rac1 in tumor progression of human colorectal adenocarcinoma cells. *The American journal of pathology*, **172**, 156–166.

Esufali, S., Charames, G.S., Pethe, V.V., Buongiorno, P. and Bapat, B. (2007): Activation of tumor-specific splice variant Rac1b by dishevelled promotes canonical Wnt signaling and decreased adhesion of colorectal cancer cells. *Cancer research*, **67**, 2469–2479.

Ezponda, T., Pajares, M.J., Agorreta, J., Echeveste, J.I., López-Picazo, J.M., Torre, W., Pio, R. and Montuenga, L.M. (2010): The oncoprotein SF2/ASF promotes non-small cell lung cancer survival by enhancing survivin expression. *Clinical cancer research*, **16**, 4113–4125.

Fagoonee, S., Picco, G., Orso, F., Arrigoni, A., Longo, D.L., Forni, M., Scarfò, I., Cassenti, A., Piva, R., Cassoni, P., Silengo, L., Tolosano, E., Aime, S., Taverna, D., Pandolfi, P.P., Brancaccio, M., Medico, E. and Altruda, F. (2017): The RNA-binding protein ESRP1 promotes human colorectal cancer progression. *Oncotarget*, **8**, 10007–10024.

Fardi, M., Alivand, M., Baradaran, B., Farshdousti Hagh, M. and Solali, S. (2019): The crucial role of ZEB2: From development to epithelial-to-mesenchymal transition and cancer complexity. *Journal of cellular physiology*, 1–17.

Faria, M., Capinha, L., Simões-Pereira, J., Bugalho, M.J. and Silva, A.L. (2016): Extending the Impact of RAC1b Overexpression to Follicular Thyroid Carcinomas. *International journal of endocrinology*, **2016**, 1972367.

Faria, M., Matos, P., Pereira, T., Cabrera, R., Cardoso, B.A., Bugalho, M.J. and Silva, A.L. (2017): RAC1b overexpression stimulates proliferation and NF-kB-mediated anti-apoptotic signaling in thyroid cancer cells. *PloS one*, **12**, 1-13.

Feig, L.A. (1999): Tools of the trade: use of dominant-inhibitory mutants of Ras-family GTPases. *Nature cell biology*, **1**, 25–27.

Fici, P., Gallerani, G., Morel, A.P., Mercatali, L., Ibrahim, T., Scarpi, E., Amadori, D., Puisieux, A., Rigaud, M. and Fabbri, F. (2017): Splicing factor ratio as an index of epithelial-mesenchymal transition and tumor aggressiveness in breast cancer. *Oncotarget*, **8**, 2423–2436.

Fiegen, D., Haeusler, L.-C., Blumenstein, L., Herbrand, U., Dvorsky, R., Vetter, I.R. and Ahmadian, M.R. (2004): Alternative splicing of Rac1 generates Rac1b, a self-activating GTPase. *The Journal of biological chemistry*, **279**, 4743–4749.

Gandhi, P.N., Gibson, R.M., Tong, X., Miyoshi, J., Takai, Y., Konieczkowski, M., Sedor, J.R. and Wilson-Delfosse, A.L. (2004): An activating mutant of Rac1 that fails to interact with Rho GDP-dissociation inhibitor stimulates membrane ruffling in mammalian cells. *The Biochemical journal*, **375**, 409–419.

Garcia-Mata, R., Boulter, E. and Burridge, K. (2011): The 'invisible hand': regulation of RHO GTPases by RHOGDIs. *Nature reviews. Molecular cell biology*, **12**, 493–504.

Gemmill, R.M., Roche, J., Potiron, V.A., Nasarre, P., Mitas, M., Coldren, C.D., Helfrich, B.A., Garrett-Mayer, E., Bunn, P.A. and Drabkin, H.A. (2011): ZEB1-responsive genes in non-small cell lung cancer. *Cancer letters*, **300**, 66–78.

Gloushankova, N.A., Rubtsova, S.N. and Zhitnyak, I.Y. (2017): Cadherin-mediated cell-cell interactions in normal and cancer cells. *Tissue barriers*, **5**, 1-15.

Gökmen-Polar, Y., Neelamraju, Y., Goswami, C.P., Gu, Y., Gu, X., Nallamothu, G., Vieth, E., Janga, S.C., Ryan, M. and Badve, S.S. (2019): Splicing factor ESRP1 controls ER-positive breast cancer by altering metabolic pathways. *EMBO reports*, **20**, 1–19.

Gonçalves, V., Henriques, A.F.A., Henriques, A., Pereira, J.F.S., Pereira, J., Neves Costa, A., Moyer, M.P., Moita, L.F., Gama-Carvalho, M., Matos, P. and Jordan, P. (2014): Phosphorylation of SRSF1 by SRPK1 regulates alternative splicing of tumor-related Rac1b in colorectal cells. *RNA*, **20**, 474–482.

Gonçalves, V., Matos, P. and Jordan, P. (2009): Antagonistic SR proteins regulate alternative splicing of tumor-related Rac1b downstream of the PI3-kinase and Wnt pathways. *Human molecular genetics*, **18**, 3696–3707.

Gout, S., Brambilla, E., Boudria, A., Drissi, R., Lantuejoul, S., Gazzeri, S. and Eymin, B. (2012): Abnormal expression of the pre-mRNA splicing regulators SRSF1, SRSF2, SRPK1 and SRPK2 in non small cell lung carcinoma. *PloS one*, **7**, 1-14.

Graveley, B.R. (2009): Alternative splicing: regulation without regulators. *Nature structural & molecular biology*, **16**, 13–15.

Grizot, S., Fauré, J., Fieschi, F., Vignais, P.V., Dagher, M.-C. and Pebay-Peyroula, E. (2001): Crystal Structure of the Rac1−RhoGDI Complex Involved in NADPH Oxidase Activation †,‡. *Biochemistry*, **40**, 10007–10013.

Grobe, H., Wüstenhagen, A., Baarlink, C., Grosse, R. and Grikscheit, K. (2018): A Rac1-FMNL2 signaling module affects cell-cell contact formation independent of Cdc42 and membrane protrusions. *PloS one*, **13**, 1-17.

Guo, R., Li, Y., Ning, J., Sun, D., Lin, L. and Liu, X. (2013): HnRNP A1/A2 and SF2/ASF regulate alternative splicing of interferon regulatory factor-3 and affect immunomodulatory functions in human non-small cell lung cancer cells. *PloS one*, **8**, 1-13.

Hage, B., Meinel, K., Baum, I., Giehl, K. and Menke, A. (2009): Rac1 activation inhibits E-cadherin-mediated adherens junctions via binding to IQGAP1 in pancreatic carcinoma cells. *Cell communication and signaling*, **7**, 1–13.

Hartsock, A. and Nelson, W.J. (2008): Adherens and tight junctions: structure, function and connections to the actin cytoskeleton. *Biochimica et biophysica acta*, **1778**, 660–669.

Hata, A. and Chen, Y.-G. (2016): TGF-β Signaling from Receptors to Smads. *Cold Spring Harbor perspectives in biology*, **8**.

Hayakawa, A., Saitoh, M. and Miyazawa, K. (2017): Dual Roles for Epithelial Splicing Regulatory Proteins 1 (ESRP1) and 2 (ESRP2) in Cancer Progression. *Advances in experimental medicine and biology*, **925**, 33–40.

Heid, I., Lubeseder-Martellato, C., Sipos, B., Mazur, P.K., Lesina, M., Schmid, R.M. and Siveke, J.T. (2011): Early requirement of Rac1 in a mouse model of pancreatic cancer. *Gastroenterology*, **141**, 719-730.

Henriques, A.F.A., Barros, P., Moyer, M.P., Matos, P. and Jordan, P. (2015): Expression of tumor-related Rac1b antagonizes B-Raf-induced senescence in colorectal cells. *Cancer letters*, **369**, 368–375.

Herbst, R.S., Heymach, J.V. and Lippman, S.M. (2008): Molecular origins of cancer - lung cancer. *The New England journal of medicine*, **359**, 1367–1380.

Hofer, M.D., Menke, A., Genze, F., Gierschik, P. and Giehl, K. (2004): Expression of MTA1 promotes motility and invasiveness of PANC-1 pancreatic carcinoma cells. *British journal of cancer*, **90**, 455–462.

Horiguchi, K., Sakamoto, K., Koinuma, D., Semba, K., Inoue, A., Inoue, S., Fujii, H., Yamaguchi, A., Miyazawa, K., Miyazono, K. and Saitoh, M. (2012): TGF-β drives epithelial-mesenchymal transition through δEF1-mediated downregulation of ESRP. *Oncogene*, **31**, 3190–3201.

Huang, R.Y.-J., Guilford, P. and Thiery, J.P. (2012): Early events in cell adhesion and polarity during epithelial-mesenchymal transition. *Journal of cell science*, **125**, 4417–4422.

Imamichi, Y., Waidmann, O., Hein, R., Eleftheriou, P., Giehl, K. and Menke, A. (2005): TGF beta-induced focal complex formation in epithelial cells is mediated by activated ERK and JNK MAP kinases and is independent of Smad4. *Biological chemistry*, **386**, 225–236.

Iovanna, J., Mallmann, M.C., Gonçalves, A., Turrini, O. and Dagorn, J.-C. (2012): Current knowledge on pancreatic cancer. *Frontiers in oncology*, **2**, 1–24.

Ishii, H., Saitoh, M., Sakamoto, K., Kondo, T., Katoh, R., Tanaka, S., Motizuki, M., Masuyama, K. and Miyazawa, K. (2014): Epithelial splicing regulatory proteins 1 (ESRP1) and 2 (ESRP2) suppress cancer cell motility via different mechanisms. *The Journal of biological chemistry*, **289**, 27386–27399.

Ishiyama, N., Lee, S.-H., Liu, S., Li, G.-Y., Smith, M.J., Reichardt, L.F. and Ikura, M. (2010): Dynamic and static interactions between p120 catenin and E-cadherin regulate the stability of cell-cell adhesion. *Cell*, **141**, 117–128.

Izumi, D., Toden, S., Ureta, E., Ishimoto, T., Baba, H. and Goel, A. (2019): TIAM1 promotes chemoresistance and tumor invasiveness in colorectal cancer. *Cell death & disease*, **10**, 267.

Jeong, H.M., Han, J., Lee, S.H., Park, H.-J., Lee, H.J., Choi, J.-S., Lee, Y.M., Choi, Y.-L., Shin, Y.K. and Kwon, M.J. (2017): ESRP1 is overexpressed in ovarian cancer and promotes switching from mesenchymal to epithelial phenotype in ovarian cancer cells. *Oncogenesis*, **6**, 1-13.

Jia, R., Cuiling, L., McCoy, J.P., Deng, C.-X. and Zheng, Z.-M. (2010): SRp20 is a proto-oncogene critical for cell proliferation and tumor induction and maintenance. *International Journal of Biological Sciences*, **6**, 806–826.

Jordan, P., Brazao, R., Boavida, M.G., Gespach, C. and Chastre, E. (1999): Cloning of a novel human Rac1b splice veriant with increased expression in colorectal tumors. *Oncogene*, **18**, 6835–6839.

Kadara, H., Kabbout, M. and Wistuba, I.I. (2012): Pulmonary adenocarcinoma: a renewed entity in 2011. *Respirology (Carlton, Vic.)*, **17**, 50–65.

Kalluri, R. and Weinberg, R.A. (2009): The basics of epithelial-mesenchymal transition. *The Journal of clinical investigation*, **119**, 1420–1428.

Kamato, D., Burch, M.L., Piva, T.J., Rezaei, H.B., Rostam, M.A., Xu, S., Zheng, W., Little, P.J. and Osman, N. (2013): Transforming growth factor-β signalling: role and consequences of Smad linker region phosphorylation. *Cellular signalling*, **25**, 2017–2024.

Kawashima, T., Bao, Y.C., Nomura, Y., Moon, Y., Tonozuka, Y., Minoshima, Y., Hatori, T., Tsuchiya, A., Kiyono, M., Nosaka, T., Nakajima, H., Williams, D.A. and Kitamura, T. (2006): Rac1 and a GTPase-activating protein, MgcRacGAP, are required for nuclear translocation of STAT transcription factors. *The Journal of cell biology*, **175**, 937–946.

Kim, J. and Kim, S.H. (2013): CK2 inhibitor CX-4945 blocks TGF-β1-induced epithelial-to-mesenchymal transition in A549 human lung adenocarcinoma cells. *PloS one*, **8**, 1-13.

Kölbl, A.C., Jeschke, U. and Andergassen, U. (2016): The Significance of Epithelial-to-Mesenchymal Transition for Circulating Tumor Cells. *International journal of molecular sciences*, **17**, 1–12.

Kourtidis, A., Ngok, S.P. and Anastasiadis, P.Z. (2013): p120 catenin: an essential regulator of cadherin stability, adhesion-induced signaling, and cancer progression. *Progress in molecular biology and translational science*, **116**, 409–432.

Lam, B.D. and Hordijk, P.L. (2013): The Rac1 hypervariable region in targeting and signaling: a tail of many stories. *Small GTPases*, **4**, 78–89.

Lamouille, S., Xu, J. and Derynck, R. (2014): Molecular mechanisms of epithelial–mesenchymal transition. *Nature reviews. Molecular cell biology*, **15**, 178-196.

Lanning, C.C., Daddona, J.L., Ruiz-Velasco, R., Shafer, S.H. and Williams, C.L. (2004): The Rac1 C-terminal polybasic region regulates the nuclear localization and protein degradation of Rac1. *The Journal of biological chemistry*, **279**, 44197–44210.

Lanning, C.C., Ruiz-Velasco, R. and Williams, C.L. (2003): Novel mechanism of the co-regulation of nuclear transport of SmgGDS and Rac1. *The Journal of biological chemistry*, **278**, 12495–12506.

Lawson, C.D. and Ridley, A.J. (2018): Rho GTPase signaling complexes in cell migration and invasion. *The Journal of cell biology*, **217**, 447–457.

Lee, Y. and Rio, D.C. (2015): Mechanisms and Regulation of Alternative Pre-mRNA Splicing. *Annual review of biochemistry*, **84**, 291–323.

Livak, K.J. and Schmittgen, T.D. (2001): Analysis of relative gene expression data using real-time quantitative PCR and the 2(-Delta Delta C(T)) Method. *Methods*, **25**, 402–408.

Lokman, N.A., Elder, A.S.F., Ricciardelli, C. and Oehler, M.K. (2012): Chick chorioallantoic membrane (CAM) assay as an in vivo model to study the effect of newly identified molecules on ovarian cancer invasion and metastasis. *International journal of molecular sciences*, **13**, 9959–9970.

Luo, Y., Yu, T., Zhang, Q., Fu, Q., Hu, Y., Xiang, M., Peng, H., Zheng, T., Lu, L. and Shi, H. (2018): Upregulated N-cadherin expression is associated with poor prognosis in epithelial-derived solid tumours: A meta-analysis. *European journal of clinical investigation*, **48**, 1–14.

Makrodouli, E., Oikonomou, E., Koc, M., Andera, L., Sasazuki, T., Shirasawa, S. and Pintzas, A. (2011): BRAF and RAS oncogenes regulate Rho GTPase pathways to mediate migration and invasion properties in human colon cancer cells: a comparative study. *Molecular Cancer*, **10**, 1–21.

Mali, P., Yang, L., Esvelt, K.M., Aach, J., Guell, M., DiCarlo, J.E., Norville, J.E. and Church, G.M. (2013): RNA-guided human genome engineering via Cas9. *Science*, **339**, 823–826.

Marei, H. and Malliri, A. (2017): GEFs: Dual regulation of Rac1 signaling. *Small GTPases*, **8**, 90–99.

Marone, M., Mozzetti, S., De Ritis, D., Pierelli, L. and Scambia, G. (2001): Semiquantitative RT-PCR analysis to assess the expression levels of multiple transcripts from the same sample. *Biochemical procedures online*, **3**, 19–25.

Matos, P., Collard, J.G. and Jordan, P. (2003): Tumor-related alternatively spliced Rac1b is not regulated by Rho-GDP dissociation inhibitors and exhibits selective downstream signaling. *The Journal of biological chemistry*, **278**, 50442–50448.

Matos, P. and Jordan, P. (2005): Expression of Rac1b stimulates NF-kappaB-mediated cell survival and G1/S progression. *Experimental cell research*, **305**, 292–299.

Matos, P., Oliveira, C., Velho, S., Gonçalves, V., da Costa, L.T., Moyer, M.P., Seruca, R. and Jordan, P. (2008): B-Raf(V600E) cooperates with alternative spliced Rac1b to sustain colorectal cancer cell survival. *Gastroenterology*, **135**, 899–906.

Mehner, C., Miller, E., Khauv, D., Nassar, A., Oberg, A.L., Bamlet, W.R., Zhang, L., Waldmann, J., Radisky, E.S., Crawford, H.C. and Radisky, D.C. (2014): Tumor cell-derived MMP3 orchestrates Rac1b and tissue alterations that promote pancreatic adenocarcinoma. *Molecular cancer research*, **12**, 1430–1439.

Melzer, C., Ohe, J. von der, Hass, R. and Ungefroren, H. (2017): TGF-β-Dependent Growth Arrest and Cell Migration in Benign and Malignant Breast Epithelial Cells Are Antagonistically Controlled by Rac1 and Rac1b. *International journal of molecular sciences*, **18**, 1–16.

Menke, A. and Giehl, K. (2012): Regulation of adherens junctions by Rho GTPases and p120-catenin. *Archives of biochemistry and biophysics*, **524**, 48–55.

Micalizzi, D.S., Farabaugh, S.M. and Ford, H.L. (2010): Epithelial-mesenchymal transition in cancer: parallels between normal development and tumor progression. *Journal of mammary gland biology and neoplasia*, **15**, 117–134.

Michaelson, D., Abidi, W., Guardavaccaro, D., Zhou, M., Ahearn, I., Pagano, M. and Philips, M.R. (2008): Rac1 accumulates in the nucleus during the G2 phase of the cell cycle and promotes cell division. *The Journal of cell biology*, **181**, 485–496.

Montero, J.C., Seoane, S., Ocaña, A. and Pandiella, A. (2011): P-Rex1 participates in Neuregulin-ErbB signal transduction and its expression correlates with patient outcome in breast cancer. *Oncogene*, **30**, 1059–1071.

Morgan, R.T., Woods, L.K., Moore, G.E., Quinn, L.A., McGavran, L. and Gordon, S.G. (1980): Human cell line (COLO 357) of metastatic pancreatic adenocarcinoma. *International Journal of Cancer*, **25**, 591–598.

Morrison, C.D., Parvani, J.G. and Schiemann, W.P. (2013): The relevance of the TGF-β Paradox to EMT-MET programs. *Cancer letters*, **341**, 30–40.

Nagano, M., Hoshino, D., Koshikawa, N., Akizawa, T. and Seiki, M. (2012): Turnover of focal adhesions and cancer cell migration. *International journal of cell biology*, **2012**, 310616.

Nicholson, R.C., Mader, S., Nagpal, S., Leid, M., Rochette-Egly, C. and Chambon, P. (1990): Negative regulation of the rat stromelysin gene promoter by retinoic acid is mediated by an AP1 binding site. *The EMBO journal*, **9**, 4443–4454.

Nimnual, A.S., Taylor, L.J., Nyako, M., Jeng, H.-H. and Bar-Sagi, D. (2010): Perturbation of cytoskeleton dynamics by the opposing effects of Rac1 and Rac1b. *Small GTPases*, **1**, 89–97.

Nuessle, J.M., Giehl, K., Herzog, R., Stracke, S. and Menke, A. (2011): TGFβ1 suppresses vascular smooth muscle cell motility by expression of N-cadherin. *Biological chemistry*, **392**, 461–474.

Orlichenko, L., Geyer, R., Yanagisawa, M., Khauv, D., Radisky, E.S., Anastasiadis, P.Z. and Radisky, D.C. (2010): The 19-amino acid insertion in the tumor-associated splice isoform Rac1b confers specific binding to p120 catenin. *The Journal of biological chemistry*, **285**, 19153–19161.

Pastushenko, I. and Blanpain, C. (2019): EMT Transition States during Tumor Progression and Metastasis. *Trends in cell biology*, **29**, 212–226.

Peixoto, P., Etcheverry, A., Aubry, M., Missey, A., Lachat, C., Perrard, J., Hendrick, E., Delage-Mourroux, R., Mosser, J., Borg, C., Feugeas, J.-P., Herfs, M., Boyer-Guittaut, M. and Hervouet, E. (2019): EMT is associated with an epigenetic signature of ECM remodeling genes. *Cell death & disease*, **10**, 205.

Pelisch, F., Khauv, D., Risso, G., Stallings-Mann, M., Blaustein, M., Quadrana, L., Radisky, D.C. and Srebrow, A. (2012): Involvement of hnRNP A1 in the matrix metalloprotease-3-dependent regulation of Rac1 pre-mRNA splicing. *Journal of cellular biochemistry*, **113**, 2319–2329.

Pennisi, E. (2005): Why do humans have so few genes? *Science*, **309**, 80.

Pethe, V.V., Charames, G.S. and Bapat, B. (2011): Rac1b recruits Dishevelled and β-catenin to Wnt target gene promoters independent of Wnt3A stimulation. *International journal of oncology*, **39**, 805–810.

Peurois, F., Veyron, S., Ferrandez, Y., Ladid, I., Benabdi, S., Zeghouf, M., Peyroche, G. and Cherfils, J. (2017): Characterization of the activation of small GTPases by their GEFs on membranes using artificial membrane tethering. *The Biochemical journal*, **474**, 1259–1272.

Phillips, S. and Kuperwasser, C. (2014): SLUG: Critical regulator of epithelial cell identity in breast development and cancer. *Cell adhesion & migration*, **8**, 578–587.

Piekielko-Witkowska, A., Wiszomirska, H., Wojcicka, A., Poplawski, P., Boguslawska, J., Tanski, Z. and Nauman, A. (2010): Disturbed expression of splicing factors in renal cancer affects alternative splicing of apoptosis regulators, oncogenes, and tumor suppressors. *PloS one*, **5**, 1-12.

Pieters, T., van Roy, F. and van Hengel, J. (2012): Functions of p120ctn isoforms in cell-cell adhesion and intracellular signaling. *Frontiers in Bioscience*, **17**, 1669–1694.

Pirozzi, G., Tirino, V., Camerlingo, R., Franco, R., La Rocca, A., Liguori, E., Martucci, N., Paino, F., Normanno, N. and Rocco, G. (2011): Epithelial to mesenchymal transition by TGFβ-1 induction increases stemness characteristics in primary non small cell lung cancer cell line. *PloS one*, **6**, 1-11.

Pradella, D., Naro, C., Sette, C. and Ghigna, C. (2017): EMT and stemness: flexible processes tuned by alternative splicing in development and cancer progression. *Molecular Cancer*, **16**, 1–19.

Radulovich, N., Qian, J.-y. and Tsao, M.-S. (2008): Human pancreatic duct epithelial cell model for KRAS transformation. *Methods in enzymology*, **439**, 1–13.

Raftopoulou, M. and Hall, A. (2004): Cell migration: Rho GTPases lead the way. *Developmental Biology*, **265**, 23–32.

Reinke, L.M., Xu, Y. and Cheng, C. (2012): Snail represses the splicing regulator epithelial splicing regulatory protein 1 to promote epithelial-mesenchymal transition. *The Journal of biological chemistry*, **287**, 36435–36442.

Remorino, A., Beco, S. de, Cayrac, F., Di Federico, F., Cornilleau, G., Gautreau, A., Parrini, M.C., Masson, J.-B., Dahan, M. and Coppey, M. (2017): Gradients of Rac1 Nanoclusters Support Spatial Patterns of Rac1 Signaling. *Cell reports*, **21**, 1922–1935.

Richardson, D.N., Rogers, M.F., Labadorf, A., Ben-Hur, A., Guo, H., Paterson, A.H. and Reddy, A.S.N. (2011): Comparative analysis of serine/arginine-rich proteins across 27 eukaryotes: insights into sub-family classification and extent of alternative splicing. *PloS one*, **6**, 1-16.

Roy, R., Huang, Y., Seckl, M.J. and Pardo, O.E. (2017): Emerging roles of hnRNPA1 in modulating malignant transformation. *Wiley interdisciplinary reviews*, **8**, 1–18.

Ryan, D.P., Hong, T.S. and Bardeesy, N. (2014): Pancreatic adenocarcinoma. *The New England journal of medicine*, **371**, 1039–1049.

Sahu, V., Gupta, A., Kumar, R., Gupta, T., Mohan, A. and Dey, S. (2016): Quantification of Rac1 and Rac1b in serum of non small cell lung cancer by label free real time assay. *Clinica chimica acta*, **460**, 231–235.

Sandrock, K., Bielek, H., Schradi, K., Schmidt, G. and Klugbauer, N. (2010): The nuclear import of the small GTPase Rac1 is mediated by the direct interaction with karyopherin alpha2. *Traffic*, **11**, 198–209.

Santibáñez, J.F., Kocić, J., Fabra, A., Cano, A. and Quintanilla, M. (2010): Rac1 modulates TGF-beta1-mediated epithelial cell plasticity and MMP9 production in transformed keratinocytes. *FEBS letters*, **584**, 2305–2310.

Schindelin, J., Arganda-Carreras, I., Frise, E., Kaynig, V., Longair, M., Pietzsch, T., Preibisch, S., Rueden, C., Saalfeld, S., Schmid, B., Tinevez, J.-Y., White, D.J., Hartenstein, V., Eliceiri, K., Tomancak, P. and Cardona, A. (2012): Fiji: an open-source platform for biological-image analysis. *Nature methods*, **9**, 676–682.

Schnelzer, A., Prechtel, D., Knaus, U., Dehne, K., Gerhard, M., Graeff, H., Harbeck, N., Schmitt, M. and Lengyel, E. (2000): Rac1 in human breast cacner: overexpression, mutation analysis, and characterization of a new isoform, Rac1b. *Oncogene*, **19**, 3013–3020.

Seiz, J.R., Klinke, J., Scharlibbe, L., Lohfink, D., Heipel, M., Ungefroren, H., Giehl, K. and Menke, A. (2019): Different signaling and functionality of Rac1 and Rac1b in the progression of lung adenocarcinoma. *Biological chemistry*, 1–22.

Shen, H.-j., Sun, Y.-h., Zhang, S.-j., Jiang, J.-x., Dong, X.-w., Jia, Y.-l., Shen, J., Guan, Y., Zhang, L.-h., Li, F.-f., Lin, X.-x., Wu, X.-m., Xie, Q.-m. and Yan, X.-f. (2014): Cigarette smoke-induced alveolar epithelial-mesenchymal transition is mediated by Rac1 activation. *Biochimica et biophysica acta*, **1840**, 1838–1849.

Shi, M., Zhu, J., Wang, R., Chen, X., Mi, L., Walz, T. and Springer, T.A. (2011): Latent TGF-β structure and activation. *Nature*, **474**, 343–349.

Shin, S.H., Kim, H.J., Hwang, D.W., Lee, J.H., Song, K.B., Jun, E., Shim, I.K., Hong, S.-M., Park, K.-M., Lee, Y.-L. and Kim, S.C. (2017): The DPC4/SMAD4 genetic status determines recurrence patterns and treatment outcomes in resected pancreatic ductal adenocarcinomas: a prospective cohort study. *Oncotarget*, **8**, 11945–11959.

Singh, A., Karnoub, A.E., Palmby, T.R., Lengyel, E., Sondek, J. and Der, C.J. (2004): Rac1b, a tumor associated, constitutively active Rac1 splice variant, promotes cellular transformation. *Oncogene*, **23**, 9369–9380.

St Johnston, D. and Ahringer, J. (2010): Cell polarity in eggs and epithelia: parallels and diversity. *Cell*, **141**, 757–774.

Stallings-Mann, M.L., Waldmann, J., Zhang, Y., Miller, E., Gauthier, M.L., Visscher, D.W., Downey, G.P., Radisky, E.S., Fields, A.P. and Radisky, D.C. (2012): Matrix metalloproteinase induction of Rac1b, a key effector of lung cancer progression. *Science translational medicine*, **4**, 1-12.

Steeg, P.S. (2016): Targeting metastasis. *Nature reviews. Cancer*, **16**, 201–218.

Tanaka, M. and Herr, W. (1990): Differential transcriptional activation by Oct-1 and Oct-2: Interdependent activation domains induce Oct-2 phosphorylation. *Cell*, **60**, 375–386.

Tang, H., Massi, D., Hemmings, B.A., Mandalà, M., Hu, Z., Wicki, A. and Xue, G. (2016): AKT-ions with a TWIST between EMT and MET. *Oncotarget*, **7**, 62767–62777.

Tran, D.D., Corsa, C.A.S., Biswas, H., Aft, R.L. and Longmore, G.D. (2011): Temporal and spatial cooperation of Snail1 and Twist1 during epithelial-mesenchymal transition predicts for human breast cancer recurrence. *Molecular cancer research : MCR*, **9**, 1644–1657.

Ueda, J., Matsuda, Y., Yamahatsu, K., Uchida, E., Naito, Z., Korc, M. and Ishiwata, T. (2014): Epithelial splicing regulatory protein 1 is a favorable prognostic factor in pancreatic cancer that attenuates pancreatic metastases. *Oncogene*, **33**, 4485–4495.

Ungefroren, H., Groth, S., Sebens, S., Lehnert, H., Gieseler, F. and Fändrich, F. (2011): Differential roles of Smad2 and Smad3 in the regulation of TGF-β1-mediated growth inhibition and cell migration in pancreatic ductal adenocarcinoma cells: control by Rac1. *Molecular Cancer*, **10**, 1–16.

Ungefroren, H., Sebens, S., Giehl, K., Helm, O., Groth, S., Fändrich, F., Röcken, C., Sipos, B., Lehnert, H. and Gieseler, F. (2013): Rac1b negatively regulates TGF-β1 induced cell motility in pancreatic ductal epithelial cells by suppressing Smad signalling. *Oncotarget*, **5**, 277–290.

Vanharanta, S., Marney, C.B., Shu, W., Valiente, M., Zou, Y., Mele, A., Darnell, R.B. and Massaguè, J. (2014): Loss of the multifunctional RNA-binding protein RBM47 as a source of selectable metastatic traits in breast cancer. *eLife*, **3**, 1-24.

Vázquez, P.F., Carlini, M.J., Daroqui, M.C., Colombo, L., Dalurzo, M.L., Smith, D.E., Grasselli, J., Pallotta, M.G., Ehrlich, M., Bal de Kier Joffé, E.D. and Puricelli, L. (2013): TGF-beta specifically enhances the metastatic attributes of murine lung adenocarcinoma: implications for human non-small cell lung cancer. *Clinical & experimental metastasis*, **30**, 993–1007.

Veit, C., Genze, F., Menke, A., Hoeffert, S., Gress, T.M., Gierschik, P. and Giehl, K. (2004): Activation of phophatidylinositol 3-kinase and extracellular signal-regulated kinase Is required for glial cell line-derived neurotrophic factor-induced migration and invasion of pancreatic carcinoma cells. *Cancer research*, **64**, 5291–5300.

Venables, J.P., Brosseau, J.-P., Gadea, G., Klinck, R., Prinos, P., Beaulieu, J.-F., Lapointe, E., Durand, M., Thibault, P., Tremblay, K., Rousset, F., Tazi, J., Abou Elela, S. and Chabot, B. (2013): RBFOX2 is an important regulator of mesenchymal tissue-specific splicing in both normal and cancer tissues. *Molecular and cellular biology*, **33**, 396–405.

Vetter, I.R. and Wittinghofer, A. (2001): The guanine nucleotide-binding switch in three dimensions. *Science*, **294**, 1299–1304.

Walser, T.C., Jing, Z., Tran, L.M., Lin, Y.Q., Yakobian, N., Wang, G., Krysan, K., Zhu, L.X., Sharma, S., Lee, M.-H., Belperio, J.A., Ooi, A.T., Gomperts, B.N., Shay, J.W., Larsen, J.E., Minna, J.D., Hong, L.-S., Fishbein, M.C. and Dubinett, S.M. (2018): Silencing the Snail-Dependent RNA Splice Regulator ESRP1 Drives Malignant Transformation of Human Pulmonary Epithelial Cells. *Cancer research*, **78**, 1986–1999.

Wang, F., Fu, X., Chen, P., Wu, P., Fan, X., Li, N., Zhu, H., Jia, T.-T., Ji, H., Wang, Z., Wong, C.C.L., Hu, R. and Hui, J. (2017a): SPSB1-mediated HnRNP A1 ubiquitylation regulates alternative splicing and cell migration in EGF signaling. *Cell research*, **27**, 540–558.

Wang, H., Wu, Q., Zhang, Y., Zhang, H.-N., Wang, Y.-B. and Wang, W. (2017b): TGF-β1-induced epithelial-mesenchymal transition in lung cancer cells involves upregulation of miR-9 and downregulation of its target, E-cadherin. *Cellular & molecular biology letters*, **22**, 1–10.

Warzecha, C.C. and Carstens, R.P. (2012): Complex changes in alternative pre-mRNA splicing play a central role in the epithelial-to-mesenchymal transition (EMT). *Seminars in cancer biology*, **22**, 417–427.

Warzecha, C.C., Jiang, P., Amirikian, K., Dittmar, K.A., Lu, H., Shen, S., Guo, W., Xing, Y. and Carstens, R.P. (2010): An ESRP-regulated splicing programme is abrogated during the epithelial-mesenchymal transition. *The EMBO journal*, **29**, 3286–3300.

Warzecha, C.C., Sato, T.K., Nabet, B., Hogenesch, J.B. and Carstens, R.P. (2009a): ESRP1 and ESRP2 are epithelial cell-type-specific regulators of FGFR2 splicing. *Molecular cell*, **33**, 591–601.

Warzecha, C.C., Shen, S., Xing, Y. and Carstens, R.P. (2009b): The epithelial splicing factors ESRP1 and ESRP2 positively and negatively regulate diverse types of alternative splicing events. *RNA biology*, **6**, 546–562.

Wawruszak, A., Kalafut, J., Okon, E., Czapinski, J., Halasa, M., Przybyszewska, A., Miziak, P., Okla, K., Rivero-Muller, A. and Stepulak, A. (2019): Histone Deacetylase Inhibitors and Phenotypical Transformation of Cancer Cells. *Cancers*, **11**, 1–31.

Wertheimer, E., Gutierrez-Uzquiza, A., Rosemblit, C., Lopez-Haber, C., Sosa, M.S. and Kazanietz, M.G. (2012): Rac signaling in breast cancer: a tale of GEFs and GAPs. *Cellular signalling*, **24**, 353–362.

Witte, D., Otterbein, H., Förster, M., Giehl, K., Zeiser, R., Lehnert, H. and Ungefroren, H. (2017): Negative regulation of TGF-β1-induced MKK6-p38 and MEK-ERK signalling and epithelial-mesenchymal transition by Rac1b. *Scientific reports*, **7**, 1–15.

Yalim-Camci, I., Balcik-Ercin, P., Cetin, M., Odabas, G., Tokay, N., Sayan, A.E. and Yagci, T. (2019): ETS1 is coexpressed with ZEB2 and mediates ZEB2-induced epithelial-mesenchymal transition in human tumors. *Molecular carcinogenesis*, **58**, 1068–1081.

Yanagisawa, M., Huveldt, D., Kreinest, P., Lohse, C.M., Cheville, J.C., Parker, A.S., Copland, J.A. and Anastasiadis, P.Z. (2008): A p120 catenin isoform switch affects Rho activity, induces tumor cell invasion, and predicts metastatic disease. *The Journal of biological chemistry*, **283**, 18344–18354.

Yang, F., Sun, L., Li, Q., Han, X., Lei, L., Zhang, H. and Shang, Y. (2012): SET8 promotes epithelial-mesenchymal transition and confers TWIST dual transcriptional activities. *The EMBO journal*, **31**, 110–123.

Yang, M.-H., Hsu, D.S.-S., Wang, H.-W., Wang, H.-J., Lan, H.-Y., Yang, W.-H., Huang, C.-H., Kao, S.-Y., Tzeng, C.-H., Tai, S.-K., Chang, S.-Y., Lee, O.K.-S. and Wu, K.-J. (2010): Bmi1 is essential in Twist1-induced epithelial-mesenchymal transition. *Nature cell biology*, **12**, 982–992.

Yang, Y., Park, J.W., Bebee, T.W., Warzecha, C.C., Guo, Y., Shang, X., Xing, Y. and Carstens, R.P. (2016): Determination of a Comprehensive Alternative Splicing Regulatory Network and Combinatorial Regulation by Key Factors during the Epithelial-to-Mesenchymal Transition. *Molecular and cellular biology*, **36**, 1704–1719.

Yatabe, Y., Borczuk, A.C. and Powell, C.A. (2011): Do all lung adenocarcinomas follow a stepwise progression? *Lung cancer (Amsterdam, Netherlands)*, **74**, 7–11.

Yilmaz, M. and Christofori, G. (2009): EMT, the cytoskeleton, and cancer cell invasion. *Cancer metastasis reviews*, **28**, 15–33.

Ying, L., Li, G., Wei, S.-s., Wang, H., An, P., Wang, X., Guo, K., Luo, X.-j., Gao, J.-m., Zhou, Q., Li, W., Yu, Y., Li, Y.-g., Duan, J.-l. and Wang, Y.-p. (2015): Sanguinarine inhibits Rac1b-rendered cell survival enhancement by promoting apoptosis and blocking proliferation. *Acta pharmacologica Sinica*, **36**, 229–240.

Zhang, L., Zhou, F. and Dijke, P. ten (2013): Signaling interplay between transforming growth factor-β receptor and PI3K/AKT pathways in cancer. *Trends in biochemical sciences*, **38**, 612–620.

Zhang, Y., Zhao, Y., Jiang, G., Zhang, X., Zhao, H., Wu, J., Xu, K. and Wang, E. (2014): Impact of p120-catenin isoforms 1A and 3A on epithelial mesenchymal transition of lung cancer cells expressing E-cadherin in different subcellular locations. *PloS one*, **9**, 1-9.

Zhang, Y.E. (2017): Non-Smad Signaling Pathways of the TGF-β Family. *Cold Spring Harbor perspectives in biology*, **9**, 1–18.

Zhao, P., Guo, S., Tu, Z., Di, L., Zha, X., Zhou, H. and Zhang, X. (2016): Grhl3 induces human epithelial tumor cell migration and invasion via downregulation of E-cadherin. *Acta biochimica et biophysica Sinica*, **48**, 266–274.

Zhou, C., Licciulli, S., Avila, J.L., Cho, M., Troutman, S., Jiang, P., Kossenkov, A.V., Showe, L.C., Liu, Q., Vachani, A., Albelda, S.M. and Kissil, J.L. (2013a): The Rac1 splice form Rac1b promotes K-ras-induced lung tumorigenesis. *Oncogene*, **32**, 903–909.

Zhou, Z.-J., Dai, Z., Zhou, S.-L., Fu, X.-T., Zhao, Y.-M., Shi, Y.-H., Zhou, J. and Fan, J. (2013b): Overexpression of HnRNP A1 promotes tumor invasion through regulating CD44v6 and indicates poor prognosis for hepatocellular carcinoma. *International Journal of Cancer*, **132**, 1080–1089.

Zhu, G., Zhang, Y., Wang, Q., Che, S., Yang, Y., Chen, L. and Lin, Z. (2019): The prognostic value of Tiam1 correlates with its roles in epithelial-mesenchymal transition progression and angiogenesis in lung adenocarcinoma. *Cancer management and research*, **11**, 1741–1752.

8 Appendix

8.1 Raw data

Due to the large amount and size of the raw data generated in the course of this work, two DVD data disks were attached to the printed version of this work. These disks contain western blot and agarose gel images as well as Microsoft Excel and Graph Pad Prism sheets of the densitometric as well as the qRT-PCR evaluations. The raw data of all the experiments, which were described in this work, was sorted in the order of the figures shown in chapter 3 (see folder "2. Raw data"). The figures were also provided as Microsoft Powerpoint and high resolution PNG files (see folder "3. Figures"). Furthermore, the results and data which were described, but not shown in this work, were included and sorted in the order of the chapters, in which they were mentioned (see folder "4. Data not shown"). Additionally, this work was attached as a Microsoft Word and PDF file (see folder "1. Dissertation").

8.2 Curriculum vitae

The curriculum vitae has been removed from this version of the doctoral thesis for data protection reasons.

8.3 Publications and conference contributions

Seiz, J.R.*, Klinke, J.*, Scharlibbe, L., Lohfink, D., Heipel, M. Ungefroren, H., Giehl, K. and Menke, A. (2019): Different signaling and functionality of Rac1 and Rac1b in the progression of lung adenocarcinoma. *Biological Chemistry*. (* shared first authors).

Klinke, J., Sauer, M., Menke, A. and Giehl, K. (2017): Novel insights into the cooperation of Epithelial Splicing Regulatory Proteins (ESRPs) and Rac1b (poster presentation). *21th Joint Meeting of the Society of Signal (STS): Signal Transduction – Receptors, Mediators and Genes. Weimar, Germany (08.-10.11.2017).*

Klinke, J. and Giehl, K. (2016) Functional differences of the GTPase isoforms Rac1 and Rac1b (talk). *8th Meeting of the GBM study group „Biochemical Pharmacology and Toxicology": Young Scientists meet Experience. Günzburg/Donau, Germany (02.-03.12.2016).*

Klinke, J., Heipel, M., Sauer, M. Menke, A. and Giehl, K. (2016): Differential localization and activity of GTPase isoforms Rac1 and Rac1b (poster presentation*). 20th Joint Meeting of the Society of Signal (STS): Signal Transduction – Receptors, Mediators and Genes. Weimar, Germany (09.-11.11.2016).*

Klinke, J., Menke, A. and Giehl, K. (2014) The SNAP-/CLIP-tag technology as a tool for spatial localization of Galectin-8 (poster presentation). *7th Meeting of the GBM study group „Biochemical Pharmacology and Toxicology": Young Scientists meet Experience. Günzburg/Donau, Germany (12.-13.09.2014).*

8.4 Acknowledgements

I would like to thank everyone who contributed to the successful outcome of this work.

First and foremost, I would like to thank Prof. Dr. Klaudia Giehl for her continuous support of my Ph.D. project and supervising me over the last three and a half years. Her outstanding counseling and the intriguing discussions helped me during my research and the writing of this thesis.

I would also like to express my sincere gratitude to Prof. Dr. Reinhard Dammann of the Institute of Genetics for his insightful comments and encouragements as well as his willingness to participate as my external supervisor. Additionally, my sincere appreciation go to Prof. Dr. Sandra Hake and Prof. Dr. Albrecht Bindereif, who support me as members of my thesis committee.

I also thank Prof. Dr. Andre Menke for introducing me to various RT-PCR methods and counseling me, whenever I had questions regarding this and other topics.

My gratitude also goes to Felicitas Genze for introducing me to the CAM invasion model and teaching me all, that was necessary to establish the method in our lab in Gießen. I also want to thank Ida Oberst and Ewa Bieniek for training me in microtome sectioning. Additionally, I want to express my gratitude to Britta Dorn for lending me her support, not only in material questions, but also for the helpful insights on HE staining protocols.

I would also like to thank all my lab mates. I especially appreciate the time spent with Christopher Meinohl, Marisa Heipel and Julia Seiz as colleagues. They created a great work climate and supported me during the last three and a half years, not only in questions regarding lab work and my research, but also as good friends outside of the laboratory.

Last but not least, I want to thank my parents, Diane and Markus Klinke, my siblings, Michaela and Christopher Klinke as well as my uncle, Michael Klinke. Equally, I want to thank Anja Templin and her parents, Susanne and Stephan Templin. All of them supported me considerably in the completion of this work and guided me throughout the last couple of years by giving me the moral support I needed to keep going.

I dedicate this work to my aunt and god mother Maria Achinger.

8.5 Affidavit of authorship

I hereby declare, that I have completed this dissertation single-handedly without the unauthorized help of a second party and only with the assistance acknowledged therein. I have appropriately acknowledged and cited all text passages, that are derived verbatim from or are based on the content of published work of others, and all information relating to verbal communications. I consent to the use of an anti-plagiarism software to check my thesis. I have abided by the principles of good scientific conduct laid down in the charter of the Justus-Liebig-University Gießen "Satzung der Justus-Liebig-Universität Gießen zur Sicherung guter wissenschaftlicher Praxis" in carrying out the investigations described in the dissertation.

Gießen, February 20th, 2020 Signature: _____

Johannes Klinke